July 1996 •

Wind Tunnel Testing of Three S809 Aileron Configurations for use on Horizontal Axis Wind Turbines

Airfoil Performance Report

R. R. Ramsay
J. M. Janiszewska
G.M. Gregorek
The Ohio State University
Columbus, Ohio

National Renewable Energy Laboratory
1617 Cole Boulevard
Golden, Colorado 80401-3393
A national laboratory of the U.S. Department of Energy
Managed by Midwest Research Institute
for the U.S. Department of Energy
under contract No. DE-AC36-83CH10093

Foreword

Airfoils for wind turbines have been selected by comparing data from different wind tunnels, tested under different conditions, making it difficult to make accurate comparisons. Most wind tunnel data sets do not contain airfoil performance in stall commonly experienced by turbines operating in the field. Wind turbines commonly experience extreme roughness for which there is very little data. Finally, recent tests have shown that dynamic stall is a common occurrence for most wind turbines operating in yawed, stall or turbulent conditions. Very little dynamic stall data exists for the airfoils of interest to wind turbine designer. In summary, very little airfoil performance data exists which is appropriate for a wind turbine design.

Recognizing the need for a wind turbine airfoil performance data base, the National Renewable Energy Laboratory (NREL), funded by the US Department of Energy, awarded a contract to Ohio State University (OSU) to conduct a wind tunnel test program. Under this program, OSU tested a series of popular wind turbine airfoils. A standard test matrix was developed to assure that each airfoil was tested under the same conditions. The test matrix was developed in partnership with industry and is intended to include all of the operating conditions experienced by wind turbines. These conditions include airfoil performance at high angles of attack, rough leading edge (bug simulation), steady and unsteady angles of attack.

Special care has been taken to report as much of the test conditions and raw data as practical so that designers can make their own comparisons and focus on details of the data relevant to their design goals. Some of the airfoil coordinates are proprietary to NREL or an industry partner. To protect the information which defines the exact shape of the airfoil, the coordinates have not been included in the report. Instructions on how to obtain these coordinates may be obtained by contacting C.P. (Sandy) Butterfield at NREL.

C. P. (Sandy) Butterfield
Wind Technology Division
National Renewable Energy Laboratory
1617 Cole Blvd.
Golden, Colorado, 80401 USA
Internet Address: Sandy_Butterfield@NREL.GOV
Phone 303-384-6902
FAX 303-384-6901

Abstract

Wind turbines in the field can be subjected to varying wind conditions, including high winds with the rotor locked or with yaw excursions. In some cases, the rotor blades may be subjected to unusually large angles of attack that can result in unexpected loads and deflections. The operation of the wind turbines also makes it necessary to be able to stop the rotor and to modulate the power output. The incorporation of ailerons on rotor blades has been proposed as one means of controlling the speed of a wind turbines under these adverse conditions. Wind tunnel tests of aileron designs are thus necessary to provide a better understanding of the performance of the ailerons and the loadings at unusual angles of attack.

An 18-inch constant-chord model of the NREL S809 airfoil section with three different aileron configurations was tested under two dimensional steady state conditions in The Ohio State University Aeronautical and Astronautical Research Laboratory 7x10 Subsonic Wind Tunnel. The objective of these tests was to document section lift, drag and moment characteristics under various model configurations and conditions. The three model configurations were designated as unvented aileron, vented aileron and spoiler flap. The aileron deflections used were +5° to -90° for the unvented and vented aileron configurations and -5° to +90° for the spoiler flap. Most of the testing was done for -6° to 27° angle of attack and 1 million Reynolds number. Additional testing was conducted for 0°, 45°, 60° and 90° aileron deflections were the range of angles of attack was extended to -6° to 270°. For the unvented aileron, 2 million Reynolds number tests were also ran. The model was tested under both clean and leading edge grit roughness (LEGR) applied conditions. The LEGR was used to simulate the accumulation of insects and dust on the leading edge of the rotor blades found in the field.

The three configurations exhibited clean maximum lift coefficients of 1.12 for the unvented aileron and spoiler flap and 1.21 for the vented aileron. The application of LEGR reduced the maximum lift coefficient and increased the drag for low angles of attack and low aileron deflections. The LEGR was found to have negligible effect at high angles of attack (above 20°) and high aileron deflection (above 45°), where the drag coefficients were already high.

The suction coefficient provides a measure of the aerodynamic braking ability of the configuration. The coefficient should be negative, but the exact value has to be determined from the actual design of the rotor. At high aileron deflections, the suction coefficient was negative in the region of -6° to 30° angle of attack. The spoiler flap configuration resulted in a negative suction coefficient for aileron deflections greater than 30°. The application of LEGR had a minor effect on the suction coefficient. For small aileron deflection the suction coefficient values with LEGR applied were only slightly lower than for the clean cases. At high aileron deflection, the LEGR did not affect the drag coefficient significantly and so the suction coefficient remained almost unchanged.

The hinge moment was also calculated from the surface pressure data taken. It varied greatly from one configuration to the other. The unvented aileron configuration resulted in much higher magnitudes of the hinge moment than the vented aileron or the spoiler flap. Over the 276° angle of attack range, the hinge moment coefficients varied from -0.81 to 0.91, -0.35 to 0.31, and -0.16 to 0.15 for the unvented aileron, the vented aileron, and the spoiler flap, respectively.

Contents Page

List of Figures Page

List of Tables Page

List of Symbols

AOA	Angle of Attack
A/C	Alternating current
c	Chord length
C_{dmin}	Minimum drag coefficient
C_{dp}	Pressure (form) drag coefficient
C_{dw}	Drag coefficient, calculated from wake momentum deficit
C_h	Hinge moment coefficient
C_l	Lift coefficient
C_{lmax}	Maximum lift coefficient
C_m	Pitching moment coefficient
C_{mo}	Pitching moment coefficient at zero degrees angle of attack
$C_{m¼}$	Pitching moment coefficient about the quarter chord
C_p	Pressure coefficient
C_{pmin}	Minimum pressure coefficient
C_s	Suction coefficient
D	Drag force
HP	Horsepower
k	Roughness element height
k/c	Roughness element height divided by airfoil model chord length
L	Lift force
L/D	Lift to drag ratio
p_w	Static pressure through the model wake
$p_{□□}$	Free steam pressure

q	Dynamic pressure
q_w	Dynamic pressure through the model wake
$q_{\square\square}$	Free stream dynamic pressure
Re	Reynolds number
x	Axis parallel to airfoil reference line
y	Axis perpendicular to airfoil reference line
α	Angle of attack
δ	Control surface deflection angle

Acknowledgements

This work was made possible by the efforts and financial support of the National Renewable Energy Laboratory which provided major funding and technical monitoring and the U.S. Department of Energy, which is credited for its funding of this document through the National Renewable Energy Laboratory under contract number DE-AC36-83CH10093. The staff of the Ohio State University Aeronautical and Astronautical Research Laboratory appreciate the contributions made by personnel from both organizations. The authors would like to thank the undergraduate student research assistants: Mònica Angelats i Coll and Fernando Falasca.

Introduction

Aileron devices have been installed on horizontal axis wind turbines for several purposes including aerodynamic braking and for power modulation. Aerodynamic braking may be used to stop rotor rotation when mechanical braking is not sufficient especially in runaway conditions. The aerodynamic brakes can be a light weight alternative to equivalent mechanical brakes. A consistent power output also may be obtained with the uses of ailerons. Power modulation is achieved by deflecting the aileron to compensate for conditions such as high or low wind speeds or debris buildup on the airfoil leading edges. To better describe the benefits and disadvantages of aileron devices, three configurations designated vented aileron, unvented aileron, and spoiler flap, were tested in The Ohio State University Aeronautical and Astronautical Research Laboratory 7'x10' Subsonic Wind Tunnel facility.

Wind turbines in the field can be subjected to varying wind conditions, including high winds with the rotor locked or with yaw excursions. In some cases, the rotor blades are subjected to unusually large angles of attack that can result in unexpected loads and deflections. To better understand these loads, tests were performed up to 270° angle of attack for some of the aileron deflections. In addition to conducting tests on a clean airfoil, leading edge grit roughness (LEGR) was applied to the model to simulate the degradation due to surface irregularities from the accumulation of insect debris, ice, and/or the aging process.

Each of the three aileron configurations had an overall chord of 457-mm (18-in), which was constant over the span of the 2.1-m (7-ft) test section. The aileron device was nominally 40% of the chord of the model. Testing of the three configurations, was performed at 1 million Reynolds number and the unvented configuration, was also tested at 2 million Reynolds number. The vented and unvented ailerons were deflected from +5° to -90° and the spoiler flap was deflected in the opposite direction from +90° to -5°. The standard angle of attack range for most of the tests was from -6° to 27°; however, for the 0°, 45°, 60°, and 90° aileron deflections and 1 million Reynolds number, the range included angles of attack up to 270°.

Test Facility

Testing was performed in the OSU/AARL 7x10 subsonic wind tunnel. A schematic of the tunnel is shown in figure 1. There are two test sections in this tunnel: a 2.1-m (7-ft) by 3-m (10-ft) section in which these tests were conducted, and a 4.9-m (16-ft) by 4.3-m (14-ft) section in which very low speed and high angle of attack testing is performed with large models. The wind tunnel is a closed-circuit, single-return, continuous-flow system. A velocity range of 18 to 92 m/s (35 to 180 knots) is developed in the 7x10 test section by a six-blade, fixed-pitch, 6.1-m (20-ft) diameter fan directly driven by a 2000-HP, variable-speed motor. The tunnel's steel outer shell is water spray cooled to control internal air temperature. Its test section floor contains a rotating table which allows adjustment of the model angle of attack through a 290° range about a vertical axis.

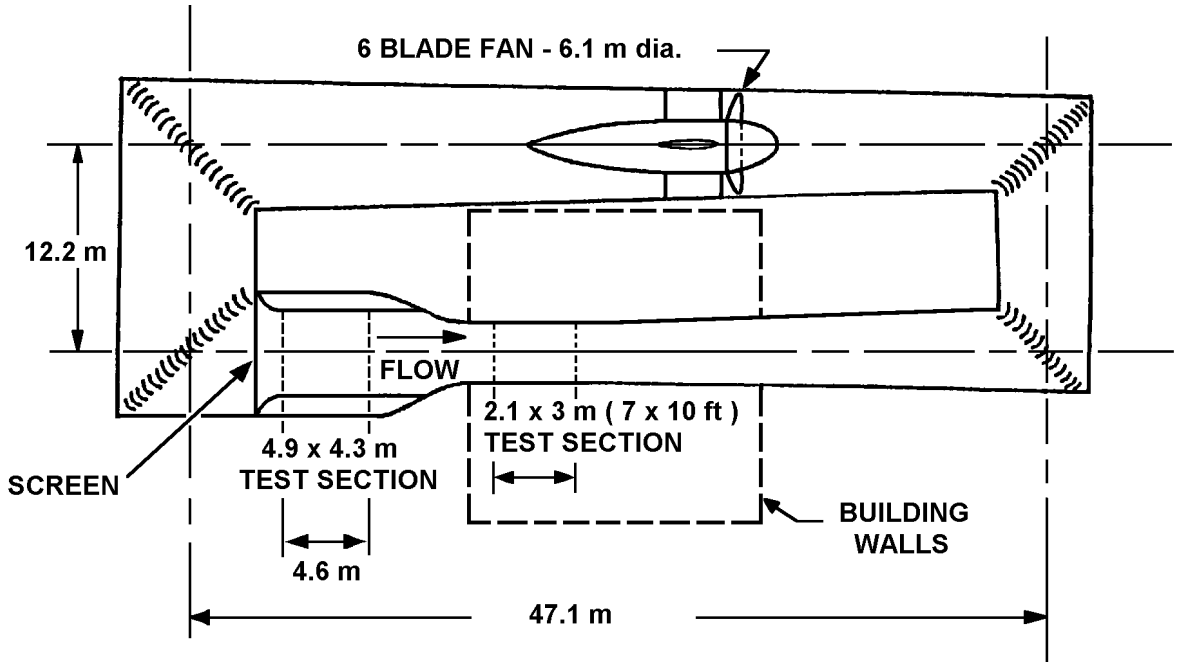

Figure 1. OSU/AARL 7x10 Subsonic Wind Tunnel.

To determine drag accurately, the wake momentum method was used and a horizontally traversing wake survey system was installed in the test section. The wake survey system consists of three total and static probe pairs attached to aerodynamic tubing, spaced approximately every 61-cm (2-ft). This arrangement allowed for 274-cm (9-ft) coverage within the test section. Figure 2 shows the detail of the wake probes. The total wake probes were internally chamfered at 45° and the static probes had four 0.635-mm (0.025-in) diameter static ports equally distributed around the probe periphery. The wake survey system was vertically supported about 61-cm (2-ft) off the center line of the tunnel on both sides. Wake probe data were taken at 122-cm (4-ft) from the floor of the tunnel and 2.4 chord lengths down stream from the model. In this test all three of the probe pairs were used to capture the wake.

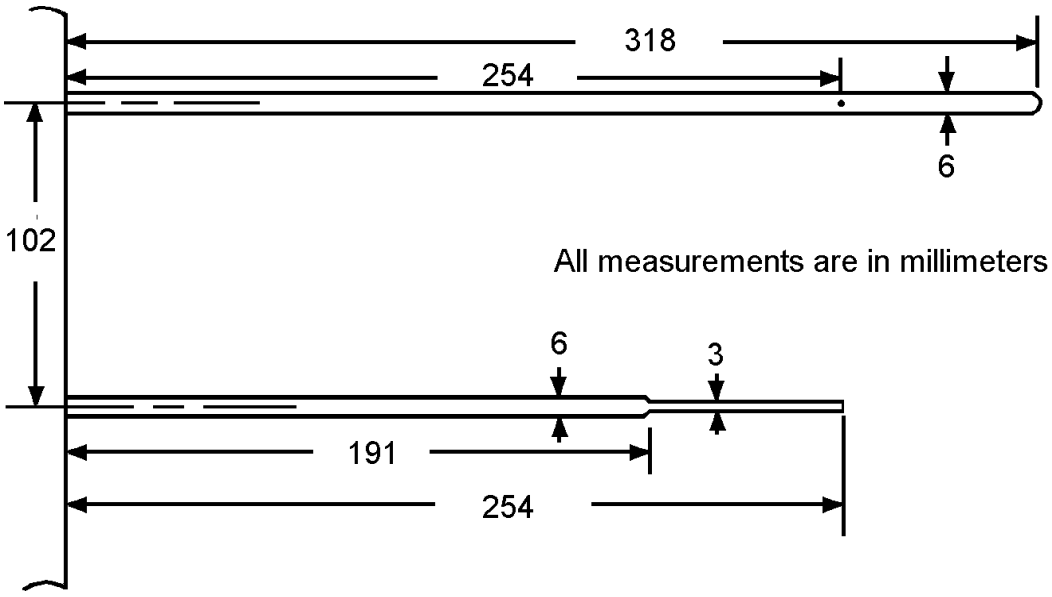

Figure 2. Wake probe detail.

The wake probe system was computer controlled with the operator choosing the limits of travel. Ten differential transducers were used to acquire the static and total pressures from the wake probe system (6) and the wind tunnel conditions (4).

Model Details

An 457-mm (18-in) constant chord aileron model was designed by OSU/AARL personnel and manufactured elsewhere. This model was designed to span 2.13 m (7-ft) and have three interchangeable aileron configurations as shown in figure 3. Each configuration was designed so that the different sections could be installed without removing the model completely from the wind tunnel. The first 229 mm (9-in) of the main element and the last 127 mm (5-in) of the aileron section were common to all configurations. A nine layer composite lay up of alternating fiberglass and carbon fiber over steel ribs was used for the common main element section. The main load bearing member was a 63.5 mm (2.5-in) diameter thick-walled steel tube which passed through the overall model quarter chord location. Loads for the model were transferred through the steel ribs to this steel tube that was fixed in the tunnel floor and ceiling. The three main element trailing edges, called cove sections, were fabricated from solid aluminum and bolted to the main element through the steel ribs. Like the cove pieces the aileron sections were fabricated from solid aluminum for structural stability. The aileron or flap sections were fastened at four locations along the 2.13 m (7-ft) model span, at the ends and two intermediate location 585 mm (23-in) from either end, to eliminate any tendency for these section to flutter at the high deflection angles prescribed in the test matrix. During testing no flutter was observed over the entire test range in either the main element or the aileron/flap sections.

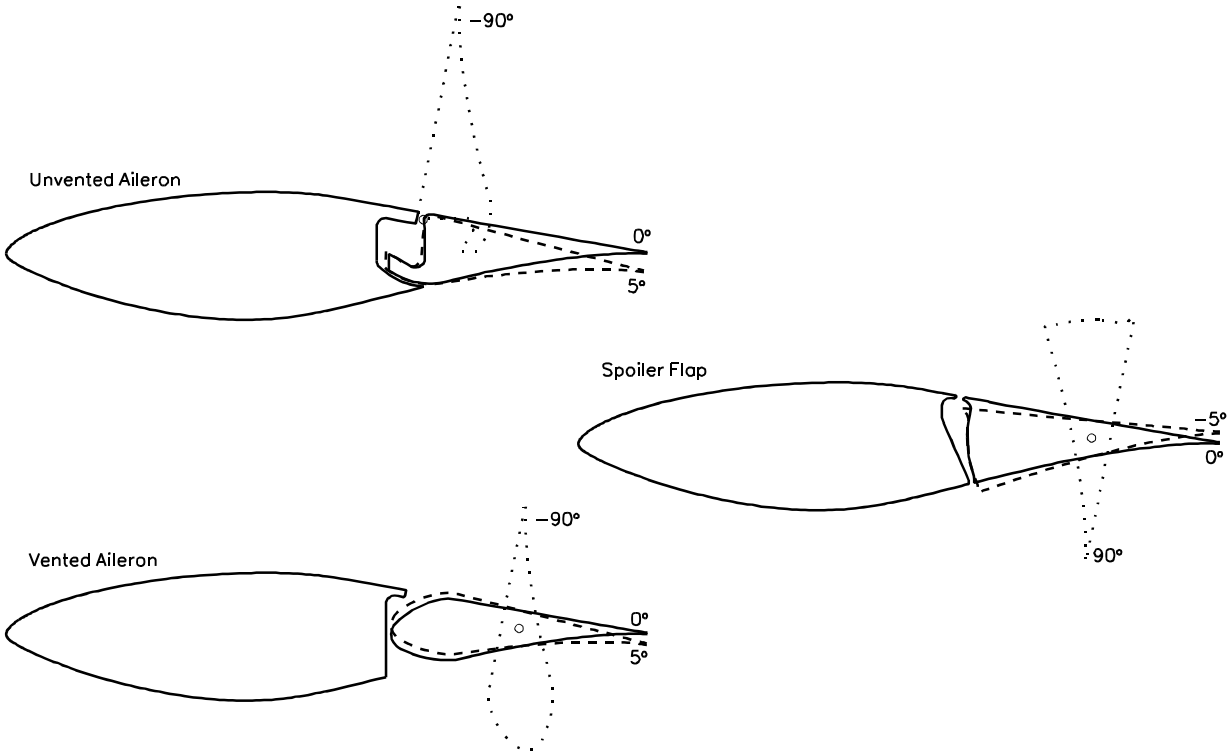

Figure 3. Aileron model sections.

The extreme aileron deflection angles for the vented aileron, unvented aileron and spoiler flap are shown figure 3.

Pressure taps were installed in the model surface during manufacturing so that pressure distributions could be obtained. The vented aileron configuration had 42 pressure taps on the main and 16 on the aileron; the unvented aileron had 43 on the main and 15 on the aileron; and the spoiler flap configuration had 41 on the main and 16 on the flap. Location of the taps are shown in figure 4 and listed in appendix A.

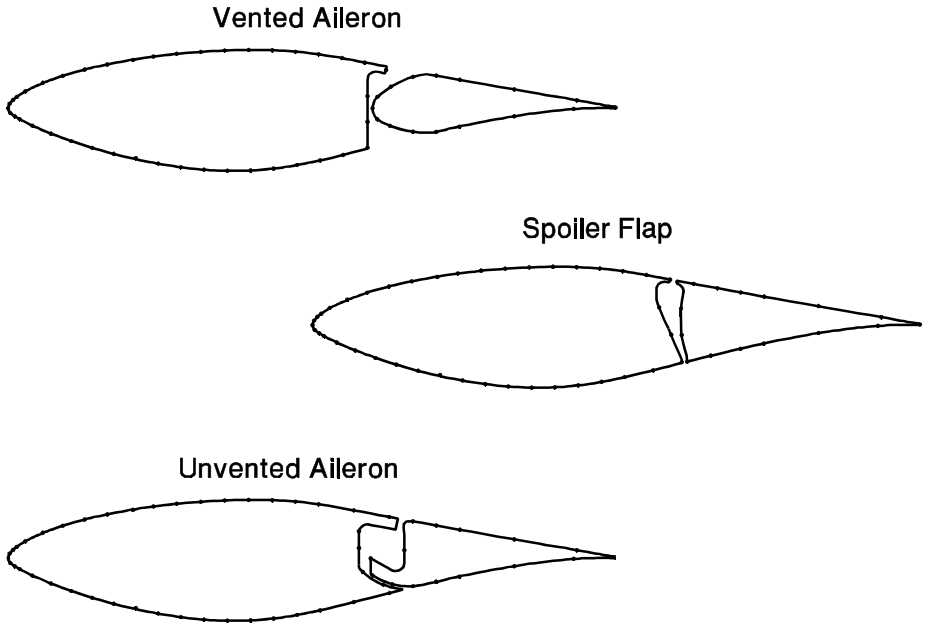

Figure 4. Pressure tap locations.

For test cases involving roughness, a standard roughness pattern developed for the National Renewable Energy Laboratory airfoil test program was used. The pattern was generated using a molded insect pattern taken from a wind turbine in the field. The particle density was 5 particles per cm^2 (32 particles per square inch) in the middle of the pattern, thinning to 1.25 particles per cm^2 (8 particles per square inch) at the edge of the pattern. Figure 5 shows the pattern. To make a usable template, the pattern was repeatedly cut into a steel sheet 102-mm (4-in) wide and 91-cm (3-ft) long with holes just large enough for one grain of grit. Based on average particle size from the field specimen, standard #40 lapidary grit was chosen for the roughness elements, giving k/c=0.0019 for a 457-mm (18-in) chord model.

To use the template, 102-mm (4-in) wide double-sided tape was applied to one side of the template and grit was poured and brushed from the opposite side. The tape was then removed from the template and transferred to the model. This method allows the same roughness pattern to be replicated for any test.

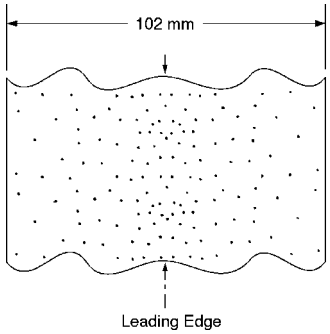

Figure 5. Roughness pattern.

Test Equipment and Procedures

Data Acquisition

Data were acquired and processed from up to 58 surface pressure taps, 10 individual tunnel pressure transducers, an angle of attack encoder, a wake probe position slide-wire, and a tunnel thermocouple. The data acquisition system was controlled by a 80386-based PC which utilized a Pressure Systems Incorporated (PSI) data scanning system. The PSI system included a 780B Data Acquisition and Control Unit (DACU), 780B Pressure Calibration Unit (PCU), 81-IFC scanning module interface, two 32-port 2.5-psid pressure scanning modules (32-ESP) and one 16-port 2.5-psid pressure scanning module (16-ESP). Figure 6 shows the schematic of the data acquisition system.

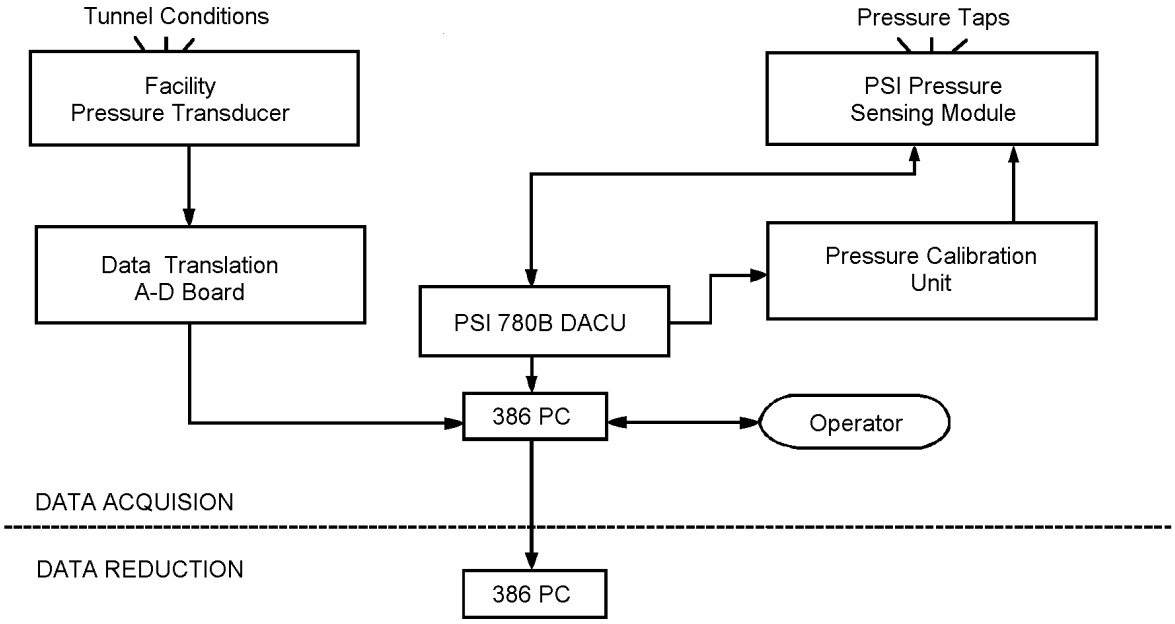

Figure 6. Data Acquisition Schematic.

Four individual pressure transducers read tunnel east total pressure, tunnel east static pressure, tunnel west total pressure, and tunnel west static pressure. Six individual pressure transducers were used to measure the wake probe total and static pressures. All transducers were powered by signal conditioners and their outputs were amplified to the proper voltage required for the data translation A-D board. Before the test, these transducers were bench calibrated using a water manometer to determine their sensitivities and offsets and related values were incorporated into the data acquisition and reduction program.

Three ESPs were calibrated simultaneously using the DACU and PCU. The DACU controlled the PCU which applied known regulated pressures to the ESPs and read the output voltages from each integrated pressure sensor. From these values, the DACU calculated the calibration coefficients and stored them internally until the coefficients were requested by the controlling computer. The calibration of the ESPs installed in the model was performed frequently during a run set to minimize the output drifts due to the temperature changes which occur during a test sequence.

Finally, pressure measurements from the airfoil surface taps and the transducers were acquired and stored by the DACU and subsequently passed to the controlling computer for final processing.

Data Reduction

The data reduction routine was incorporated as a section of the data acquisition program. This combination of data acquisition and reduction routines allowed for data to be reduced on-line during a test. By reducing runs during the test series, integrity checks could be made to insure the equipment was working properly and allow for on-the-spot updates of the test matrix.

The ambient pressure was manually input into the computer and was updated regularly. This value, as well as the measurements from the tunnel pressure transducers and tunnel thermocouple, were used to calculate tunnel airspeed.

A datum point was derived by acquiring 200 data scans of all channels over a 6-second window at each angle of attack and tunnel condition. The reduction portion of the program processed each data scan to coefficient forms (C_p, C_l, $C_{m¼}$, C_h, and C_{dp}) using the measured surface pressure voltages, calibration coefficients, tap locations and wind tunnel conditions. All scan sets for a given condition were then ensemble averaged to provide one set. All data were saved in electronic form. The data were not corrected for any tunnel wall effects.

Measured wake probe pressures were used to calculate the total drag coefficient using the following equation from Schlichting (1976).

$$C_d = \frac{2}{c} \int \sqrt{\frac{q_w + p_\infty - p_w}{q_\infty}} \left(1 - \sqrt{\frac{q_w}{q_\infty}} \right) dy$$

The integration was done automatically except the operator chose the end points of the integration from a plot of the wake survey displayed on the screen. Wake drag data were used for moderate angles of attack and low control surface deflection angles because at higher values, the wake becomes too turbulent for an accurate pitot/static probe measurement to be taken. The wake probe measurements listed in Appendix B are considered reliable.

The suction coefficient can be used as a measure of an airfoil's ability to produce aerodynamic braking forces for a wind turbine. This coefficient is defined using the following equation:

$$C_s = C_l \sin\alpha - C_d \cos\alpha$$

Aerodynamic braking can only occur if the suction coefficient is negative. The actual design of the rotor is required to determine the maximum value of negative suction coefficient, since many factors affect the ailerons ability to stop rotation.

Test Matrix

This test series included aileron angles ranging from +5° to -90° or -5° to +90° and the angles of attack in some cases ranged from -6° up to +270°. All configurations were tested at 1 million Reynolds number and the unvented aileron was additionally tested at 2 million Reynolds number. Table 1 shows the test conditions for which each configuration was tested. All aileron deflections and Reynolds numbers were repeated with LEGR applied for the angle of attack range from -6° to +27°.

Table 1. Test Matrix

	Vented	Unvented		Spoiler Flap	
δ	$Re=1x10^6$	$Re=1x10^6$	$Re=2x10^6$	δ	$Re=1x10^6$
5°	Set 1	Set 1	Set 1	-5°	Set 1
0°	Set 1 and 2	Set 1 and 2	Set 1	0°	Set 1 and 2
-5°	Set 1	Set 1	Set 1	5°	Set 1
-10°	Set 1	Set 1	Set 1	10°	Set 1
-20°	Set 1	Set 1	Set 1	20°	Set 1
-30°	Set 1	Set 1	Set 1	30°	Set 1
-45°	Set 1 and 2	Set 1 and 2	Set 1	45°	Set 1 and 2
-60°	Set 1 and 2	Set 1 and 2	Set 1	60°	Set 1 and 2
-90°	Set 1 and 2	Set 1 and 2	Set 1	90°	Set 1 and 2
Angle of Attack Set 1: -6°, 0°, 3°, 6°, 9°, 12°, 15°, 18°, 20°, 24°, 27°					
Angle of Attack Set 2: 30°, 35°, 40°, 45°, 60°, 70°, 80°, 90°, 120°, 150°, 180°, 210°, 240°, 270°					

Results and Discussion

Baseline Configuration

A baseline clean configuration was tested to provide a reference. For the baseline tests, the spoiler flap configuration was used with the spoiler flap set at zero degrees deflection and both the upper and lower surface gaps were taped over. Additionally, the tap file was modified by removing taps located in the interior of the airfoil once the gap was taped, see figure 4. These taps were not used in the integration of the performance coefficients.

The maximum pre-stall lift coefficient for the baseline configuration was 1.04 and occurred at 15° angle of attack, presented in figure 7. Over the entire test range, a secondary peak was produced in the lift coefficient beyond stall at 45° and had a value of 1.23. The lift then decreased until a minimum was reached near 120° angle of attack. The minimum drag was measured using a wake survey probe and was 0.0088. The pitching moment about the quarter chord location at zero lift was -0.027. Although the lift reached a secondary peak the drag increased substantially until it reached a maximum at 90° as shown in figure 8. Since both lift and drag were high and the resulting lift-to-drag ratio was actually less than 5 as seen in figure 10. At lower lift coefficient, the lift-to-drag ratio had a maximum of 72 which occurred at 6° angle of attack. The suction coefficient, shown in figure 9, is negative only in a narrow angle of attack region.

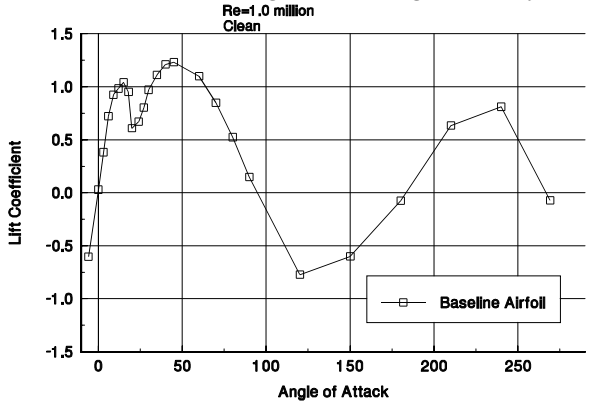

Figure 7. S809 Baseline, Re=1x10^6, C_l vs α.

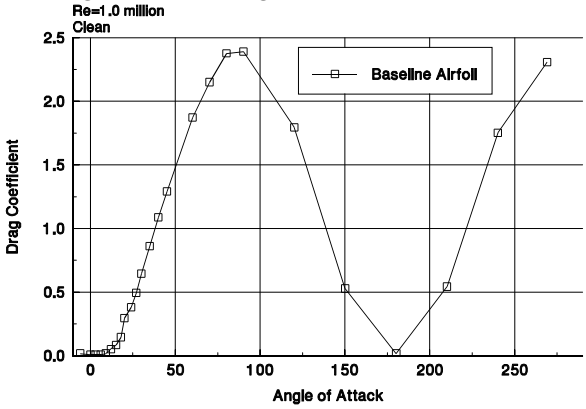

Figure 8. S809 Baseline, Re=1x10^6, C_d vs α.

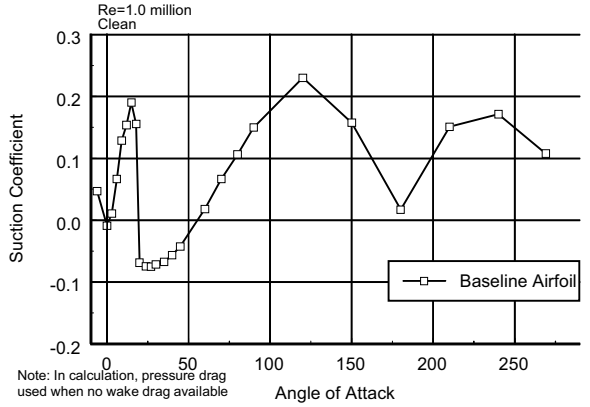

Figure 9. S809 Baseline, Re=1x10^6, C_s vs α.

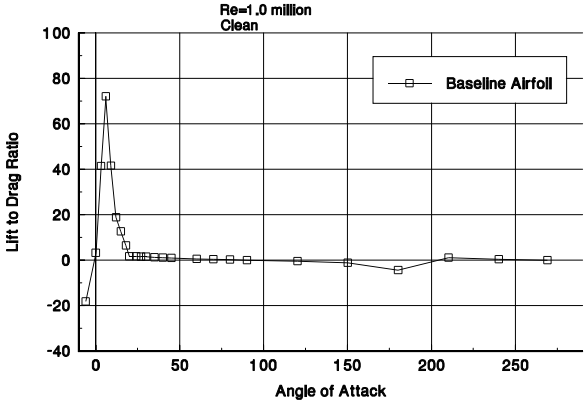

Figure 10. S809 Baseline, Re=1x10^6, L/D vs α.

Unvented Aileron

Re=1 million

Clean

The pivot point for the flap rotation was located at the leading edge upper surface of the flap for the unvented aileron configuration; making it unique from the other two configurations. The maximum lift coefficient measured occurred for a positive 5° deflection and was 1.12. As the flap was deflected in a more negative direction, the lift curves shifted to the right and to more negative values as seen in figures 11 and 12. Additionally, the slopes of the curves were reduced as the flap deflection angle was decreased to -90°. The maximum lift curve slope was found for an aileron deflection of 5° and was 0.11 and the minimum occurred for the -90° aileron deflection and was 0.03.

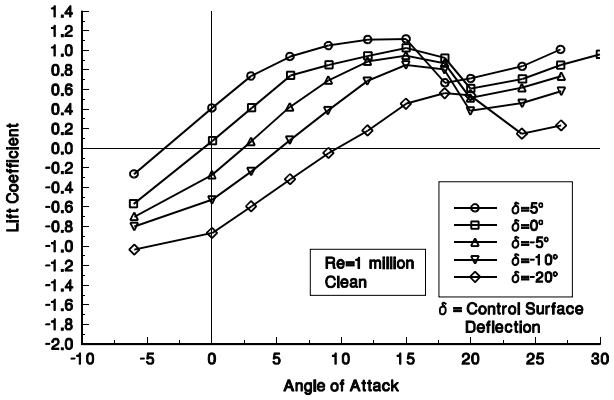

Figure 11. Unvented aileron, clean, Re=1x10^6, C_l vs α.

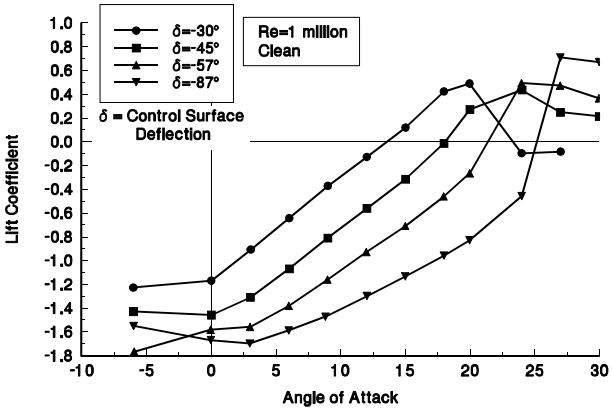

Figure 12. Unvented aileron, clean, Re=1x10^6, C_l vs α.

The drag coefficients, shown in figures 13 and 14 increased with decreased control surface deflection angle. Moreover, the minimum drag occurred for the 0° control surface deflection and 0° angle of attack and had a value of 0.0089. As the control surface deflection decreased, the characteristic drag bucket became less apparent and at -90° aileron deflection, there was no drag bucket to speak of. At the -90° deflection, the overall drag coefficient was near 0.5, making it over five times higher than the measured minimum drag.

The unvented aileron, 1 million Reynolds number suction coefficients, in figures 15 and 16, show positive or near positive results for all of the control surface deflections tested in the -6° to 30° angle of attack range. Regions of positive or nearly positive flap deflection can be problematic since suction coefficients should be negative to stop the rotation of the rotor. For angles of attack less than 20° and control surface deflection of -90°; the suction coefficient was -0.7, which could be enough to stop the wind turbine rotation.

The clean hinge moment curves show that for a flap deflection of 5°, figure 17, the hinge moments are all negative from -6° to 30° angle of attack and range from -0.071 to -0.325. At a control surface deflection of -90°, shown in figure 18, the slope of the hinge moment curve is actually positive for a range of angles of attack from 0° to 10°. Through this range, the hinge moment coefficients tended to be around 0.55. An interesting feature was that the hinge moment coefficient dropped substantially between 24° and 27° angle of attack. This was also reflected in a distinct rise the suction coefficient as shown figure 16.

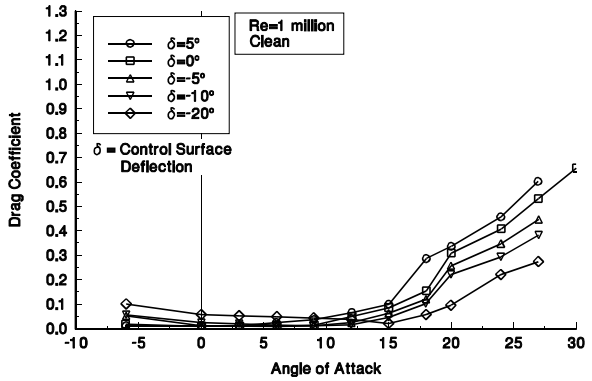

Figure 13. Unvented aileron, clean, Re=1x10^6, C_d vs α.

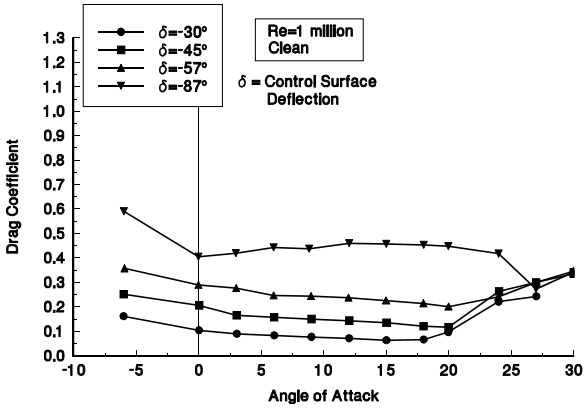

Figure 14. Unvented aileron, clean, Re=1x10^6, C_d vs α.

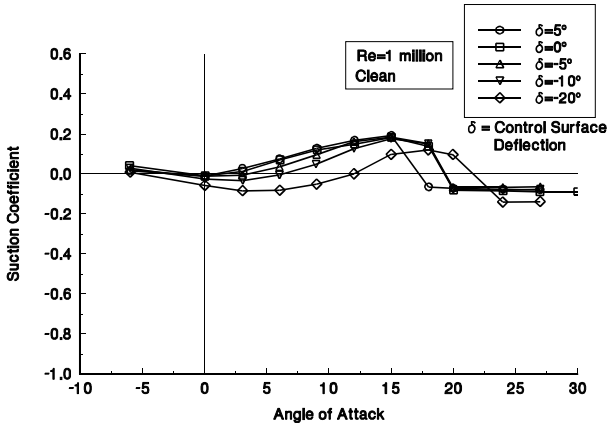

Figure 15. Unvented aileron, clean, Re=1x10^6, C_s vs α.

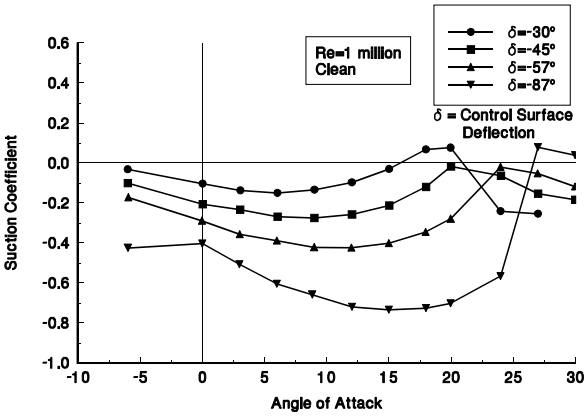

Figure 16. Unvented aileron, clean, Re=1x10^6, C_s vs α.

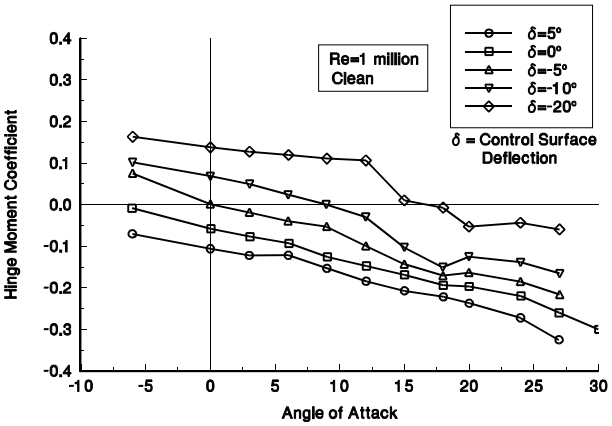

Figure 17. Unvented aileron, clean, Re=1x10^6, C_h vs α.

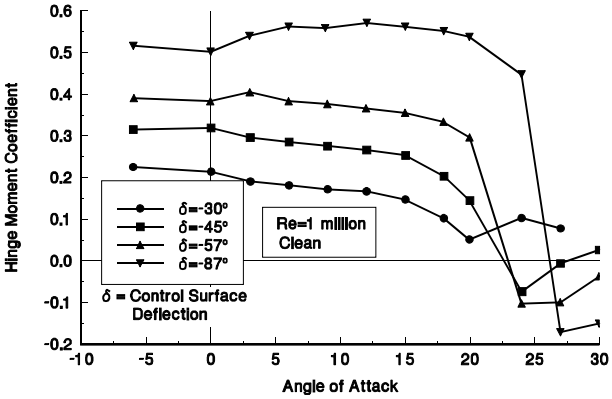

Figure 18. Unvented aileron, clean, Re=1x10^6, C_h vs α.

The maximum lift-to-drag ratio for this configuration and Reynolds number occurred for a 0° control surface deflection angle and 6° angle of attack. The maximum value was 87. As seen from figures 19 and 20, the

maximum of each individual curve decreased consistently with decreasing aileron deflection and the maximum was located at higher angles of attack for each consecutive deflection.

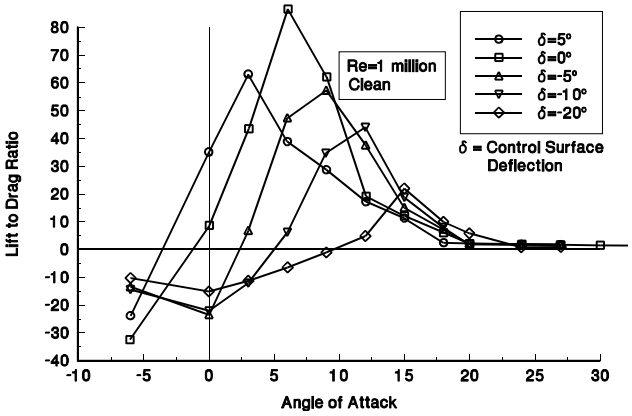

Figure 19. Unvented aileron, clean, Re=1x10^6, L/D vs α.

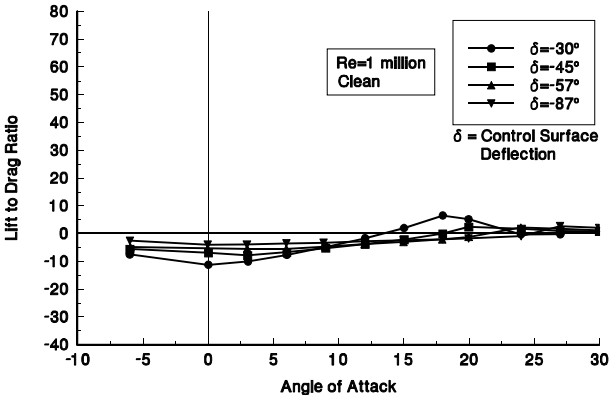

Figure 20. Unvented aileron, clean, Re=1x10^6, L/D vs α.

LEGR

LEGR was applied to the main section of the unvented aileron configuration to investigate its effect on the performance characteristics of the model. The LEGR lowered the lift curves as compared to the clean case for control surface deflections from 5° to -20° resulting in a reduced maximum lift coefficient, seen in figure 21. The maximum lift coefficient for this test configuration was reduced to 1.00 from the clean value of 1.12, about an 11% reduction. All maximum lift coefficients were reduced anywhere from 9% to 22% below the clean values for aileron deflections of greater than -30°. In addition to a reduction in the maximum lift coefficient, the application of LEGR caused a reduction in the lift curve slopes. It can also be observed from figure 21, that just beyond the maximum lift coefficient, the curves were somewhat flatter than the same region for the clean case. In other words, the reduction in lift coefficient beyond the normal lift coefficient maximum was less for the LEGR cases. Comparing figure 22 for the most negative flap deflections to the clean cases in figure 12, it can be seen that the lift curves were very similar.

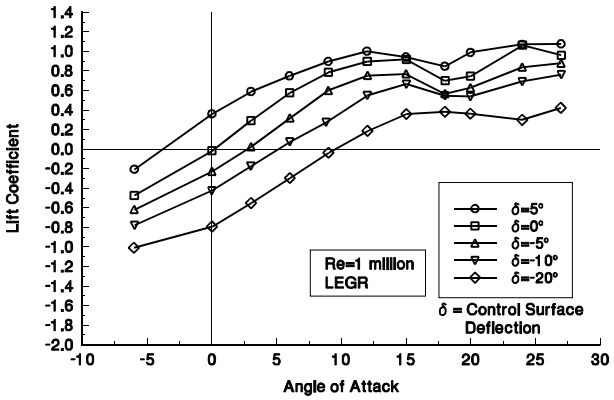

Figure 21. Unvented aileron, LEGR, C_l vs α.

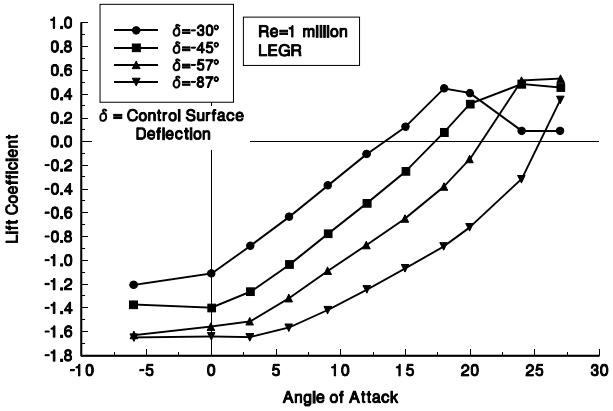

Figure 22. Unvented aileron, LEGR, C_l vs α.

With the addition of LEGR, the trend showed increased drag coefficient and especially an increase in the minimum drag coefficient. The minimum drag coefficient for this 1 million Reynolds number, unvented

aileron, LEGR case was 0.0138 and occurred, at a 0° aileron deflection and 0° angle of attack, as it did for the clean case. This was an increase of 56% over the 0.0089 clean case minimum drag coefficient. A feature of the drag data were that the drag "bucket" which was apparent in the clean data shown in figure 13 was not as clearly defined in the LEGR drag curves shown in figure 23. The drag coefficient did show increased values as the control surface deflection angle was decreased as seen in figure 24. In comparison to the clean drag data, the lowest control surface deflection LEGR applied drag data were very similar. If plotted together, they would nearly lie on top of one another especially for moderate angles of attack up to 20°.

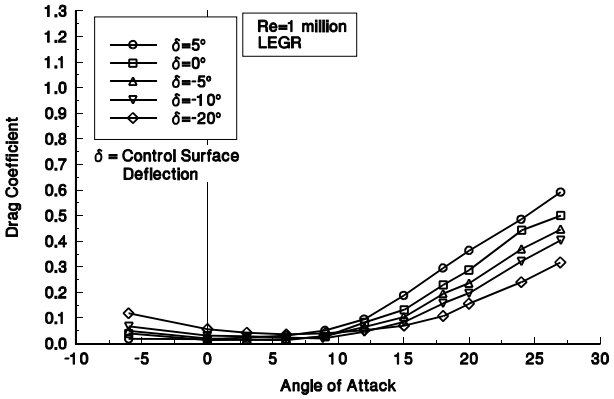

Figure 23. Unvented aileron, LEGR, C_d vs α.

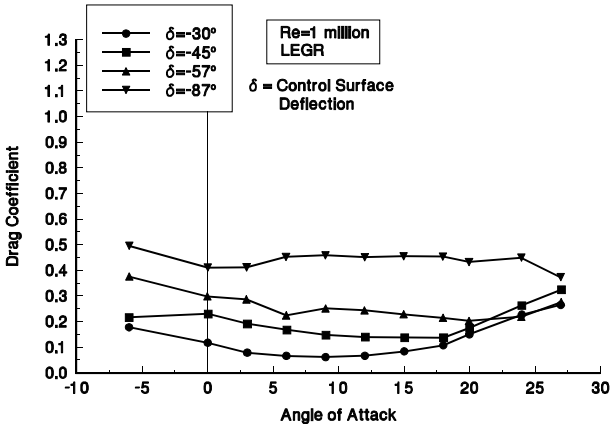

Figure 24. Unvented aileron, LEGR, C_d vs α.

As expected, suction coefficient was affected by LEGR application since it is a function of the lift and drag coefficients. From figure 25, it can be seen that the application of LEGR to control deflection cases down to -30° flattened the curves so that they were closer to zero through the angle of attack range tested than for the clean cases. The 0° deflection case had suction coefficient values ranging from 0.11 to -0.016. Alternatively, the lowest control surface deflections of -30° to -87° shown in figure 26 had LEGR applied suction coefficient curves that were very similar to those for the clean cases. This was especially true for angles of attack up to 10°. At slightly higher angles of attack, the -87° case for the LEGR and clean cases diverge slightly with the LEGR case being less negative. Although this was true, the suction coefficient was still quite negative having a value of -0.71. Beyond 20° angle of attack, however, the suction coefficient rose steeply.

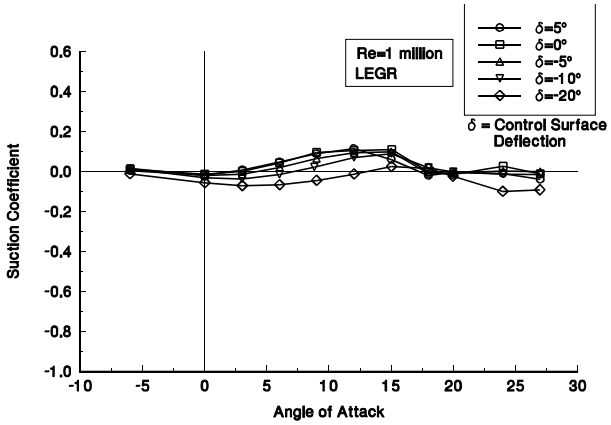

Figure 25. Unvented aileron, LEGR, C_s vs α.

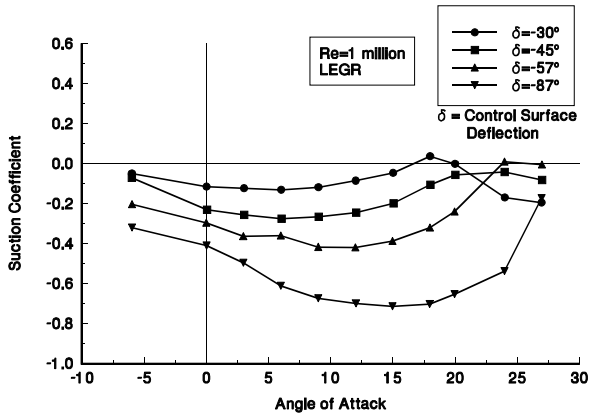

Figure 26. Unvented aileron, LEGR, C_s vs α.

The application of LEGR also affected the hinge moment of the unvented aileron. The slope of the hinge moment curves were more negative once LEGR was applied for the 5° and 0° control surface deflection angles, figure 27. For the lower control surface deflections in figure 28, the LEGR hinge moment data and clean hinge moment data showed similar features. The only differences in the data occurred for the angle of attack region of maximum lift.

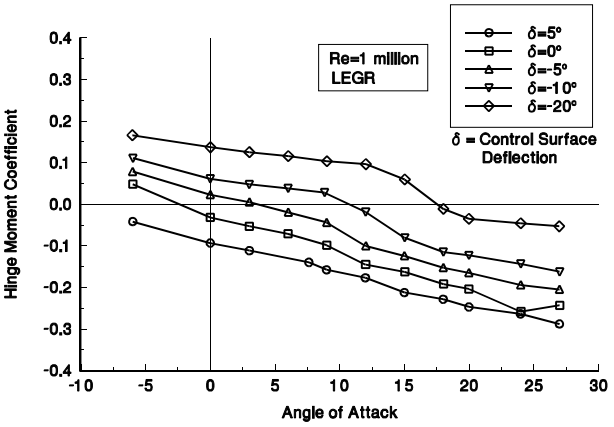

Figure 27. Unvented aileron, LEGR, C_h vs α.

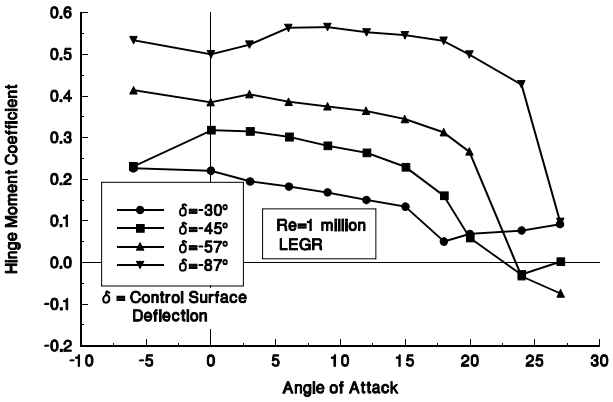

Figure 28. Unvented aileron, LEGR, C_h vs α.

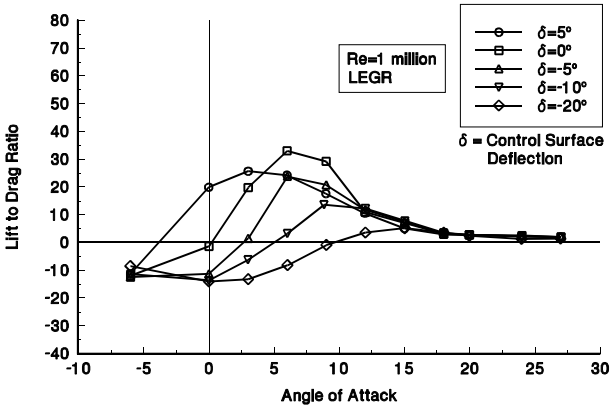

Figure 29. Unvented aileron, LEGR, L/D vs α.

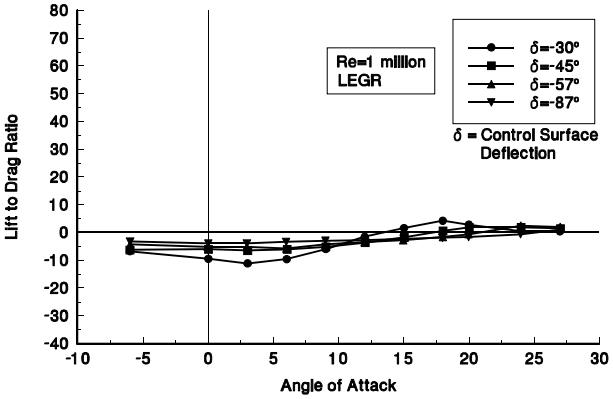

Figure 30. Unvented aileron, LEGR, L/D vs α.

The application of LEGR caused a significant reduction in the lift-to-drag ratio, as seen in figures 29 and 30, from the clean case. Similarly to the clean cases, the maximum lift-to-drag ratio occurred for the 0° control device deflection and had a value of 33. This value was much lower than the maximum found for the clean case which was 87. Otherwise, the same trends that were observed for the clean case were also observed for the application of LEGR. For example, the maximum lift-to-drag ratio shifted to higher angle of attack with decreasing control surface deflection angle.

At 1 million Reynolds number the unvented aileron configuration was tested through an angle of attack range from -6° to 270°. The model was clean and the aileron deflection angles were 0°, 45°, 57°, and 87°. Figures 31 through 34 show lift coefficient, drag coefficient, suction coefficient, and hinge moment coefficient versus angle of attack. At 0° deflection of the aileron, the lift coefficient data showed a secondary peak at 45° of 1.2. Although this peak was high, the drag coefficient increased substantially through this angle of attack and consequently drove down the lift-to-drag ratio. The hinge moment coefficient went from -0.81 to 0.91

for the deflections and angles of attack tested. The data shown graphically here and in tabular form in Appendix B can help in determining the loads on blades under extreme angle of attack conditions.

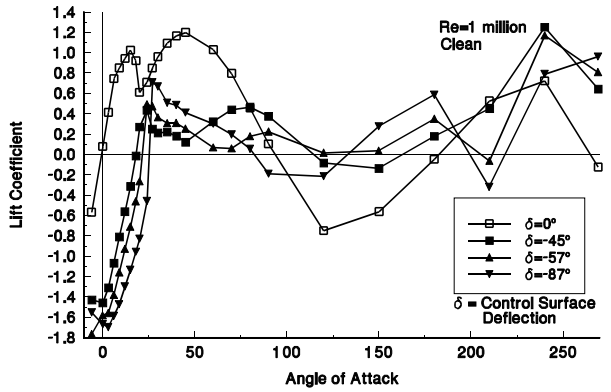

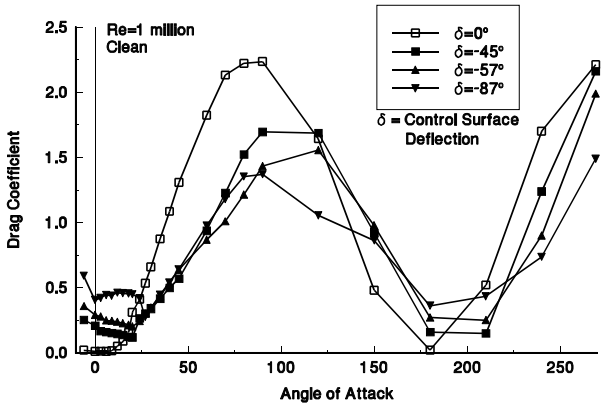

Figure 31. Unvented aileron, full sweep, C_l vs α. Figure 32. Unvented aileron, full sweep, C_d vs α.

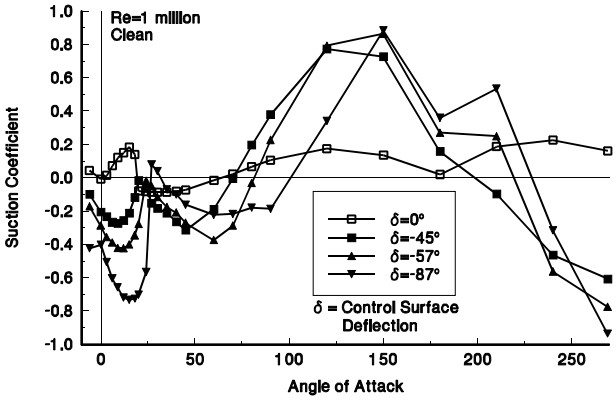

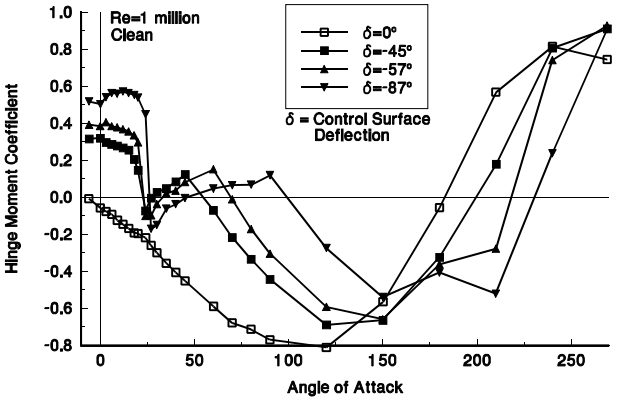

Figure 33. Unvented aileron, full sweep, C_s vs α. Figure 34. Unvented aileron, full sweep, C_h vs α.

Re=2 million

Clean

One of the purposes of these tests was to determine the Reynolds number effect on the aileron braking capabilities. The unvented aileron configuration was chosen from the three configuration for additional higher Reynolds number testing.

The increase in Reynolds number caused a slight increase in maximum lift coefficient for most of the aileron deflections tested. Through the linear range of the lift curves, there were no changes. These lift coefficient curves are shown in figures 35 and 36. The maximum lift coefficient occurred, at the 5° aileron deflection and was 1.19 as compared to the lower Reynolds number which had a maximum lift coefficient of 1.12 for the same aileron deflection angle.

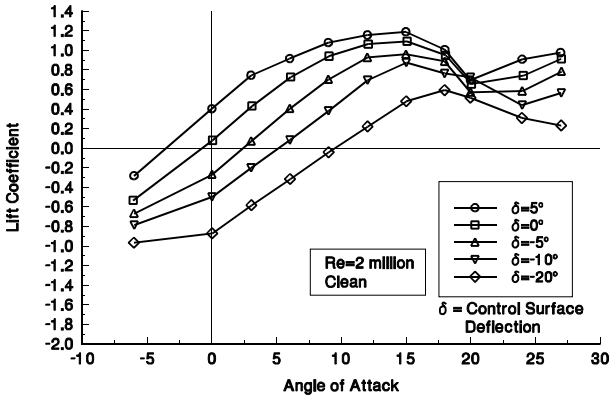

Figure 35. Unvented aileron, clean, Re=2x10^6, C_l vs α.

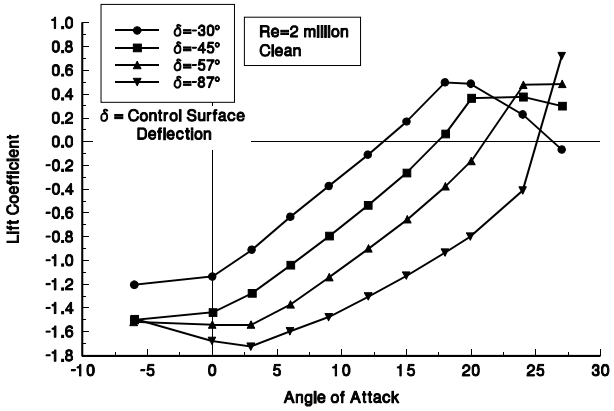

Figure 36. Unvented aileron, clean, Re=2x10^6, C_l vs α.

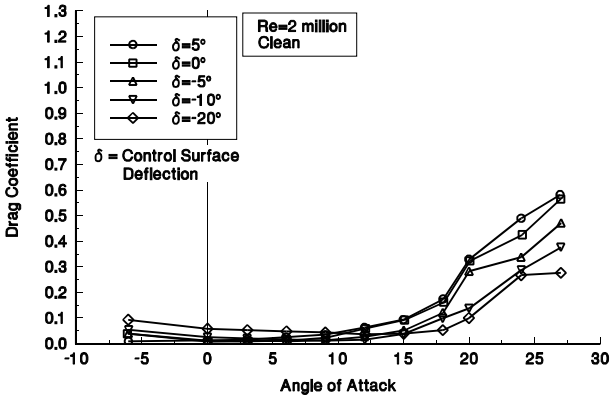

Figure 37. Unvented aileron, clean, Re=2x10^6, C_d vs α.

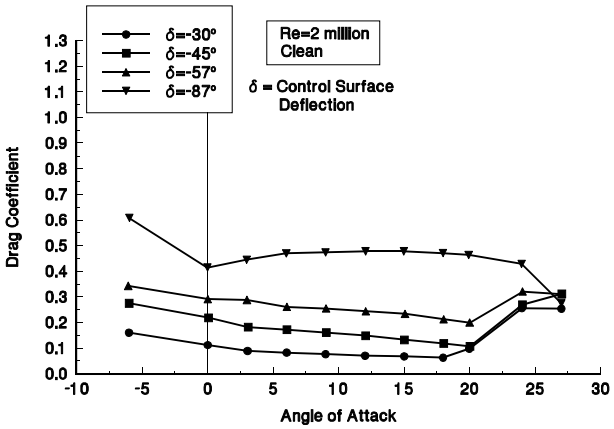

Figure 38. Unvented aileron, clean, Re=2x10^6, C_d vs α.

Increased Reynolds number also affected the drag coefficient. The minimum drag for the 2 million Reynolds number case was 0.0075 and occurred for 0° angle of attack and aileron deflection. Additionally the increase in speed caused a slight increase in the size of the drag bucket for the 5°to -10° aileron deflection angles shown in figure 37. For the other control surface deflection angles shown in figure 38, the drag curves were almost the same as the lower Reynolds number case, especially for angles of attack from 0° to 20°. Therefore, the speed difference shown here produced little change in the drag coefficient at control surface deflection angles less than -20°.

Suction coefficient was affected by the Reynolds number change for angles of attack beyond 15° as shown in figures 39 and 40. This was expected since the lift and drag coefficient changed significantly for angles of attack greater than 15°. The most negative suction coefficient was again found for a -87° control surface deflection where the suction coefficient varied from -0.414 to -0.753 for up to 24° angle of attack. The -57° aileron deflection case had suction coefficients which varied from -0.056 to a minimum of -0.431 through the angle of attack range tested.

For the higher Reynolds number case, the hinge moment showed little change for moderate angles of attack as compared to the lower Reynolds number case. Figures 41 and 42 show the hinge moment coefficient data

for this case. The hinge moment curves did diverge slightly from the 1 million Reynolds number data for angles of attack higher than 20°. In one case, the hinge moment had 0.15 change in magnitude due to the Reynolds number change but the average increased in magnitude was only 0.023.

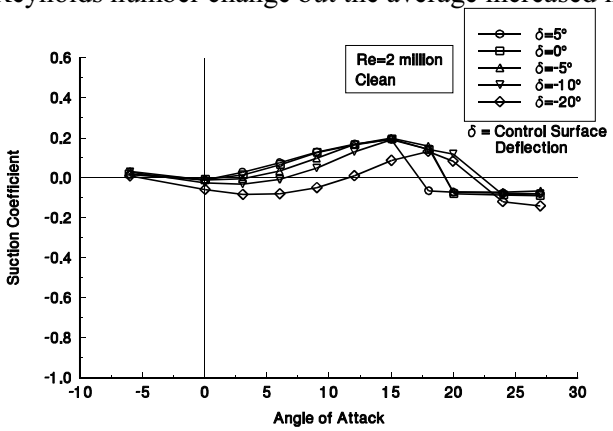

Figure 39. Unvented aileron, clean, Re=2x10^6, C_s vs α.

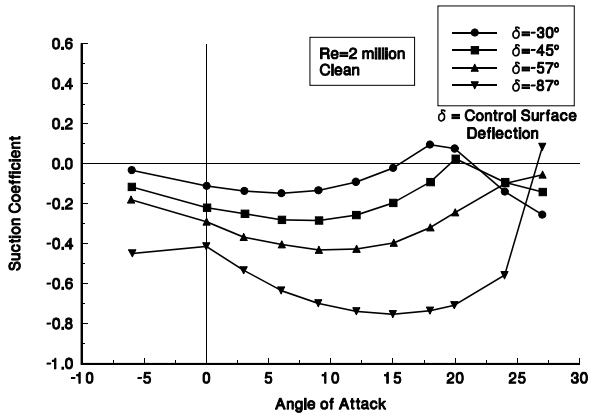

Figure 40. Unvented aileron, clean, Re=2x10^6, C_s vs α.

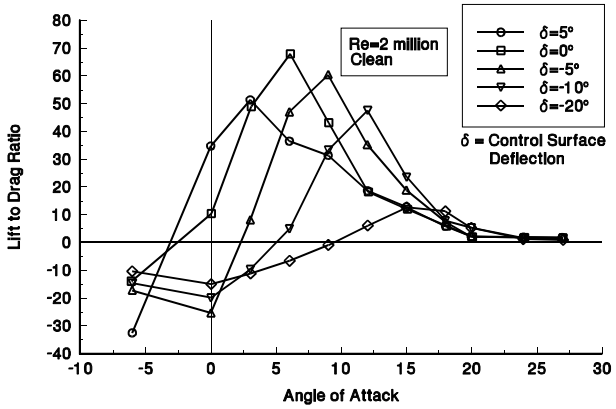

Figure 41. Unvented aileron, clean, Re=2x10^6, L/D vs α.

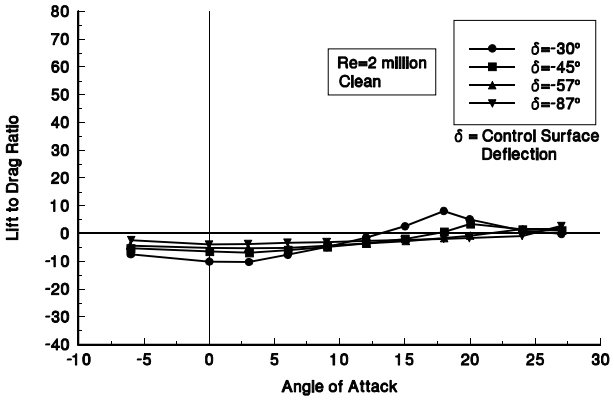

Figure 42. Unvented aileron, clean, Re=2x10^6, L/D vs α.

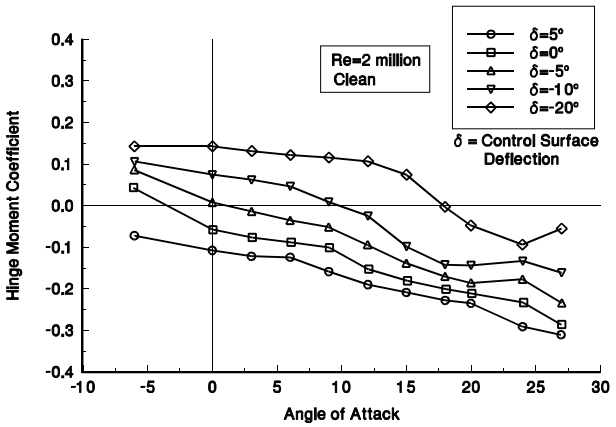

Figure 43. Unvented aileron, clean, Re=2x10^6, C_h vs α.

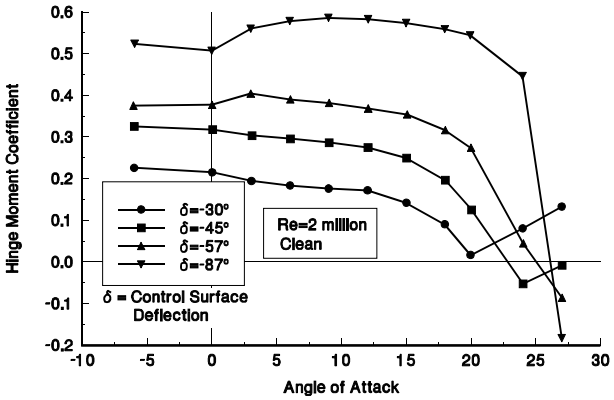

Figure 44. Unvented aileron, clean, Re= 2x10^6, C_h vs α.

The lift-to-drag ratios for the 2 million Reynolds number case are shown in figures 43 and 44. Much of the same trends appeared in this case as for the 1 million Reynolds number case. The maximum lift-to-drag ratio occurred at 0° control surface deflection and 6° angle of attack and had a value of 70.

Please note that all of the data previously discussed can be found in tabular form in Appendix B.

Vented Aileron

The vented aileron as shown in figure 3 was tested under the same conditions as the unvented aileron but at only 1 million Reynolds number.

Clean

The maximum lift coefficient occurred for the vented aileron at 5° control surface deflection and was 1.21. Generally, the maximum lift coefficient decreased with decreasing control surface deflection. This is shown in figures 47 and 48. Additionally, the slope of the lift coefficient curve decreased with decreasing control surface deflection. The -20° aileron deflection case showed an increase in lift coefficient near 15° angle of attack. The pressure distributions shown in figures 45 and 46 are for 12° and 15° angle of attack. The pressure coefficient became nearly -2 on the lower surface of the aileron device for the 12° case and was also apparent for angles of attack less than 12°. It appears from this figure that the flow through the gap from the upper surface could cause this type of pressure distribution. Beyond this angle of attack to 15°, it appears that this type of flow no longer occurs; probably because the main element then shields the aileron.

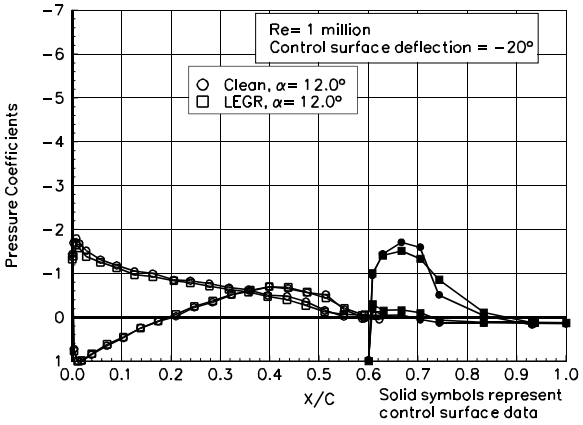

Figure 45. Vented aileron, pressure distribution, α=12°, δ=-20°.

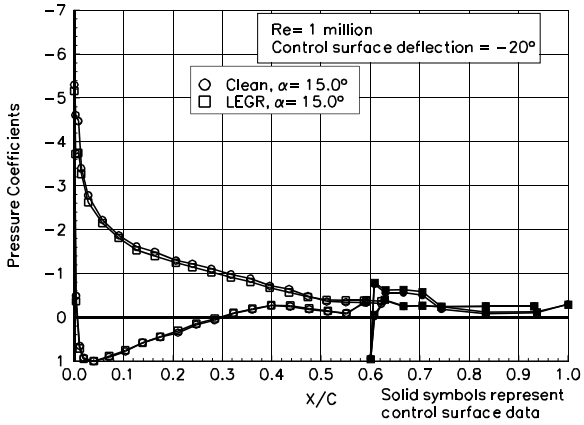

Figure 46. Vented aileron, pressure distribution, α=15°, δ=-20°.

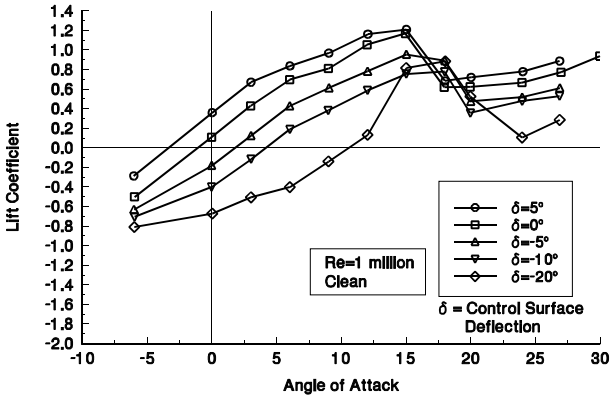

Figure 47. Vented aileron, Clean, C_l vs α.

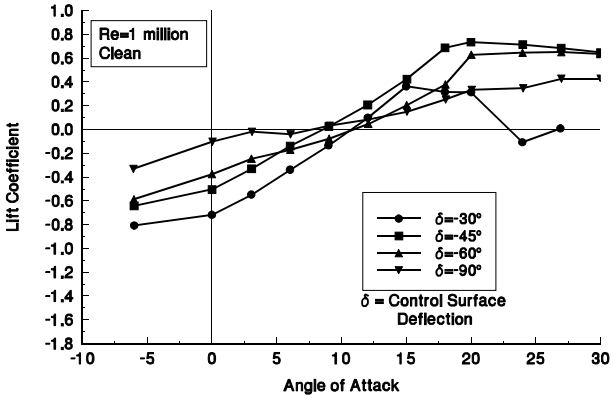

Figure 48. Vented aileron, Clean, C_l vs α.

The drag coefficient is shown in figures 49 and 50 for the vented aileron configuration. A minimum drag of 0.012 occurred for this case at a flap deflection and angle of attack of 0°. The drag levels increased for

each decrease in control device deflection angle. A maximum drag coefficient of approximately 0.5 occurred for a -90° control surface deflection at the range of angles of attack.

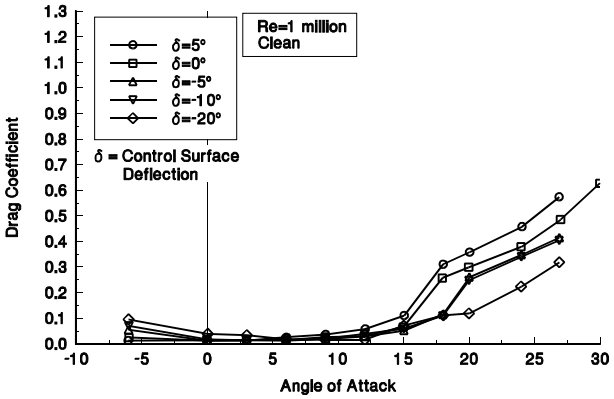

Figure 49. Vented aileron, Clean, C_d vs α.

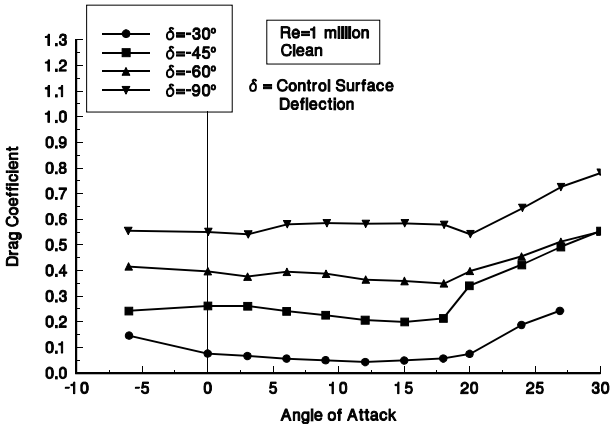

Figure 50. Vented aileron, Clean, C_d vs α.

Figure 51 shows that the suction coefficient had substantial region of positive value for control surface deflection of less than -10°. For a control device deflection of -20°, there was a region of negative values up to nearly 12° angle of attack. When the aileron deflection was -30°, the suction coefficient was more negative and it became positive between 12° and 20° angle of attack, as shown in figure 52. For more and more negative deflection, the suction coefficient grew to a fairly substantially negative value; between -0.39 and -0.58 for angles of attack up to 30° and for -90° aileron deflection.

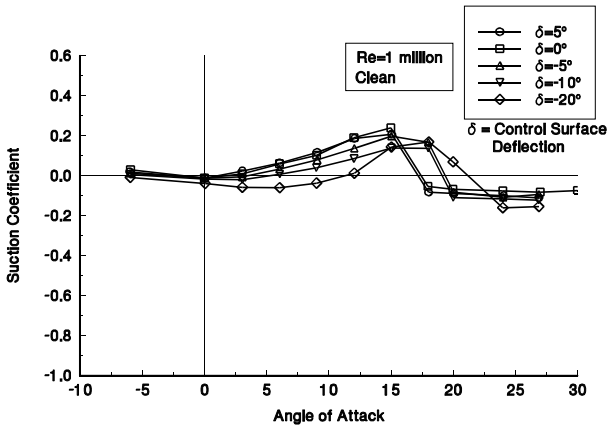

Figure 51. Vented aileron, Clean, C_s vs α.

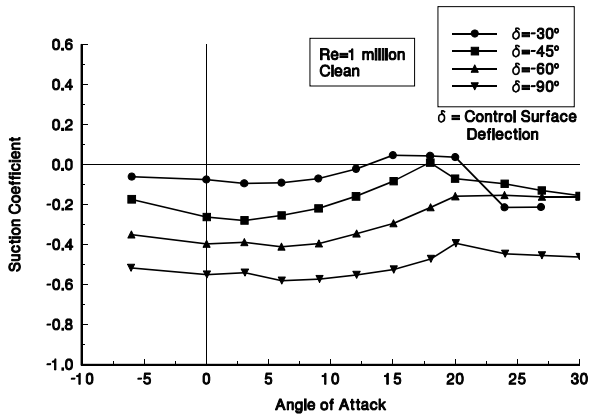

Figure 52. Vented aileron, Clean, C_s vs α.

An indication of the forces required to deflect the aileron is given by the hinge moment values. The slope of the curve also indicates the direction in which the control device would want to rotate if allowed to do so freely. At low angles of attack and control surface deflection angles of greater than -10°, the hinge moment coefficient was between -0.07 and 0.07. The slope tended to be positive on these curves in figure 53, which indicates that the device would want to rotate in the negative direction; the trailing edge toward the upper surface. For higher control surface deflections, shown in figure 54, the hinge moments are more negative for angles of attack up to 30° and the slopes of the curves are both negative and positive depending on the angle of attack range. Through this angle of attack range, only a control surface deflection of -90° shows negative slope through the entire angle of attack range.

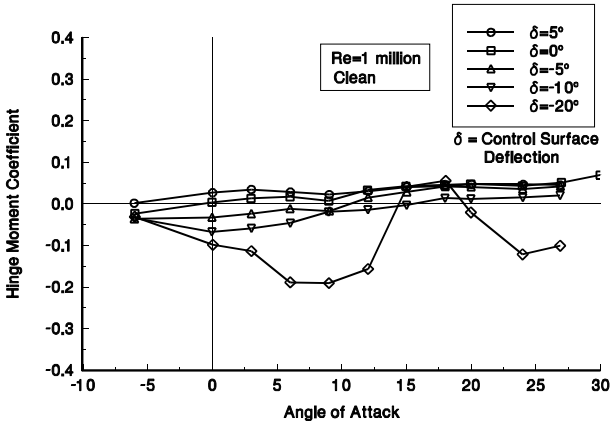

Figure 53. Vented aileron, Clean, C_h vs α.

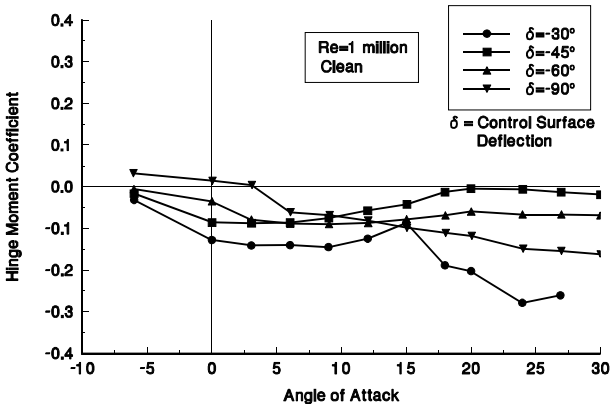

Figure 54. Vented aileron, Clean, C_h vs α.

The lift-to-drag ratio data are shown in figures 55 and 56. The maximum lift-to-drag ratio for this case was 53 and occurred for an aileron deflection of 5° and an angle of attack of 3°. The maximum value of lift-to drag-ratio decreased with decreasing control surface deflection.

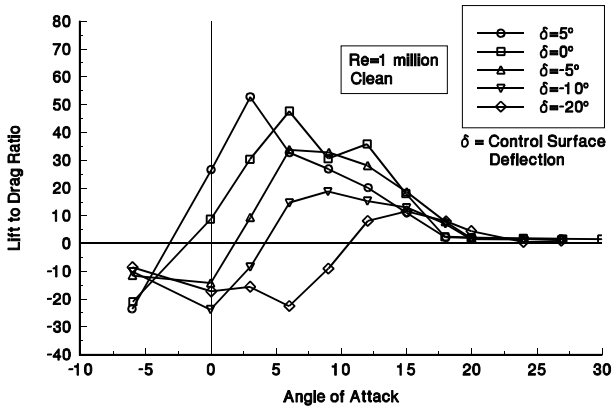

Figure 55. Vented aileron, Clean, L/D vs α.

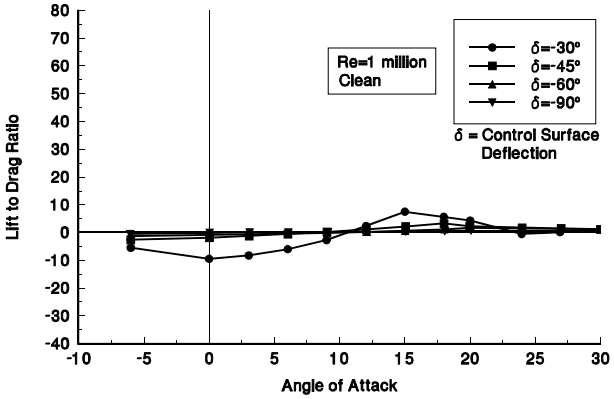

Figure 56. Vented aileron, Clean, L/D vs α.

LEGR

Application of LEGR generally caused a drop in the lift coefficient curves and a reduction of the maximum lift coefficient, especially at angles of attack less than 10° as shown in figures 57 and 58. When the control surface was at the higher deflections, as in figure 58, and the angle of attack was greater than 10°, the effect of LEGR was less apparent since the LEGR has less effect at higher angles of attack. The LEGR data showed less of a lift coefficient reduction beyond stall than did the clean cases at higher angles of attack. The LEGR maximum lift coefficient of 1.06 occurred for a control surface deflection of +5°. Therefore, if a wind turbine is designed such that normal operating conditions use 0° flap deflection, then the blades degradation in lift performance due to LEGR may be counteracted by using a positive flap deflection. This of course, would have to be balanced with other factors such as drag and moment.

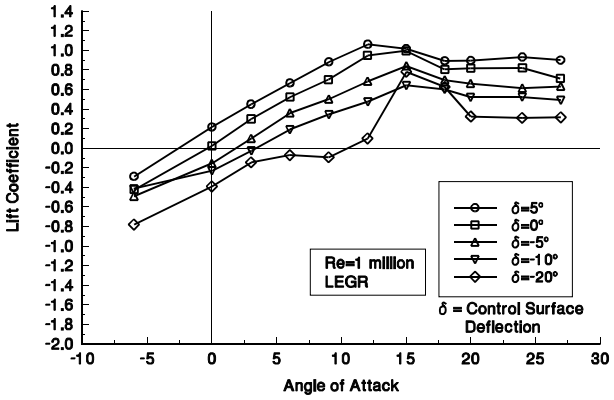

Figure 57. Vented aileron, LEGR, C_l vs α.

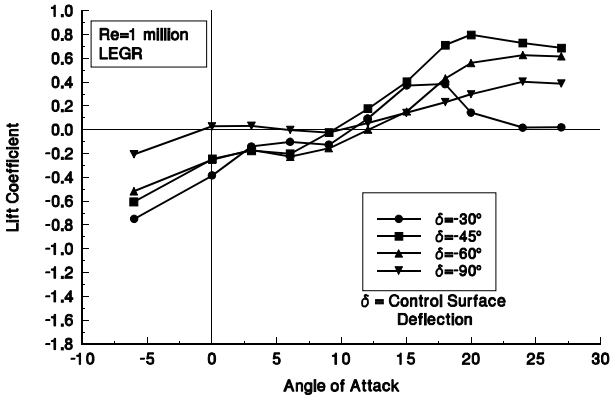

Figure 58. Vented aileron, LEGR, C_l vs α.

The drag coefficient presented in figure 59, was generally higher throughout the -6° to 24° angle of attack range for LEGR than for the clean data. But at control surface deflections greater than 20°, as in figure 60, the drag coefficient difference between the cases with LEGR applied and clean was nearly negligible. Consequently at high control surface deflections and high angles of attack the clean and LEGR applied drag coefficients are comparable.

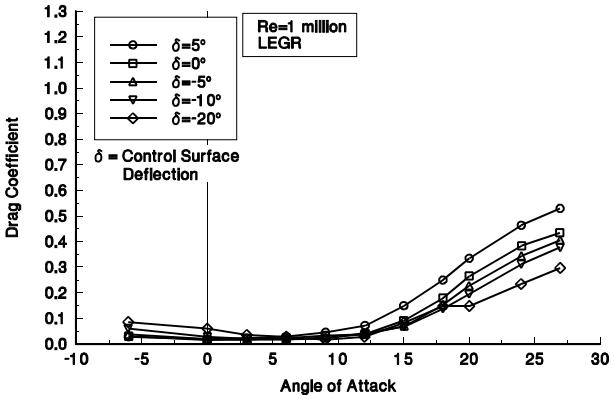

Figure 59. Vented aileron, LEGR, C_d vs α.

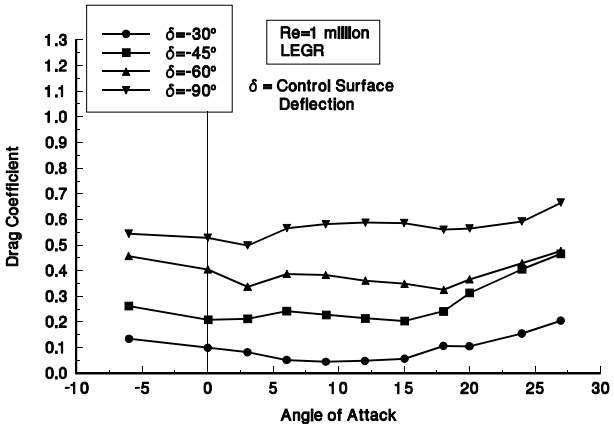

Figure 60. Vented aileron, LEGR, C_d vs α.

For the suction coefficient, the application of LEGR lowered the curves in the negative direction or had no effect on them as seen in figures 61 and 62. This trend would indicate that the application of LEGR to this aileron configuration would not affect its aerodynamic braking ability. It is useful to know that when a blade is contaminated, the braking ability is not effected. As in the clean case, the control surface deflection angles lower than -45° were those which created negative suction coefficient throughout the entire angle of attack range tested. An actual wind turbine design is required to determine if -45° control surface device deflection is enough to stop rotation or if -90° would be required.

The hinge moment coefficients for the vented aileron configuration are shown in figures 63 and 64. When LEGR was applied to the airfoil, the hinge moments for control surface deflection angles greater than -10°, were ranging between -0.05 and 0.06, which is closer to zero than the clean case. For high control surface deflections, the hinge moments became less negative for angle of attack less than 15° and stayed relatively the same as the clean data for angles of attack that were higher than 15°.

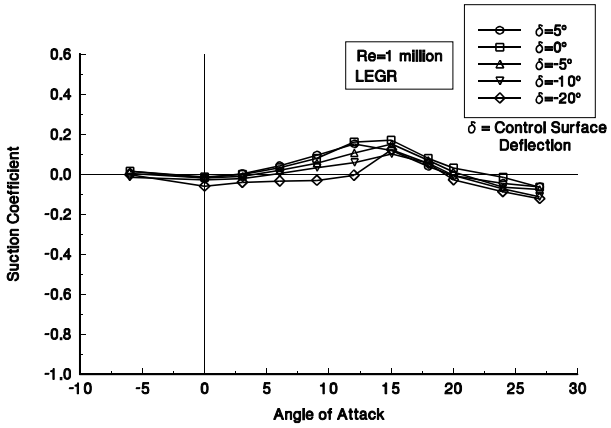

Figure 61. Vented aileron, LEGR, C_s vs α.

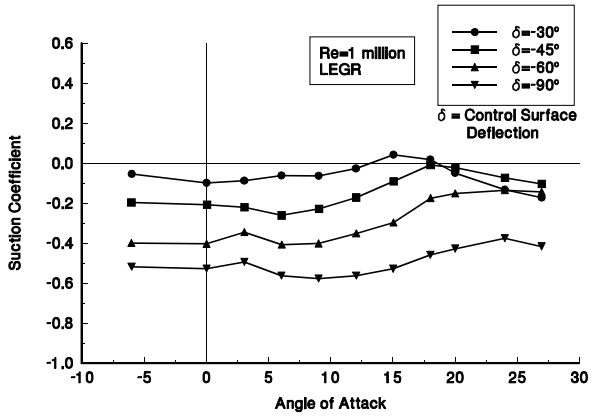

Figure 62. Vented aileron, LEGR, C_s vs α.

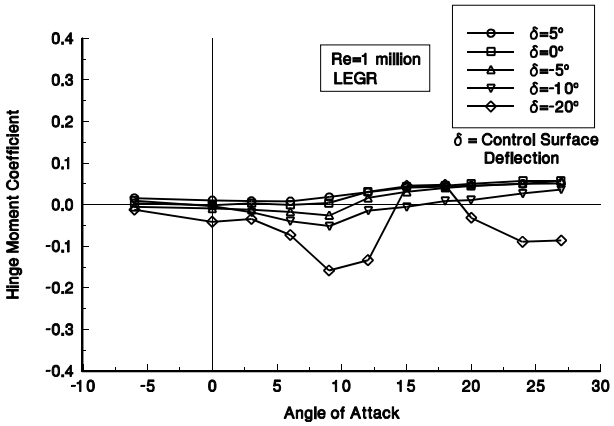

Figure 63. Vented aileron, LEGR, C_h vs α.

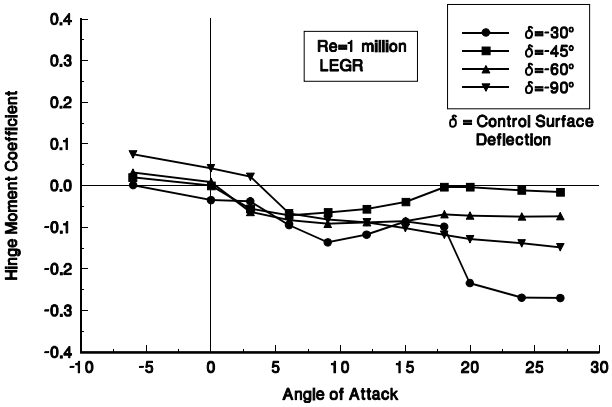

Figure 64. Vented aileron, LEGR, C_h vs α.

As would be expected from the previous discussion, i.e. lower lift and higher drag coefficients, the lift-to-drag ratio decreased markedly for control surface deflections of 5°, 0°, and -5° as presented in figure 65. For the deflection of -10° or less, the lift-to-drag ratio was not impacted as greatly. In fact, from figure 66, it can be seen that at the most negative control surface deflections, the lift-to-drag ratios were on the order of -1.

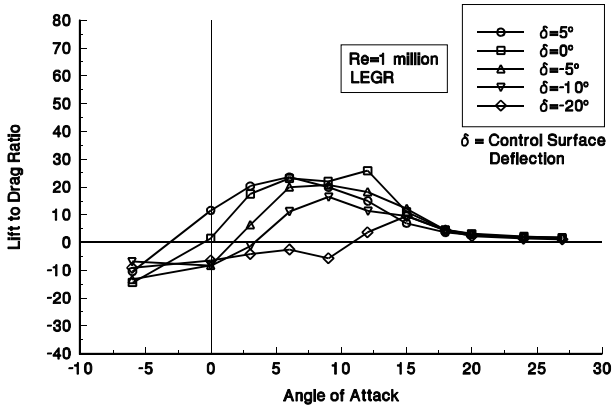

Figure 65. Vented aileron, LEGR, L/D vs α.

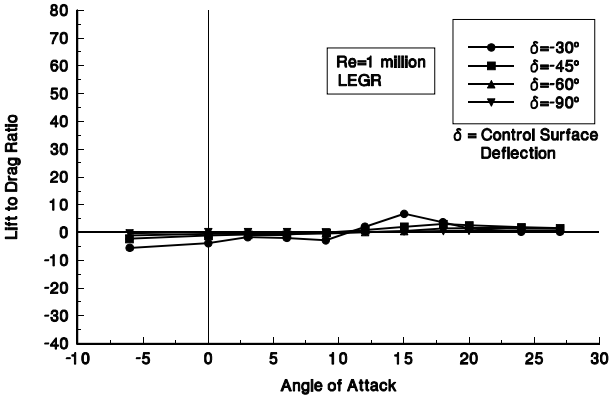

Figure 66. Vented aileron, LEGR, L/D vs α.

As was done for the unvented case, selected aileron deflection angles were tested at extreme angles of attack up to 270° and are shown in figures 67 - 70. The model was tested using a clean configuration and 1 million Reynolds number. At angles of attack between 25° and 150° and from 225° to 270°, the pressure drag values were very high. The 90° aileron case, however, showed the lowest drag for these ranges. This is shown in figure 68. Because the drag coefficient was so high through the mentioned range, the lift-to-drag ratio was very low; less than 5 for angles of attack greater than 25° for all the aileron deflections tested. As shown in figure 70, the vented aileron hinge moments were not as severe between -0.35 and 0.31 as the unvented which varied between -0.81 and 0.91. Extreme angle of attack loading conditions can be studied using the results of this test.

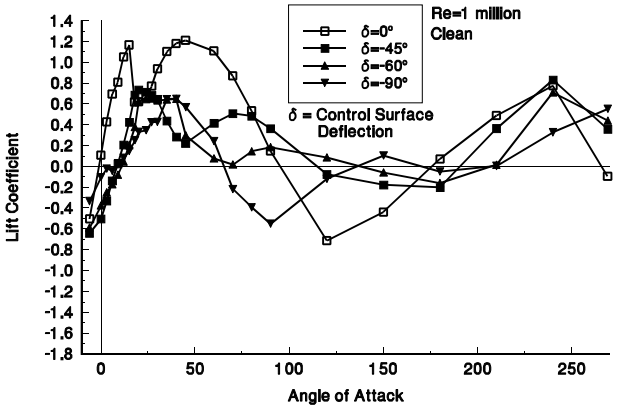

Figure 67. Vented aileron, full sweep, C_l vs α.

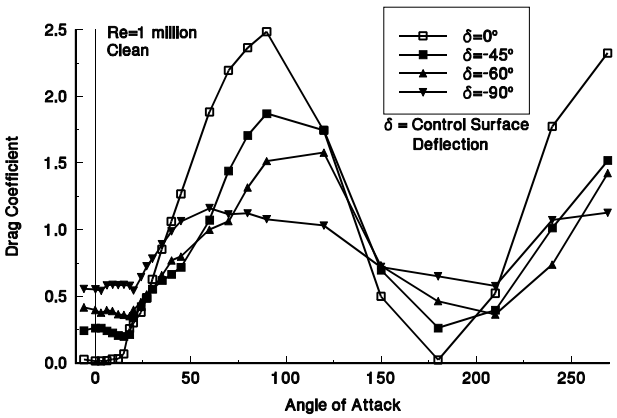

Figure 68. Vented aileron, full sweep, C_d vs α.

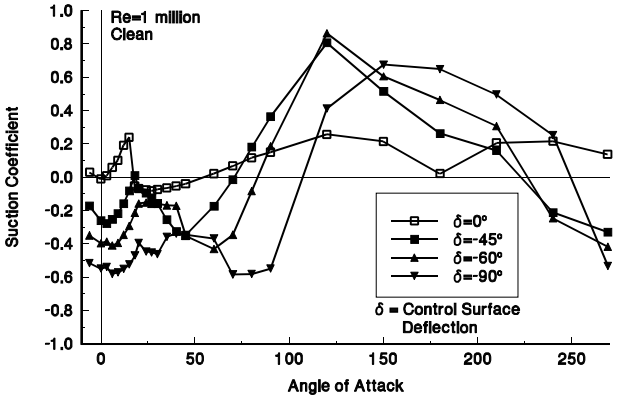

Figure 69. Vented aileron, full sweep, C_s vs α.

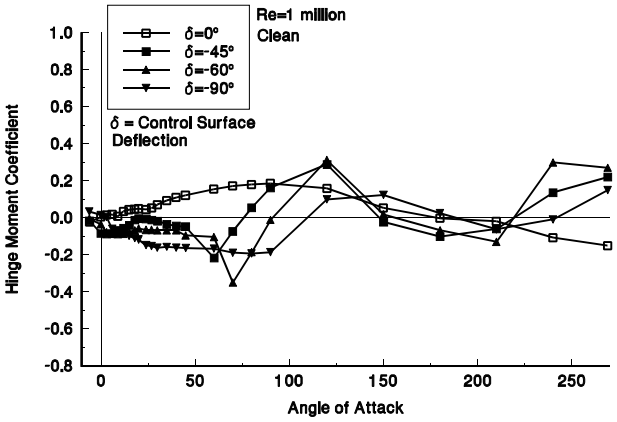

Figure 70. Vented aileron, full sweep, C_h vs α.

Spoiler Flap

The spoiler flap configuration was similar to the vented aileron in that the pivot point for both configurations are located in the same position, see figure 3. The spoiler flap, however, was deflected in the opposite direction, from -5° to 90°. This change caused the trends to be different for this case as compared to the previous cases.

Clean

Figures 71 and 72 show the lift coefficient versus angle of attack for the clean spoiler flap cases. The maximum lift coefficient occurred for a flap deflection of 10° and was 1.12. From figure 71 and 72, it can be seen that the maximum lift coefficients for control surface deflections of 0° to 45° were close to one another. In fact, the values only ranged from 1.039 to 1.123. At higher control surface deflections of 60° and 90°, the lift coefficient dropped substantially as compared to the positive deflection angles. The 90° case did not show a usual stall pattern except a small decrease beyond 20° angle of attack. At the lowest control surface deflection of -5°, the stall behavior seemed to be delayed until after 18° angle of attack.

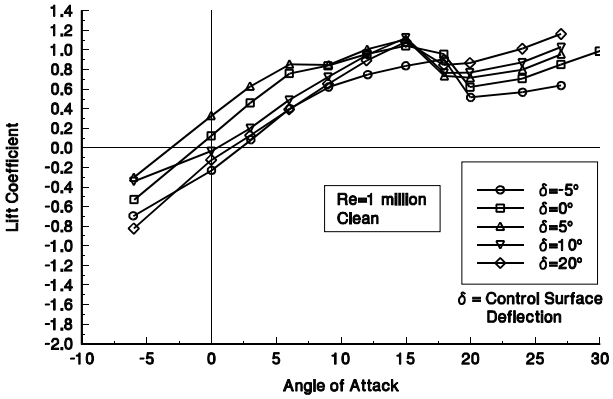

Figure 71. Spoiler flap, clean, C_l vs α.

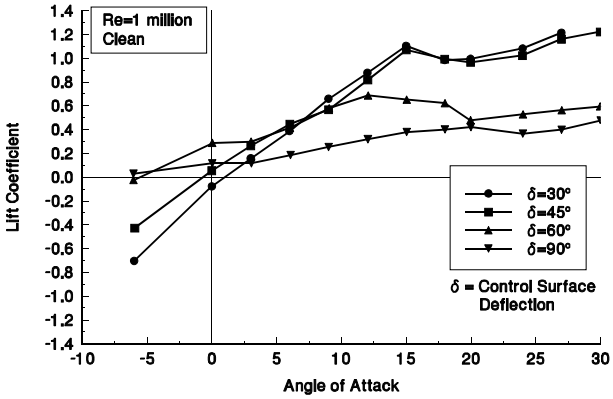

Figure 72. Spoiler flap, clean, C_l vs α.

A minimum spoiler flap drag coefficient of 0.010, was achieved at 0° flap deflection and 0° angle of attack as shown in figure 73. As the control surface deflection increased, the drag coefficient increased achieving a maximum at a flap deflection angle of 90°, as presented in figure 74. The pressure drag was near 0.65 for this flap deflection angle, at low angles of attack.

In examining the suction coefficient, the values did not become consistently negative until the flap deflection was higher than 30°, as seen in figures 75 and 76. For flap deflections of -5° to 10°, the curves were near each other and had similar trends. But for higher flap deflections the changes in suction coefficient became more apparent. The minimum overall suction coefficients occurred, as expected, at the 90° flap deflection with values around -0.6. These values persisted up to an angle of attack of 20°.

The hinge moments for the spoiler flap varied between -0.1 and 0.1 for all of the flap deflection angles. Only the -5° deflection angle in figure 77, showed a consistently negative hinge moment coefficient for the angle of attack range of -10° to 30°. For flap deflections up to 20°, the slope of the hinge moment was positive which indicates that the trailing edge would want to rotate toward the upper surface if allowed to rotate freely. For the higher flap deflections presented in figure 78, the 60° and 90° flap deflections exhibit a negative slope of the hinge moment curves.

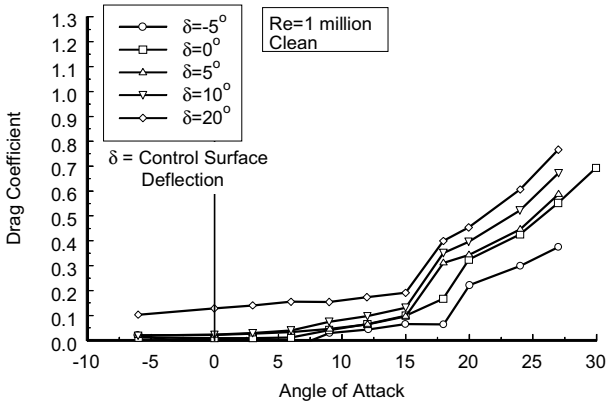

Figure 73. Spoiler flap, clean, C_d vs α.

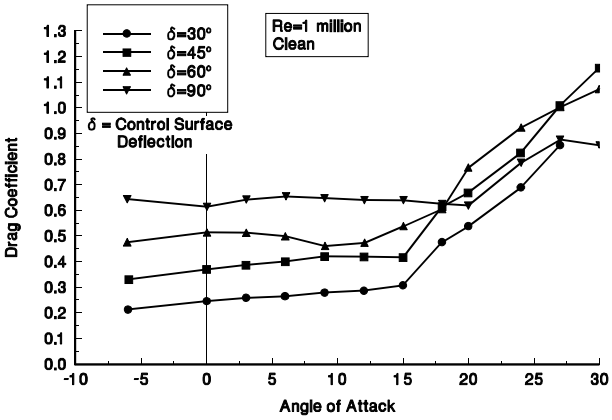

Figure 74. Spoiler flap, clean, C_d vs α.

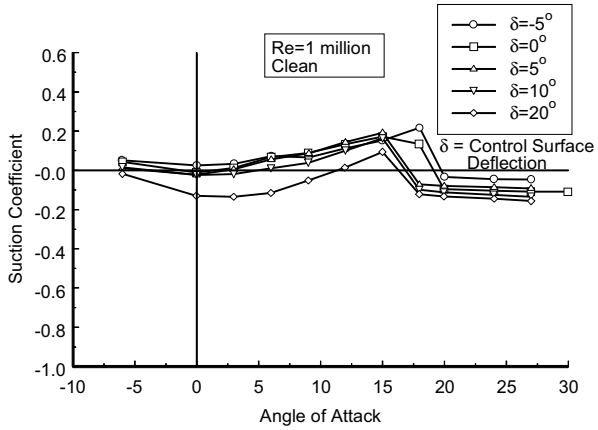

Figure 75. Spoiler flap, clean, C_s vs α.

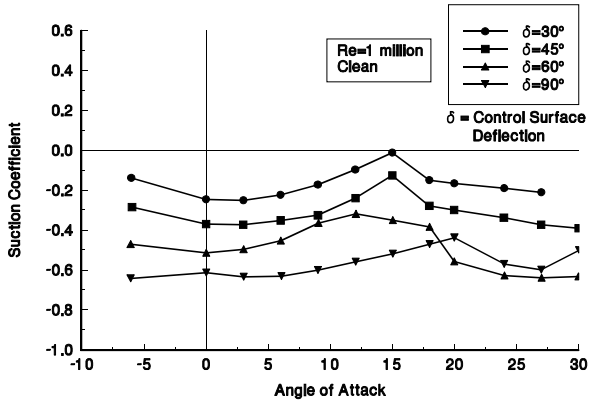

Figure 76. Spoiler flap, clean, C_s vs α.

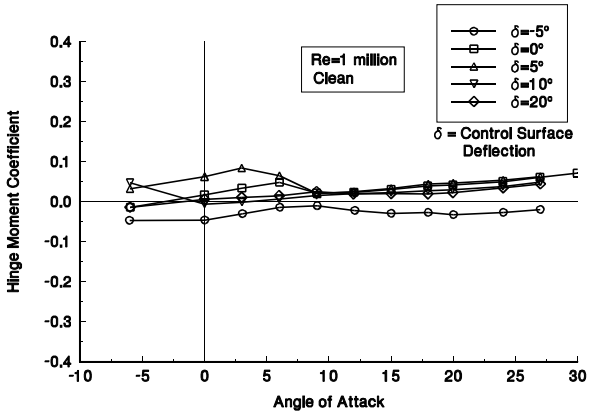

Figure 77. Spoiler flap, clean, C_h vs α.

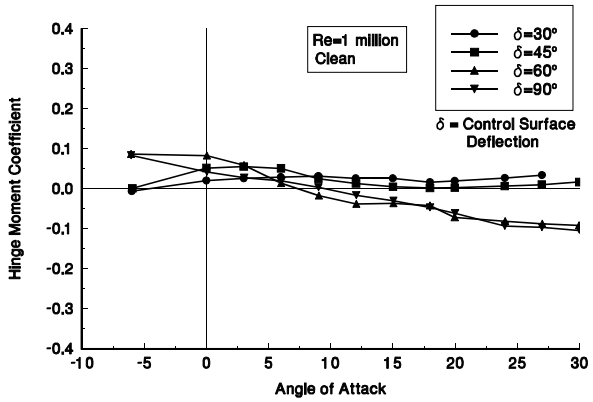

Figure 78. Spoiler flap, clean, C_h vs α.

The maximum lift-to-drag ratio occurred at 0° flap deflection and 6° angle of attack as seen in figure 79. The maximum was 68. At the highest deflections, beyond δ=30°, the lift-to-drag ratios become lower than 5 in magnitude, as shown in figure 80. A low lift-to-drag ratio is desired at the high flap deflection angles when the goal is to stop the rotation of a turbine.

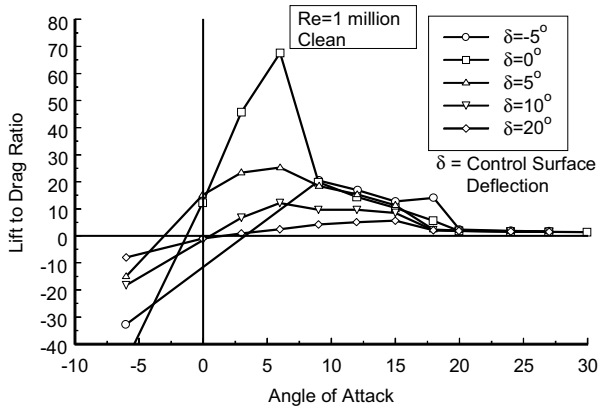

Figure 79. Spoiler flap, clean, L/D vs α.

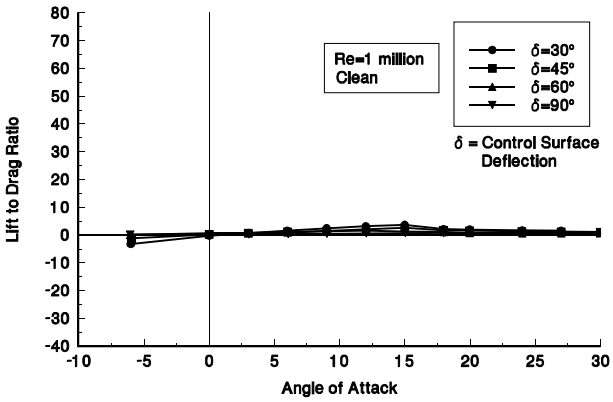

Figure 80. Spoiler flap, clean, L/D vs α.

LEGR

The effect of LEGR on the model was to shift the lift coefficient curves to lower values, as presented in figures 81 and 82. Additionally, the stall pattern was altered in that there is less of a drop in lift coefficient after the maximum lift coefficient was reached. The deflection angle of 30° produced the maximum lift of 1.07, which was a decrease from the clean case. The flap deflection angle that showed the most lift loss due to addition of LEGR was the -5° case where the reduction of the maximum lift coefficient was 22%. At the higher aileron deflections from 30° to 90°, the application of LEGR had only a minor effect on the lift curves through the angle of attack range, as shown in figure 82.

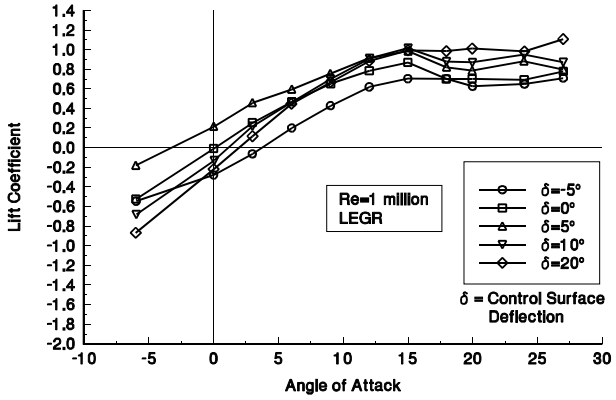

Figure 81. Spoiler flap, LEGR, C_l vs α.

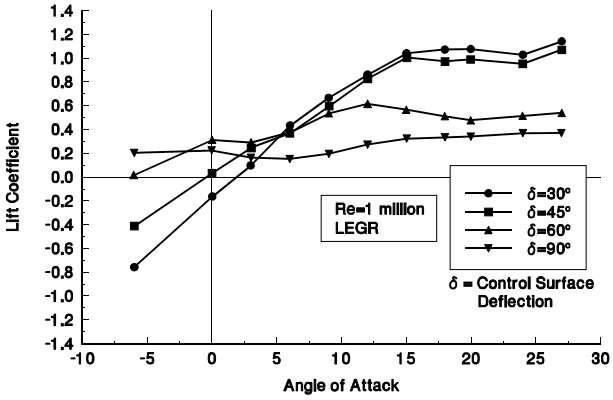

Figure 82. Spoiler flap, LEGR, C_l vs α.

In general, the application of LEGR caused the drag coefficient to increase for the airfoil, but over the -6° to 30° angle of attack range the drag coefficient did not always exceed the clean values. Through moderate angles of attack up to 20° and flap deflections below 20°, the LEGR case shown in figure 83 usually had higher drag coefficient values than the clean values. However, for the other cases beyond these values of angle of attack and flap deflection angle, the LEGR and the clean cases were quite similar, as seen in figure 84. The minimum drag for the LEGR cases on the spoiler flap was 0.015 and occurred when the flap deflection and angle of attack was 0°.

For flap deflection angles of 20° or less, figure 85, the effect of adding LEGR was to drive the suction coefficient to values closer to zero. And for all these cases, there was at least a portion of the curve that was greater than zero which is not acceptable for braking the rotation of a turbine. The deflection angles of 30° or greater, figure 86, showed that up to 30° angle of attack the suction coefficients were less than zero. Between -6° and 30°, the suction coefficient ranged from -0.03 to -0.24 for the 30° flap deflection and from -0.46 to -0.66 for the 90° flap deflection.

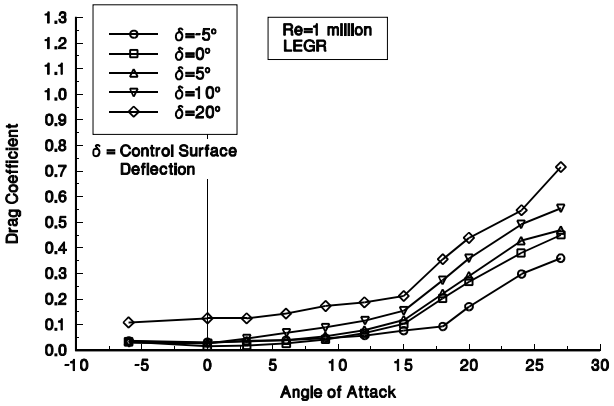

Figure 83. Spoiler flap, LEGR, C_d vs α.

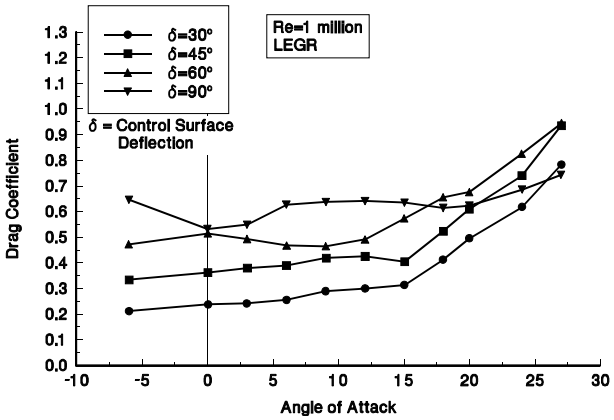

Figure 84. Spoiler flap, LEGR, C_d vs α.

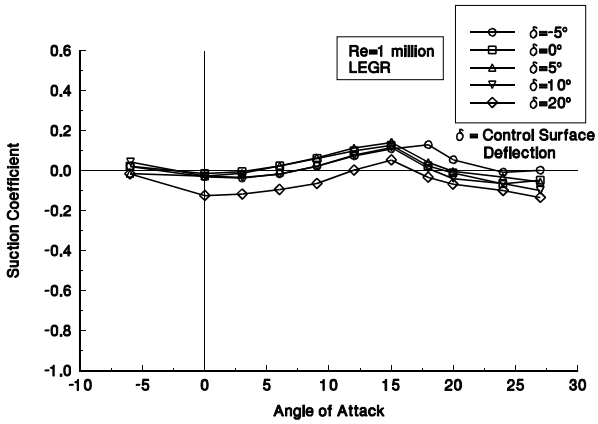

Figure 85. Spoiler flap, LEGR, C_s vs α.

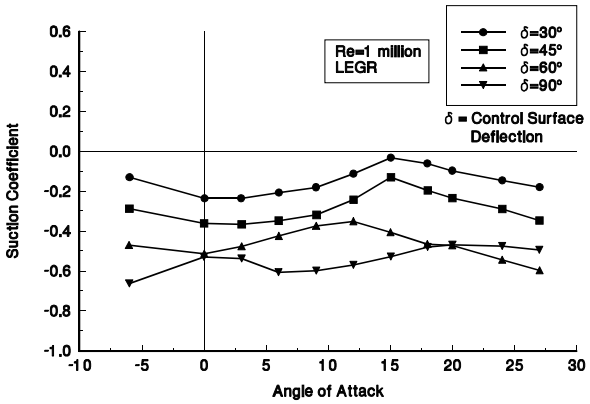

Figure 86. Spoiler flap, LEGR, C_s vs α.

Hinge moment coefficients on the spoiler flap configuration were also affected by the application of LEGR. Hinge moment coefficient curves, shown in figures 87 and 88, were shifted slightly in the negative direction except at only the highest flap deflection angles and angles of attack. The general nature of the curves has not changed; i.e. negative or positive slope occurred in the same regions for both the clean and LEGR cases.

With the application of LEGR, the lift-to-drag ratio curves dropped substantially for flap deflections less than 20°, as seen in figure 89. The maximum LEGR lift-to-drag ratio occurred at 0° flap deflection angle and 6° angle of attack. The maximum, however, was 18 for the LEGR much lower than the clean case value. The higher control surface deflections shown in figure 90 have a lift-to-drag ratio close to that of the clean data.

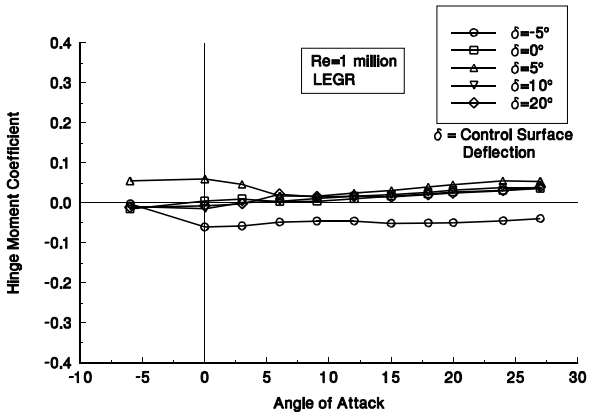

Figure 87. Spoiler flap, LEGR, C_h vs α.

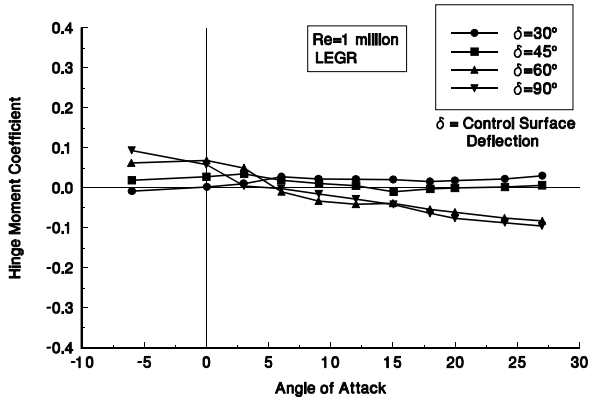

Figure 88. Spoiler flap, LEGR, C_h vs α.

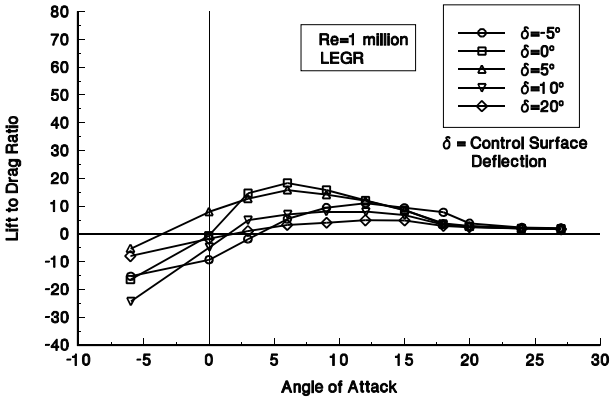

Figure 89. Spoiler flap, LEGR, L/D vs α.

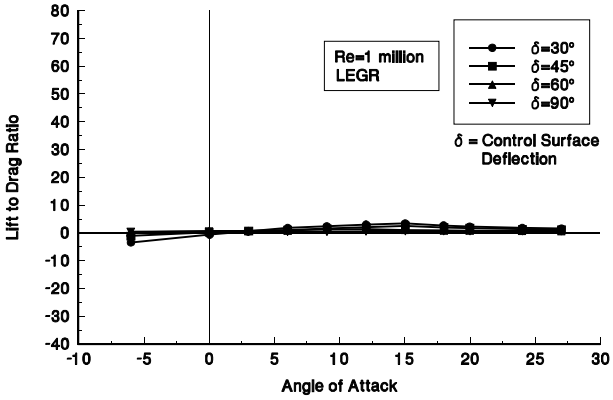

Figure 90. Spoiler flap, LEGR, L/D vs α.

The spoiler flap configuration was tested for angles of attack up to 270° at 1 million Reynolds number and aileron deflection angles of 0°, 45°, 60°, and 90°. Figures 91 through 94 show the lift, drag, suction, and hinge moment coefficients versus angle of attack. For all deflection angles shown in figure 91, there was a secondary peak in lift coefficient beyond the normal stall region around 45°; coinciding with this was increased drag coefficient as seen in figure 92. An interesting feature of this spoiler flap case was that the

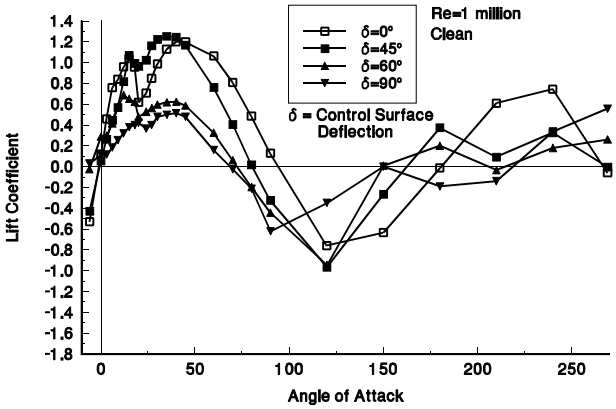

Figure 91. Spoiler flap, full sweep, C_l vs α.

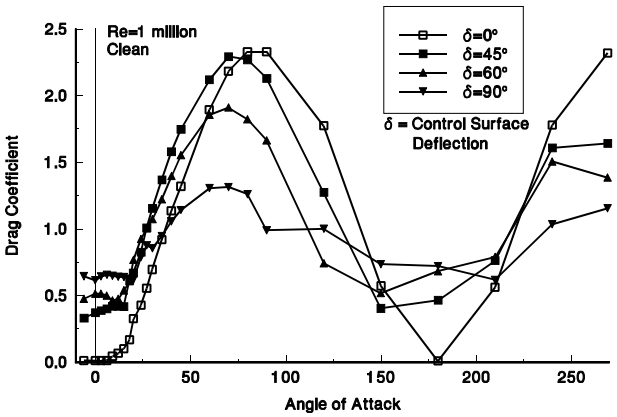

Figure 92. Spoiler flap, full sweep, C_d vs α.

suction coefficient stayed negative until 110° for the 45°, 60°, and 90° aileron deflections. This is a higher angle of attack than for the other two aileron configurations. The hinge moment coefficient for this case ranged from -0.16 to 0.15 and was the closest to zero of all of the test configurations. The values shown in these figures can indicate the loading that would occur on a wind turbine blade at extreme angles of attack.

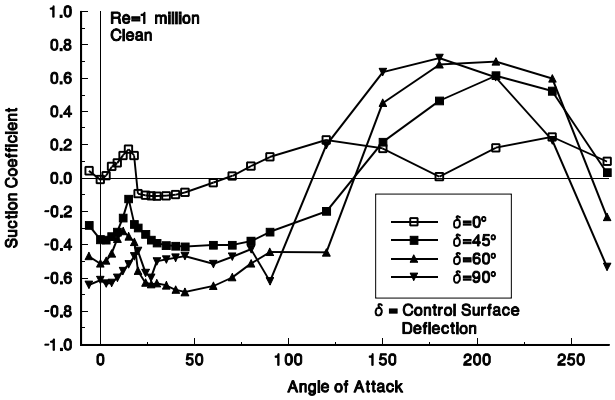

Figure 93. Spoiler flap, full sweep, C_s vs α.

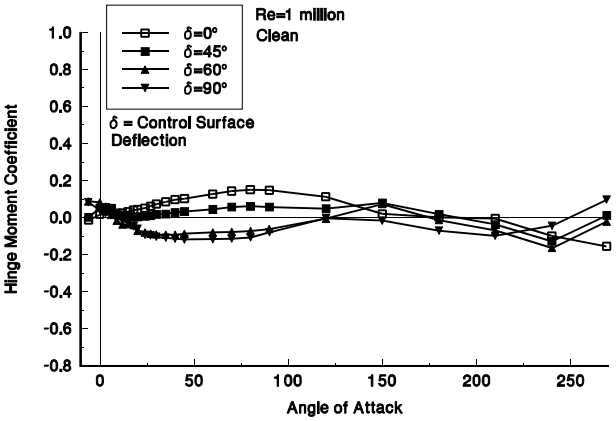

Figure 94. Spoiler flap, full sweep, C_h vs α.

Summary

Three aileron configurations were tested on an NREL S809 airfoil model to help determine the advantages and disadvantages of using them on horizontal axis wind turbines. The three configurations the unvented aileron, vented aileron, and spoiler flap were tested clean and with LEGR applied. Some general remarks can be made from the results of these tests.

The baseline S809 model was tested and it was found that the maximum lift coefficient was 1.04. Each of the three aileron configurations was able to produce a higher maximum lift coefficient with the control surface deflected slightly in the positive direction and under clean conditions. For 1 million Reynolds number, the maximum lift coefficients were 1.12, 1.21 and 1.12 for the unvented aileron, the vented aileron and the spoiler flap configurations, respectively. When LEGR was applied, the maximum lift coefficients were reduced. The LEGR lift coefficient maximums were only slightly different than the baseline S809 airfoil configuration. The lowest maximum LEGR lift coefficient was 1.00 for the unvented aileron configuration at 1 million Reynolds number. Therefore, even with this type of LEGR the clean maximum lift coefficient can be reached with a slight deflection of the aileron. This is an important point when considering using a control surface for power modulation.

It should be noted, though, that with an increase in maximum lift coefficient there is a drag penalty. For all cases, the LEGR increased the drag through the angle of attack region where the maximum lift coefficient occurred. This translated to a lower lift-to-drag ratio. In these tests it was found that the drag coefficient increased to values as high as 0.5 or 0.6 at the highest deflection angle of ±90°. This increase in drag was expected and desired because it is necessary to give a higher negative suction coefficient.

Suction coefficient values became more negative with the larger control surface deflection angles through an angle of attack range up to 30°. The unvented aileron showed an area between 20° and 30° angle of attack where the suction coefficient curves, for the highest deflection angles, had a very high positive slope. The suction coefficient became positive or nearly so for many of the high aileron deflections around this angle of attack range for the unvented aileron. The vented aileron configuration showed consistently negative values of suction coefficient for the -60° and -90° control surface deflection angles. The spoiler flap configuration consistently produced negative values of suction coefficient for the 45°, 60°, and 90° control surface deflections through 30° angle of attack. Additionally, for all aileron configurations, it was observed that for large control surface deflection angles there was little change in the suction coefficient between the clean and LEGR cases. This is desirable because it appears from this study that the effectiveness of aerodynamic brakes will not be compromised by LEGR.

Hinge moment was the most diverse of all the measurements acquired for the three aileron configurations. The hinge moments for the unvented aileron case were much higher in magnitude than the ones for the other two configurations. This can be attributed to the different location of the hinge point on the unvented aileron configuration. Over the 270° angle of attack range, the hinge moment coefficients for the unvented aileron ranged from -0.81 to 0.91. The vented aileron had hinge moment coefficients that varied from -0.35 to 0.31 over the same range. The configuration that had the least hinge moment coefficient range was the spoiler flap having values that varied from -0.16 to 0.15.

This study covered a comprehensive range of angle of attacks and control surface deflection angles for three different aileron configurations. All of the data are listed in tabular form in Appendix B. Additionally, the

pressure coefficient plots are included in Appendix C for a more detailed investigation of all of the cases studied.

References

Schlichting, H. (1979). *Boundary Layer Theory*. New York, NY: McGraw-Hill Inc.

Appendix A. Tap Locations

List of Tables Page

Table A1. S809 aileron tap locations for the first 50% chord	
X	Y
8.563	-1.780
7.871	-1.892
7.184	-1.949
6.494	-1.960
5.805	-1.924
5.119	-1.849
4.450	-1.735
3.784	-1.559
3.134	-1.431
2.491	-1.240
1.867	-1.028
1.271	-0.796
0.715	-0.545
0.344	-0.347
0.202	-0.256
0.067	-0.151
0.000	0.000
0.047	0.140
0.146	0.254
0.256	0.355
0.509	0.529
1.028	0.790
1.620	1.015
2.270	1.208
2.939	1.370
3.701	1.505
4.307	1.613
5.000	1.699
5.710	1.762

Table A1. S809 aileron tap locations for the first 50% chord		
X		Y
6.419		1.804
7.128		1.822
7.828		1.813
8.516		1.769
End of Table A1		

Table A2. S809 Unvented Aileron Cove region tap locations		
X		Y
9.246		-1.633
10.249		-1.375
11.296		-1.096
11.115		-0.830
10.513		-0.439
10.395		0.315
10.398		0.839
11.293		1.291
10.249		1.498
9.201		1.636
End of Table A2		

Table A3. S809 Unvented Aileron Flap tap locations	
X	Y
18.000	0.023
16.760	-0.022
14.999	-0.252
13.372	-0.578
12.683	-0.740
12.001	-0.878
11.383	-0.817
10.800	-0.544
10.744	-0.004
11.740	0.250
11.992	1.154
12.688	1.021
13.385	0.887
14.999	0.590
16.857	0.250
End of Table A3	

Table A4. S809 Vented Aileron Cove region tap locations	
X	Y
9.202	1.687
9.902	1.564
10.568	1.427
11.196	1.190
10.651	0.382
10.651	-0.428
10.651	-1.237
9.925	-1.462
9.247	-1.633
End of Table A4	

Table A5. S809 Vented Aileron Flap tap locations	
X	Y
18.000	0.023
16.760	-0.022
14.999	-0.252
13.372	-0.578
12.683	-0.742
12.001	-0.736
11.313	-0.551
10.937	-0.342
10.800	0.000
10.949	0.356
11.344	0.679
12.001	0.981
12.688	1.021
13.385	0.887
14.999	0.590
16.857	0.250
End of Table A5	

Table A6. S809 Spoiler Flap Cove region tap locations	
X	Y
9.198	1.686
9.900	1.564
10.600	1.428
10.276	0.560
10.629	-0.300
10.949	-1.160
10.100	-1.415
9.247	-1.632
End of Table A6	

Table A7. S809 Spoiler Flap tap locations		
X		Y
18.000		0.023
16.760		-0.022
14.999		-0.252
13.372		-0.578
12.681		-0.741
11.804		-0.954
11.101		-1.149
10.942		-0.314
10.924		0.520
10.816		1.354
11.293		1.291
11.992		1.154
12.688		1.020
13.385		0.887
14.999		0.590
16.857		0.250
End of Table A7		

Appendix B. Steady State Coefficient Data

List of Tables Page

Baseline S809 aileron

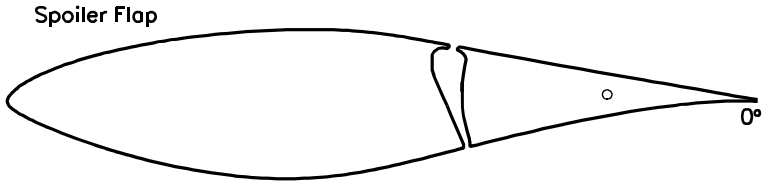

Table 1. Baseline S809 aileron data, Re=1x10^6.						
Rex10^{-6}	AOA	C_l	C_m	C_{dp}	C_{dw}	C_s
0.999	-5.99	-0.6040	0.0030	0.0161	--	0.0470
1.004	-0.01	0.0280	-0.0280	0.0049	0.0088	-0.0088
1.003	3.01	0.3820	-0.0370	0.0065	0.0092	0.0109
1.004	6.02	0.7210	-0.0430	0.0100	0.0089	0.0668
0.999	9.03	0.9250	-0.0360	0.0222	0.0166	0.1288
1.000	12.01	0.9830	-0.0380	0.0519	--	0.1538
0.997	15.00	1.0430	-0.0380	0.0826	--	0.1902
0.991	17.97	0.9520	-0.0570	0.1452	--	0.1556
0.995	19.98	0.6090	-0.1010	0.2944	--	-0.0686
1.002	24.00	0.6710	-0.1170	0.3805	--	-0.0747
0.992	27.01	0.8030	-0.1500	0.4939	--	-0.0753
0.964	30.01	0.9720	-0.1930	0.6439	--	-0.0714
0.999	34.98	1.1110	-0.2470	0.8596	--	-0.0674
0.997	39.97	1.2100	-0.3000	1.0878	--	-0.0564
1.006	45.01	1.2310	-0.3420	1.2915	--	-0.0425
0.999	60.08	1.0980	-0.4640	1.8717	--	0.0181
0.999	70.10	0.8490	-0.5240	2.1500	--	0.0665
0.990	80.07	0.5240	-0.5980	2.3761	--	0.1064
0.995	90.02	0.1490	-0.6280	2.3912	--	0.1498
0.979	120.09	-0.7730	-0.6260	1.7933	--	0.2303
1.004	150.09	-0.6010	-0.3770	0.5276	--	0.1576
1.003	180.16	-0.0740	-0.0370	0.0169	--	0.0171
0.999	210.12	0.6340	0.3860	0.5425	--	0.1511
0.946	240.06	0.8110	0.6260	1.7516	--	0.1714
0.977	269.11	-0.0720	0.6120	2.3070	--	0.1078
End of Table 1						

Unvented Aileron, Re=1x10^6

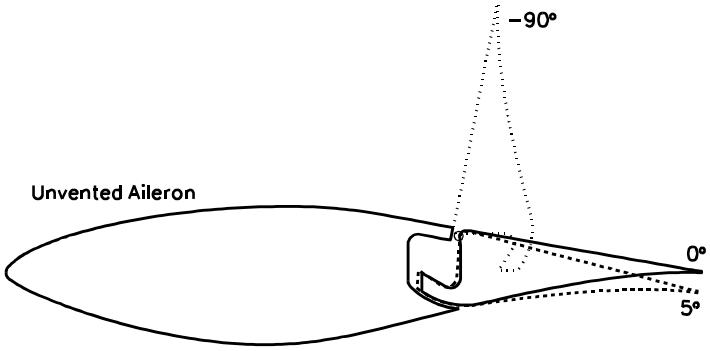

Table 2. Unvented Aileron, Clean, δ=5°, Re=1x10^6							
Rex10^{-6}	AOA	C_l	C_m	C_{dp}	C_{dw}	C_s	C_h
1.011	-6.01	-0.263	-0.066	0.0053	0.0110	0.0166	-0.0707
1.012	0.00	0.410	-0.079	0.0033	0.0117	-0.0117	-0.1063
1.006	3.03	0.738	-0.082	0.0008	0.0117	0.0273	-0.1223
1.007	6.03	0.937	-0.073	0.0117	0.0241	0.0745	-0.1222
1.005	9.02	1.049	-0.065	0.0366	--	0.1283	-0.1537
1.000	12.05	1.110	-0.060	0.0646	--	0.1686	-0.1846
0.997	15.01	1.117	-0.062	0.0993	--	0.1934	-0.2074
0.999	18.02	0.668	-0.117	0.2856	--	-0.0649	-0.2222
1.008	20.01	0.713	-0.130	0.3366	--	-0.0723	-0.2374
1.006	23.98	0.836	-0.159	0.4562	--	-0.0771	-0.2725
0.987	26.95	1.009	-0.204	0.6018	--	-0.0791	-0.3252
End of Table 2							

Table 3. Unvented Aileron, Clean, δ=0°, Re=1x10^6							
Rex10^{-6}	AOA	C_l	C_m	C_{dp}	C_{dw}	C_s	C_h
1.000	-6.04	-0.569	-0.017	0.0119	0.0175	0.0425	-0.0086
1.005	0.05	0.077	-0.031	0.0105	0.0089	-0.0088	-0.0583
1.005	3.08	0.413	-0.039	0.0074	0.0095	0.0127	-0.0773
1.008	6.08	0.744	-0.049	0.0097	0.0086	0.0702	-0.0934
1.004	9.05	0.851	-0.037	0.0261	0.0137	0.1203	-0.1259
0.997	12.06	0.942	-0.033	0.0493	--	0.1486	-0.1478
0.992	15.02	1.025	-0.041	0.0852	--	0.1833	-0.1693
0.982	18.02	0.922	-0.063	0.1543	--	0.1385	-0.1941
0.991	20.01	0.609	-0.106	0.3078	--	-0.0808	-0.1971
1.011	24.01	0.708	-0.128	0.4079	--	-0.0845	-0.2201
0.998	26.97	0.849	-0.161	0.5319	--	-0.0890	-0.2604
0.987	30.02	0.960	-0.192	0.6571	--	-0.0887	-0.3007
0.986	35.01	1.092	-0.243	0.8727	--	-0.0883	-0.3574
0.971	39.98	1.165	-0.288	1.0844	--	-0.0824	-0.4078
0.978	45.03	1.199	-0.332	1.3055	--	-0.0744	-0.4537
1.003	60.05	1.030	-0.437	1.8227	--	-0.0175	-0.5902
0.995	70.04	0.795	-0.510	2.1295	--	0.0203	-0.6794
0.990	80.04	0.455	-0.542	2.2205	--	0.0641	-0.7144
1.011	90.05	0.103	-0.579	2.2338	--	0.1049	-0.7710
1.051	120.04	-0.749	-0.584	1.6411	--	0.1732	-0.8140
1.004	150.07	-0.563	-0.351	0.4789	--	0.1341	-0.5661
1.039	180.08	-0.048	-0.026	0.0185	--	0.0186	-0.0580
1.007	210.06	0.525	0.364	0.5190	--	0.1862	0.5667
0.905	240.03	0.721	0.588	1.6999	--	0.2246	0.8135
0.947	269.09	-0.125	0.576	2.2100	--	0.1601	0.7425
End of Table 3							

Table 4. Unvented Aileron, Clean, δ=-5°, Re=1x10^6							
Rex10^{-6}	AOA	C_l	C_m	C_{dp}	C_{dw}	C_s	C_h
1.002	-6.00	-0.699	0.035	0.0398	0.0517	0.0216	0.0747
1.004	0.02	-0.271	0.027	0.0104	0.0115	-0.0116	0.0010
1.009	3.03	0.067	0.019	0.0033	0.0100	-0.0064	-0.0192
1.011	6.02	0.421	0.007	0.0027	0.0089	0.0353	-0.0396
1.004	9.01	0.693	0.007	0.0099	0.0121	0.0966	-0.0532
1.005	12.03	0.887	-0.007	0.0307	0.0236	0.1618	-0.0996
1.003	15.00	0.946	-0.018	0.0630	--	0.1840	-0.1435
1.003	17.99	0.866	-0.038	0.1204	--	0.1530	-0.1713
0.999	19.98	0.512	-0.072	0.2572	--	-0.0668	-0.1641
1.007	23.97	0.616	-0.095	0.3477	--	-0.0675	-0.1854
1.008	27.01	0.734	-0.122	0.4460	--	-0.0640	-0.2166
End of Table 4							

Table 5. Unvented Aileron, Clean, δ=-10°, Re=1x10^6							
Rex10^{-6}	AOA	C_l	C_m	C_{dp}	C_{dw}	C_s	C_h
1.005	-6.00	-0.799	0.053	0.0554	--	0.0284	0.1014
1.001	0.01	-0.528	0.072	0.0249	0.0239	-0.0240	0.0681
1.005	3.04	-0.237	0.071	0.0174	0.0195	-0.0320	0.0491
1.005	6.02	0.083	0.061	0.0130	0.0135	-0.0047	0.0235
1.008	8.97	0.385	0.057	0.0134	0.0111	0.0491	0.0003
1.009	12.01	0.686	0.043	0.0169	0.0156	0.1275	-0.0301
1.007	15.00	0.851	0.013	0.0455	--	0.1763	-0.1029
1.002	17.98	0.804	-0.013	0.1016	--	0.1515	-0.1505
0.997	19.99	0.382	-0.030	0.2212	--	-0.0773	-0.1253
1.003	23.98	0.460	-0.047	0.2933	--	-0.0810	-0.1388
1.008	27.01	0.583	-0.075	0.3824	--	-0.0759	-0.1658
End of Table 5							

Table 6. Unvented Aileron, Clean, δ=-20°, Re=1x10^6							
Rex10^{-6}	AOA	C_l	C_m	C_{dp}	C_{dw}	C_s	C_h
1.001	-5.99	-1.037	0.098	0.1001	--	0.0087	0.1629
1.003	0.02	-0.866	0.123	0.0569	--	-0.0572	0.1374
1.006	3.04	-0.594	0.125	0.0523	--	-0.0837	0.1270
1.007	6.05	-0.317	0.125	0.0484	--	-0.0815	0.1191
1.006	9.02	-0.049	0.127	0.0435	--	-0.0506	0.1105
1.005	12.02	0.181	0.132	0.0380	--	0.0005	0.1061
1.007	15.00	0.453	0.082	0.0207	--	0.0973	0.0098
1.005	18.00	0.562	0.085	0.0568	--	0.1196	-0.0076
0.997	19.98	0.541	0.059	0.0943	--	0.0962	-0.0530
1.007	23.97	0.149	0.038	0.2205	--	-0.1409	-0.0440
0.999	26.99	0.232	0.022	0.2738	--	-0.1387	-0.0601
End of Table 6							

Table 7. Unvented Aileron, Clean, δ=-30°, Re=1x10^6							
Rex10^{-6}	AOA	C_l	C_m	C_{dp}	C_{dw}	C_s	C_h
1.002	-6.01	-1.228	0.138	0.1613	--	-0.0318	0.2248
1.005	0.02	-1.170	0.171	0.1032	--	-0.1036	0.2136
1.011	3.06	-0.907	0.169	0.0892	--	-0.1375	0.1904
1.003	6.04	-0.643	0.172	0.0825	--	-0.1497	0.1810
1.007	9.02	-0.372	0.172	0.0764	--	-0.1338	0.1713
1.009	12.03	-0.128	0.178	0.0715	--	-0.0966	0.1665
1.015	15.02	0.119	0.165	0.0629	--	-0.0299	0.1467
1.009	17.99	0.423	0.137	0.0662	--	0.0677	0.1022
1.008	19.97	0.489	0.102	0.0963	--	0.0765	0.0509
0.998	23.99	-0.097	0.127	0.2205	--	-0.2409	0.1025
1.000	27.00	-0.085	0.125	0.2421	--	-0.2543	0.0776
End of Table 7							

Table 8. Unvented Aileron, Clean, δ=-45°, Re=1x10^6							
Rex10^{-6}	AOA	C_l	C_m	C_{dp}	C_{dw}	C_s	C_h
1.005	-6.01	-1.429	0.174	0.2511	--	-0.1001	0.3152
1.018	0.01	-1.459	0.224	0.2064	--	-0.2067	0.3187
1.018	3.03	-1.310	0.226	0.1648	--	-0.2338	0.2959
1.009	6.03	-1.068	0.229	0.1568	--	-0.2681	0.2854
1.003	9.01	-0.810	0.231	0.1499	--	-0.2749	0.2758
0.999	12.03	-0.562	0.232	0.1431	--	-0.2571	0.2662
0.999	15.02	-0.315	0.229	0.1355	--	-0.2125	0.2533
1.003	17.98	-0.014	0.199	0.1208	--	-0.1192	0.2031
1.007	19.99	0.271	0.156	0.1165	--	-0.0168	0.1446
1.001	24.01	0.435	-0.015	0.2629	--	-0.0632	-0.0739
1.002	26.99	0.249	0.038	0.2990	--	-0.1534	-0.0064
1.003	29.99	0.213	0.054	0.3352	--	-0.1839	0.0258
0.999	34.98	0.220	0.062	0.4136	--	-0.2128	0.0469
1.004	39.99	0.180	0.079	0.4966	--	-0.2648	0.0827
1.007	45.04	0.121	0.099	0.5671	--	-0.3151	0.1228
1.002	59.99	0.322	-0.017	0.9351	--	-0.1889	-0.0701
1.012	70.01	0.440	-0.143	1.2246	--	-0.0051	-0.2182
1.011	80.00	0.466	-0.262	1.5202	--	0.1949	-0.3356
1.001	90.04	0.376	-0.348	1.6941	--	0.3772	-0.4434
0.999	120.06	-0.084	-0.491	1.6850	--	0.7713	-0.6903
1.002	150.02	-0.137	-0.381	0.9169	--	0.7258	-0.6658
1.014	180.08	0.179	-0.061	0.1577	--	0.1574	-0.3250
0.997	210.10	0.450	0.212	0.1467	--	-0.0988	0.1771
1.008	240.03	1.250	0.540	1.2370	--	-0.4649	0.8052
0.982	269.07	0.643	0.616	2.1599	--	-0.6079	0.9083
End of Table 8							

Table 9. Unvented Aileron, Clean, δ=-57°, Re=1x10^6							
Rex10^{-6}	AOA	C_l	C_m	C_{dp}	C_{dw}	C_s	C_h
0.998	-5.95	-1.767	0.184	0.3568	--	-0.1717	0.3906
1.002	-0.04	-1.582	0.230	0.2896	--	-0.2885	0.3828
1.000	3.00	-1.558	0.253	0.2762	--	-0.3574	0.4045
1.004	6.00	-1.381	0.257	0.2463	--	-0.3893	0.3830
1.003	8.99	-1.161	0.261	0.2433	--	-0.4217	0.3766
1.004	11.99	-0.929	0.262	0.2360	--	-0.4238	0.3658
1.002	14.99	-0.710	0.263	0.2254	--	-0.4014	0.3549
1.008	17.96	-0.462	0.253	0.2142	--	-0.3462	0.3337
1.004	19.98	-0.266	0.232	0.2005	--	-0.2793	0.2962
1.006	23.98	0.493	-0.024	0.2406	--	-0.0195	-0.1031
1.000	26.97	0.472	-0.017	0.2994	--	-0.0528	-0.0996
0.995	29.97	0.364	0.016	0.3462	--	-0.1181	-0.0375
1.000	34.97	0.307	0.038	0.4316	--	-0.1777	0.0200
1.009	39.97	0.309	0.040	0.5319	--	-0.2091	0.0345
0.993	44.92	0.253	0.056	0.6346	--	-0.2707	0.0799
1.005	60.00	0.068	0.071	0.8664	--	-0.3743	0.1496
0.982	70.04	0.059	0.009	1.0066	--	-0.2882	-0.0126
0.994	80.05	0.179	-0.111	1.2126	--	-0.0332	-0.1725
0.993	90.07	0.224	-0.222	1.4309	--	0.2257	-0.3059
0.986	120.03	0.016	-0.405	1.5544	--	0.7918	-0.5933
1.003	149.93	0.036	-0.341	0.9767	--	0.8633	-0.6608
0.999	180.07	0.350	-0.043	0.2695	--	0.2691	-0.3640
1.011	210.04	-0.065	-0.059	0.2489	--	0.2480	-0.2790
0.987	240.00	1.170	0.444	0.8986	--	-0.5640	0.7401
0.944	269.05	0.808	0.559	1.9873	--	-0.7749	0.9264
End of Table 9							

Table 10. Unvented Aileron, Clean, δ=-87°, Re=1x10^6							
Rex10^{-6}	AOA	C_l	C_m	C_{dp}	C_{dw}	C_s	C_h
1.000	-5.99	-1.552	0.164	0.5899	--	-0.4247	0.5162
1.034	-0.02	-1.670	0.190	0.4044	--	-0.4038	0.5017
1.008	2.98	-1.699	0.218	0.4191	--	-0.5069	0.5398
1.008	6.00	-1.588	0.235	0.4417	--	-0.6053	0.5620
0.997	8.84	-1.473	0.247	0.4374	--	-0.6586	0.5587
0.999	12.04	-1.299	0.257	0.4594	--	-0.7203	0.5708
1.003	15.00	-1.134	0.262	0.4562	--	-0.7342	0.5616
1.007	17.99	-0.958	0.263	0.4531	--	-0.7268	0.5512
1.006	19.97	-0.828	0.259	0.4468	--	-0.7027	0.5376
1.005	23.99	-0.457	0.218	0.4172	--	-0.5670	0.4472
1.039	26.99	0.709	-0.042	0.2728	--	0.0787	-0.1718
1.003	29.99	0.669	-0.033	0.3414	--	0.0387	-0.1509
0.994	34.97	0.508	-0.003	0.4431	--	-0.0719	-0.0625
0.996	39.97	0.484	-0.003	0.5378	--	-0.1012	-0.0385
0.997	44.96	0.410	0.011	0.6399	--	-0.1631	-0.0054
0.997	59.98	0.303	-0.010	0.9739	--	-0.2249	0.0458
0.988	70.01	0.196	-0.041	1.1781	--	-0.2185	0.0637
1.001	79.98	0.055	-0.081	1.3520	--	-0.1811	0.0661
1.003	90.04	-0.188	-0.095	1.3686	--	-0.1870	0.1178
0.992	120.01	-0.215	-0.189	1.0534	--	0.3407	-0.2754
1.003	150.01	0.276	-0.207	0.8615	--	0.8841	-0.5397
1.024	180.06	0.586	0.031	0.3596	--	0.3590	-0.4073
1.010	210.00	-0.320	-0.090	0.4312	--	0.5334	-0.5216
0.954	239.98	0.790	0.231	0.7355	--	-0.3161	0.2365
0.981	269.03	0.962	0.377	1.4880	--	-0.9367	0.9066
End of Table 10							

Table 11. Unvented Aileron, LEGR, δ=5°, Re=1x10^6							
Rex10^{-6}	AOA	C_l	C_m	C_{dp}	C_{dw}	C_s	C_h
1.008	-5.99	-0.208	-0.050	0.0054	0.0182	0.0036	-0.0421
1.011	0.00	0.357	-0.061	0.0118	0.0180	-0.0180	-0.0936
1.007	3.03	0.587	-0.057	0.0000	0.0229	0.0082	-0.1120
1.009	6.00	0.747	-0.051	0.0425	0.0309	0.0473	-0.1402
1.008	8.99	0.895	-0.050	0.0510	--	0.0895	-0.1580
1.008	11.98	0.998	-0.054	0.0953	--	0.1139	-0.1773
1.001	15.00	0.938	-0.085	0.1882	--	0.0610	-0.2128
0.996	18.00	0.844	-0.124	0.2949	--	-0.0197	-0.2290
0.995	19.99	0.987	-0.139	0.3636	--	-0.0043	-0.2476
0.999	23.98	1.069	-0.153	0.4860	--	-0.0096	-0.2639
0.994	26.99	1.075	-0.182	0.5917	--	-0.0394	-0.2885
End of Table 11							

Table 12. Unvented Aileron, LEGR, δ=0°, Re=1x10^6							
Rex10^{-6}	AOA	C_l	C_m	C_{dp}	C_{dw}	C_s	C_h
0.997	-5.99	-0.475	0.005	0.0304	0.0396	0.0102	0.0478
1.006	0.01	-0.020	-0.016	0.0040	0.0138	-0.0138	-0.0321
1.010	3.03	0.290	-0.023	0.0020	0.0147	0.0006	-0.0536
1.011	6.01	0.573	-0.027	0.0139	0.0174	0.0427	-0.0715
1.006	9.01	0.783	-0.030	0.0438	0.0269	0.0960	-0.0991
1.005	12.01	0.894	-0.035	0.0823	--	0.1055	-0.1455
1.004	15.04	0.914	-0.034	0.1317	--	0.1100	-0.1632
0.989	18.03	0.697	-0.085	0.2295	--	-0.0025	-0.1921
1.001	19.99	0.743	-0.098	0.2872	--	-0.0159	-0.2042
1.002	24.01	1.060	-0.122	0.4426	--	0.0270	-0.2584
0.992	27.00	0.957	-0.123	0.5003	--	-0.0113	-0.2433
End of Table 12							

Table 13. Unvented Aileron, LEGR, δ=-5°, Re=1x10^6							
Rex10^{-6}	AOA	C_l	C_m	C_{dp}	C_{dw}	C_s	C_h
1.003	-6.00	-0.620	0.029	0.0494	--	0.0157	0.0781
1.000	0.01	-0.229	0.023	0.0051	0.0201	-0.0201	0.0225
1.002	3.03	0.021	0.024	0.0006	0.0153	-0.0142	0.0048
1.005	6.03	0.315	0.017	0.0085	0.0133	0.0199	-0.0200
1.006	9.01	0.598	0.010	0.0289	--	0.0652	-0.0442
1.009	12.02	0.751	-0.004	0.0642	--	0.0936	-0.1005
1.006	15.01	0.766	-0.006	0.1038	--	0.0981	-0.1246
1.001	18.02	0.564	-0.056	0.1947	--	-0.0107	-0.1530
0.997	19.99	0.625	-0.064	0.2353	--	-0.0075	-0.1652
0.995	24.00	0.835	-0.093	0.3694	--	0.0022	-0.1948
0.998	26.99	0.876	-0.100	0.4467	--	-0.0005	-0.2057
End of Table 13							

Table 14. Unvented Aileron, LEGR, δ=-10°, Re=1x10^6							
Rex10^{-6}	AOA	C_l	C_m	C_{dp}	C_{dw}	C_s	C_h
1.006	-5.98	-0.779	0.057	0.0677	--	0.0138	0.1102
1.007	0.00	-0.426	0.055	0.0157	0.0311	-0.0311	0.0609
1.000	3.01	-0.176	0.055	0.0082	0.0280	-0.0372	0.0473
1.001	6.02	0.073	0.058	0.0110	0.0227	-0.0149	0.0379
1.005	8.83	0.271	0.062	0.0200	--	0.0218	0.0277
1.002	12.01	0.547	0.046	0.0451	--	0.0697	-0.0187
1.004	15.03	0.662	0.027	0.0855	--	0.0891	-0.0809
0.994	18.02	0.544	-0.012	0.1571	--	0.0189	-0.1151
1.001	19.99	0.535	-0.020	0.1969	--	0.0030	-0.1231
0.990	24.00	0.688	-0.052	0.3219	--	-0.0142	-0.1438
1.007	27.00	0.760	-0.063	0.4044	--	-0.0153	-0.1628
End of Table 14							

Table 15. Unvented Aileron, LEGR, δ=-20°, Re=1x10^6							
Rex10^{-6}	AOA	C_l	C_m	C_{dp}	C_{dw}	C_s	C_h
1.003	-6.01	-1.011	0.098	0.1180	--	-0.0115	0.1656
1.000	0.02	-0.793	0.116	0.0563	--	-0.0566	0.1364
1.000	3.03	-0.555	0.118	0.0417	--	-0.0710	0.1250
1.006	6.04	-0.298	0.119	0.0363	--	-0.0674	0.1150
1.003	9.02	-0.038	0.118	0.0399	--	-0.0454	0.1031
1.005	12.02	0.184	0.117	0.0526	--	-0.0131	0.0959
1.006	15.03	0.357	0.107	0.0701	--	0.0249	0.0591
1.003	18.02	0.379	0.079	0.1073	--	0.0152	-0.0120
1.002	19.98	0.359	0.057	0.1552	--	-0.0232	-0.0356
0.995	23.99	0.295	0.034	0.2401	--	-0.0994	-0.0460
0.997	26.97	0.419	0.023	0.3164	--	-0.0920	-0.0536
End of Table 15							

Table 16. Unvented Aileron, LEGR, δ=-30°, Re=1x10^6							
Rex10^{-6}	AOA	C_l	C_m	C_{dp}	C_{dw}	C_s	C_h
0.995	-5.99	-1.207	0.136	0.1774	--	-0.0505	0.2255
1.003	0.01	-1.111	0.174	0.1162	--	-0.1164	0.2196
1.007	3.03	-0.878	0.166	0.0780	--	-0.1243	0.1940
1.010	6.02	-0.633	0.167	0.0656	--	-0.1316	0.1820
1.011	9.02	-0.370	0.165	0.0611	--	-0.1183	0.1678
1.012	12.01	-0.106	0.158	0.0661	--	-0.0867	0.1498
0.997	15.02	0.125	0.149	0.0831	--	-0.0479	0.1336
1.001	18.00	0.447	0.098	0.1070	--	0.0364	0.0498
0.996	20.00	0.407	0.099	0.1498	--	-0.0016	0.0680
1.005	24.00	0.089	0.100	0.2262	--	-0.1704	0.0762
1.001	26.97	0.089	0.116	0.2645	--	-0.1954	0.0918
End of Table 16							

Table 17. Unvented Aileron, LEGR, δ=-45°, Re=1x10^6							
Rex10^{-6}	AOA	C_l	C_m	C_{dp}	C_{dw}	C_s	C_h
0.997	-6.01	-1.373	0.125	0.2158	--	-0.0709	0.2305
1.002	0.03	-1.400	0.226	0.2296	--	-0.2303	0.3178
1.010	3.03	-1.263	0.232	0.1909	--	-0.2574	0.3146
1.009	6.05	-1.035	0.233	0.1672	--	-0.2754	0.3013
1.005	9.03	-0.776	0.227	0.1471	--	-0.2671	0.2797
1.008	12.04	-0.520	0.222	0.1394	--	-0.2448	0.2628
1.003	15.04	-0.251	0.204	0.1377	--	-0.1981	0.2285
0.996	18.01	0.076	0.161	0.1365	--	-0.1063	0.1603
0.996	20.01	0.315	0.081	0.1749	--	-0.0566	0.0591
1.012	23.99	0.483	0.022	0.2623	--	-0.0433	-0.0292
1.003	27.01	0.455	0.042	0.3242	--	-0.0822	0.0018
End of Table 17							

Table 18. Unvented Aileron, LEGR, δ=-57°, Re=1x10^6							
Rex10^{-6}	AOA	C_l	C_m	C_{dp}	C_{dw}	C_s	C_h
1.004	-5.98	-1.631	0.202	0.3753	--	-0.2033	0.4129
0.996	-0.02	-1.559	0.231	0.2980	--	-0.2975	0.3841
1.001	2.97	-1.515	0.253	0.2858	--	-0.3639	0.4034
1.000	7.61	-1.319	0.254	0.2239	--	-0.3966	0.3852
1.006	9.01	-1.089	0.255	0.2504	--	-0.4178	0.3744
1.011	11.99	-0.873	0.256	0.2437	--	-0.4197	0.3636
1.001	14.97	-0.648	0.249	0.2279	--	-0.3875	0.3437
1.009	17.99	-0.380	0.232	0.2142	--	-0.3211	0.3120
1.005	19.97	-0.149	0.201	0.2023	--	-0.2410	0.2659
1.004	23.98	0.512	0.012	0.2180	--	0.0089	-0.0333
0.998	27.00	0.529	-0.006	0.2758	--	-0.0056	-0.0749
End of Table 18							

Table 19. Unvented Aileron, LEGR, δ=-87°, Re=1x10^6							
Rex10^{-6}	AOA	C_l	C_m	C_{dp}	C_{dw}	C_s	C_h
0.999	-5.98	-1.650	0.157	0.4951	--	-0.3205	0.5337
0.999	0.01	-1.641	0.187	0.4105	--	-0.4108	0.4993
1.002	2.98	-1.648	0.212	0.4113	--	-0.4964	0.5228
1.001	5.99	-1.567	0.236	0.4516	--	-0.6127	0.5629
1.003	9.00	-1.419	0.244	0.4579	--	-0.6742	0.5648
1.004	12.02	-1.245	0.246	0.4503	--	-0.6997	0.5521
1.000	14.98	-1.067	0.248	0.4545	--	-0.7148	0.5451
1.001	17.97	-0.883	0.245	0.4530	--	-0.7033	0.5321
1.006	19.97	-0.723	0.233	0.4323	--	-0.6532	0.4988
0.997	23.97	-0.317	0.187	0.4491	--	-0.5392	0.4272
1.002	26.98	0.350	0.053	0.3725	--	-0.1732	0.0970
End of Table 19							

Table 20. Unvented Aileron, Clean, δ=5°, Re=2x10^6							
Rex10^{-6}	AOA	C_l	C_m	C_{dp}	C_{dw}	C_s	C_h
1.993	-6.02	-0.284	-0.065	0.0033	0.0087	0.0211	-0.0724
1.997	0.00	0.402	-0.078	0.0037	0.0116	-0.0116	-0.1081
1.992	3.03	0.744	-0.084	0.0017	0.0145	0.0248	-0.1220
1.993	6.02	0.914	-0.072	0.0121	0.0251	0.0709	-0.1245
1.977	9.01	1.077	-0.068	0.0344	--	0.1347	-0.1589
2.005	12.02	1.154	-0.065	0.0622	--	0.1795	-0.1903
2.007	14.99	1.188	-0.064	0.0933	--	0.2171	-0.2089
1.994	18.01	1.006	-0.088	0.1739	--	0.1457	-0.2282
1.969	19.98	0.693	-0.131	0.3294	--	-0.0728	-0.2350
1.973	23.98	0.907	-0.177	0.4891	--	-0.0783	-0.2912
2.004	26.95	0.974	-0.195	0.5818	--	-0.0772	-0.3108
End of Table 20							

Table 21. Unvented Aileron, Clean, δ=0°, Re=2x10^6							
Rex10^{-6}	AOA	C_l	C_m	C_{dp}	C_{dw}	C_s	C_h
1.994	-6.08	-0.536	0.005	0.0188	0.0382	0.0188	0.0432
1.998	0.06	0.078	-0.033	0.0042	0.0075	-0.0074	-0.0579
1.996	3.10	0.430	-0.040	0.0079	0.0088	0.0145	-0.0767
2.003	6.10	0.727	-0.042	0.0155	0.0107	0.0666	-0.0887
1.991	9.06	0.939	-0.039	0.0295	0.0218	0.1263	-0.1009
2.015	12.09	1.062	-0.047	0.0585	--	0.1652	-0.1532
1.998	15.08	1.089	-0.047	0.0917	--	0.1948	-0.1808
1.994	18.07	0.948	-0.068	0.1612	--	0.1408	-0.2012
1.998	20.06	0.653	-0.117	0.3235	--	-0.0799	-0.2118
1.979	24.06	0.740	-0.135	0.4245	--	-0.0859	-0.2332
1.986	27.00	0.911	-0.176	0.5642	--	-0.0891	-0.2864
End of Table 21							

Table 22. Unvented Aileron, Clean, δ=-5°, Re=2x10^6							
Rex10^{-6}	AOA	C_l	C_m	C_{dp}	C_{dw}	C_s	C_h
2.011	-6.02	-0.670	0.038	0.0387	--	0.0318	0.0856
1.998	0.01	-0.270	0.027	0.0056	0.0106	-0.0106	0.0076
2.013	3.04	0.070	0.019	0.0021	0.0087	-0.0050	-0.0142
2.009	6.02	0.404	0.012	0.0006	0.0086	0.0338	-0.0357
2.005	9.01	0.700	0.006	0.0075	0.0116	0.0982	-0.0519
1.999	12.01	0.925	-0.009	0.0263	--	0.1667	-0.0945
1.994	15.00	0.957	-0.012	0.0510	--	0.1984	-0.1388
2.026	17.99	0.885	-0.040	0.1202	--	0.1590	-0.1708
1.994	20.00	0.571	-0.094	0.2820	--	-0.0697	-0.1860
2.002	23.98	0.582	-0.089	0.3368	--	-0.0712	-0.1773
2.018	27.02	0.782	-0.136	0.4710	--	-0.0643	-0.2342
End of Table 22							

Table 23. Unvented Aileron, Clean, δ=-10°, Re=2x10^6							
Rex10^{-6}	AOA	C_l	C_m	C_{dp}	C_{dw}	C_s	C_h
2.002	-6.00	-0.787	0.055	0.0537	--	0.0289	0.1060
1.999	0.01	-0.500	0.069	0.0190	0.0251	-0.0252	0.0744
2.002	3.04	-0.201	0.069	0.0151	0.0206	-0.0312	0.0620
1.999	6.04	0.081	0.071	0.0108	0.0166	-0.0080	0.0461
1.991	9.02	0.379	0.060	0.0117	0.0114	0.0482	0.0085
2.008	12.04	0.694	0.044	0.0135	0.0146	0.1305	-0.0253
2.007	15.02	0.873	0.015	0.0371	--	0.1904	-0.0985
2.002	17.99	0.763	-0.013	0.0981	--	0.1423	-0.1424
1.994	20.00	0.725	-0.021	0.1379	--	0.1184	-0.1439
1.953	23.99	0.439	-0.046	0.2871	--	-0.0838	-0.1335
1.991	27.00	0.564	-0.074	0.3762	--	-0.0791	-0.1617
End of Table 23							

Table 24. Unvented Aileron, Clean, δ=-20°, Re=2x10^6							
Rex10^{-6}	AOA	C_l	C_m	C_{dp}	C_{dw}	C_s	C_h
1.992	-6.02	-0.968	0.083	0.0925	--	0.0095	0.1423
1.996	0.03	-0.871	0.124	0.0580	--	-0.0585	0.1423
1.993	3.07	-0.584	0.124	0.0519	--	-0.0831	0.1311
1.988	6.05	-0.317	0.128	0.0471	--	-0.0802	0.1216
2.001	9.03	-0.043	0.130	0.0432	--	-0.0494	0.1151
1.995	12.04	0.220	0.127	0.0363	--	0.0104	0.1062
1.993	15.02	0.477	0.113	0.0380	--	0.0869	0.0742
2.007	17.99	0.590	0.089	0.0527	--	0.1321	-0.0036
1.998	19.98	0.514	0.061	0.0991	--	0.0825	-0.0484
1.979	23.97	0.306	-0.006	0.2671	--	-0.1197	-0.0937
2.012	27.01	0.230	0.026	0.2758	--	-0.1413	-0.0555
End of Table 24							

Table 25. Unvented Aileron, Clean, δ=-30°, Re=2x10^6							
Rex10^{-6}	AOA	C_l	C_m	C_{dp}	C_{dw}	C_s	C_h
2.003	-6.01	-1.206	0.135	0.1595	--	-0.0324	0.2255
2.004	0.02	-1.136	0.172	0.1112	--	-0.1116	0.2150
2.006	3.05	-0.910	0.171	0.0883	--	-0.1366	0.1939
2.006	6.04	-0.634	0.172	0.0821	--	-0.1484	0.1829
2.002	9.02	-0.374	0.177	0.0757	--	-0.1334	0.1758
2.001	12.03	-0.111	0.176	0.0698	--	-0.0914	0.1714
1.993	15.02	0.169	0.161	0.0671	--	-0.0210	0.1417
1.995	17.99	0.498	0.127	0.0621	--	0.0947	0.0901
1.989	19.98	0.486	0.076	0.0966	--	0.0753	0.0163
1.997	24.00	0.228	0.087	0.2551	--	-0.1403	0.0804
2.026	27.02	-0.067	0.134	0.2531	--	-0.2559	0.1329
End of Table 25							

Table 26. Unvented Aileron, Clean, δ=-45, Re=2x10^6							
Rex10^{-6}	AOA	C_l	C_m	C_{dp}	C_{dw}	C_s	C_h
2.008	-6.01	-1.501	0.190	0.2747	--	-0.1160	0.3254
1.997	0.05	-1.439	0.228	0.2182	--	-0.2195	0.3177
1.995	3.09	-1.276	0.231	0.1815	--	-0.2500	0.3031
2.000	6.06	-1.040	0.236	0.1714	--	-0.2802	0.2954
1.997	9.06	-0.794	0.239	0.1605	--	-0.2835	0.2863
1.997	12.05	-0.535	0.237	0.1484	--	-0.2568	0.2747
2.024	15.03	-0.264	0.222	0.1319	--	-0.1958	0.2492
2.006	18.03	0.065	0.189	0.1177	--	-0.0918	0.1959
2.007	20.04	0.365	0.137	0.1070	--	0.0246	0.1249
2.032	24.03	0.376	0.003	0.2692	--	-0.0928	-0.0524
2.010	27.05	0.298	0.030	0.3115	--	-0.1419	-0.0080
End of Table 26							

Table 27. Unvented Aileron, Clean, δ=-57°, Re=2x10^6							
Rex10^{-6}	AOA	C_l	C_m	C_{dp}	C_{dw}	C_s	C_h
1.994	-6.06	-1.519	0.173	0.3422	--	-0.1799	0.3748
2.000	0.02	-1.541	0.226	0.2904	--	-0.2909	0.3770
1.994	3.00	-1.541	0.255	0.2876	--	-0.3679	0.4037
1.995	6.06	-1.371	0.261	0.2604	--	-0.4037	0.3898
1.996	9.06	-1.142	0.265	0.2542	--	-0.4309	0.3812
1.996	12.08	-0.900	0.266	0.2433	--	-0.4263	0.3680
1.992	15.08	-0.655	0.263	0.2333	--	-0.3957	0.3533
1.997	18.03	-0.378	0.242	0.2124	--	-0.3190	0.3159
1.997	20.02	-0.164	0.216	0.1992	--	-0.2433	0.2736
1.995	24.05	0.477	0.035	0.3200	--	-0.0978	0.0442
1.994	27.05	0.484	-0.016	0.3098	--	-0.0558	-0.0865
End of Table 27							

Table 28. Unvented Aileron, Clean, δ=-87°, Re=2x10^6							
Rex10^{-6}	AOA	C_l	C_m	C_{dp}	C_{dw}	C_s	C_h
1.992	-5.97	-1.493	0.167	0.6072	--	-0.4486	0.5234
2.033	-0.01	-1.679	0.192	0.4140	--	-0.4137	0.5068
2.002	2.99	-1.727	0.226	0.4446	--	-0.5341	0.5597
1.997	6.01	-1.598	0.242	0.4696	--	-0.6343	0.5779
1.994	9.01	-1.478	0.255	0.4732	--	-0.6988	0.5853
1.988	12.06	-1.304	0.261	0.4773	--	-0.7392	0.5822
1.995	14.99	-1.130	0.265	0.4770	--	-0.7530	0.5731
1.998	17.99	-0.935	0.263	0.4699	--	-0.7357	0.5584
1.999	19.95	-0.799	0.257	0.4634	--	-0.7082	0.5435
2.004	23.99	-0.412	0.213	0.4283	--	-0.5588	0.4459
2.062	27.02	0.721	-0.047	0.2741	--	0.0834	-0.1836
End of Table 28							

Table 29. Unvented Aileron, LEGR, δ=5°, Re=2x10^6							
Rex10^{-6}	AOA	C_l	C_m	C_{dp}	C_{dw}	C_s	C_h
1.998	-6.00	-0.202	-0.045	0.0094	0.0224	-0.0012	-0.0338
2.001	-0.01	0.411	-0.067	0.0108	0.0220	-0.0221	-0.0958
1.998	3.01	0.663	-0.066	0.0036	0.0267	0.0082	-0.1107
1.998	6.01	0.871	-0.064	0.0308	0.0353	0.0561	-0.1391
1.994	9.00	1.002	-0.063	0.0671	--	0.0905	-0.1757
2.010	12.00	1.057	-0.057	0.1052	--	0.1169	-0.1941
2.004	15.01	1.046	-0.077	0.1790	--	0.0980	-0.2094
2.006	17.98	0.851	-0.128	0.3329	--	-0.0536	-0.2311
2.005	19.99	0.940	-0.144	0.3743	--	-0.0304	-0.2479
1.993	23.98	0.895	-0.162	0.4742	--	-0.0695	-0.2566
2.012	26.99	0.949	-0.193	0.5827	--	-0.0885	-0.2904
End of Table 29							

Table 30. Unvented Aileron, LEGR, δ=0°, Re=2x10^6							
Rex10^{-6}	AOA	C_l	C_m	C_{dp}	C_{dw}	C_s	C_h
1.994	-6.01	-0.468	0.006	0.0332	--	0.0160	0.0565
2.00	0.01	-0.036	-0.015	0.0015	0.0121	-0.0121	-0.0294
1.998	3.05	0.283	-0.023	0.0030	0.0135	0.0016	-0.0515
1.996	6.01	0.571	-0.026	0.0203	0.0167	0.0432	-0.0668
1.990	9.01	0.786	-0.027	0.0506	0.0256	0.0978	-0.0895
2.000	12.01	0.890	-0.031	0.0898	--	0.0974	-0.1381
1.994	15.02	0.940	-0.035	0.1315	--	0.1166	-0.1636
1.990	18.01	0.797	-0.072	0.2179	--	0.0392	-0.1920
1.997	19.99	0.708	-0.098	0.2865	--	-0.0272	-0.2000
2.025	23.99	0.919	-0.129	0.4310	--	-0.0201	-0.2346
1.988	27.01	0.830	-0.138	0.4828	--	-0.0532	-0.2364
End of Table 30							

Table 31. Unvented Aileron, LEGR, δ=-5°, Re=2x10^6							
Rex10^{-6}	AOA	C_l	C_m	C_{dp}	C_{dw}	C_s	C_h
2.010	-6.00	-0.608	0.031	0.0530	--	0.0108	0.0850
2.005	-0.01	-0.251	0.028	0.0082	0.0219	-0.0219	0.0310
1.998	3.02	0.005	0.029	0.0042	0.0148	-0.0145	0.0130
2.007	6.01	0.300	0.021	0.0132	0.0135	0.0180	-0.0133
2.004	9.01	0.589	0.013	0.0342	--	0.0585	-0.0370
1.994	12.02	0.763	0.000	0.0702	--	0.0902	-0.0868
2.007	15.00	0.805	-0.005	0.1059	--	0.1061	-0.1230
2.005	18.00	0.605	-0.050	0.1905	--	0.0058	-0.1512
2.003	19.99	0.612	-0.067	0.2460	--	-0.0220	-0.1634
1.984	24.00	0.866	-0.100	0.3914	--	-0.0053	-0.2005
2.000	26.99	0.723	-0.108	0.4316	--	-0.0565	-0.1958
End of Table 31							

Table 32. Unvented Aileron, LEGR, δ=-10°, Re=2x10^6							
Rex10^{-6}	AOA	C_l	C_m	C_{dp}	C_{dw}	C_s	C_h
1.993	-6.00	-0.749	0.053	0.0682	--	0.0105	0.1125
1.995	0.01	-0.447	0.058	0.0182	0.0320	-0.0321	0.0688
1.989	3.03	-0.195	0.059	0.0113	0.0273	-0.0376	0.0556
1.990	6.03	0.066	0.062	0.0150	0.0234	-0.0163	0.0461
1.989	9.01	0.310	0.064	0.0268	--	0.0221	0.0354
2.009	12.00	0.556	0.052	0.0492	--	0.0675	-0.0047
2.002	15.01	0.688	0.030	0.0860	--	0.0951	-0.0727
1.995	18.01	0.575	-0.004	0.1552	--	0.0302	-0.1050
1.993	19.99	0.522	-0.019	0.2013	--	-0.0107	-0.1165
0.986	24.00	0.609	-0.050	0.3165	--	-0.0414	-0.1418
1.988	26.99	0.638	-0.061	0.3870	--	-0.0553	-0.1490
End of Table 32							

Table 33. Unvented Aileron, LEGR, δ=-20°, Re=2x10^6							
Rex10^{-6}	AOA	C_l	C_m	C_{dp}	C_{dw}	C_s	C_h
2.013	-6.00	-0.981	0.096	0.1187	--	-0.0155	0.1678
2.023	0.02	-0.804	0.119	0.0595	--	-0.0598	0.1420
2.007	3.04	-0.574	0.122	0.0447	--	-0.0751	0.1316
2.002	6.04	-0.315	0.124	0.0385	--	-0.0714	0.1221
2.005	9.04	-0.045	0.122	0.0429	--	-0.0494	0.1108
2.003	12.04	0.227	0.114	0.0557	--	-0.0071	0.0928
1.997	15.06	0.494	0.094	0.0761	--	0.0549	0.0537
1.993	18.03	0.452	0.100	0.1159	--	0.0297	0.0529
2.002	20.02	0.304	0.088	0.1492	--	-0.0361	0.0342
2.010	23.98	0.249	0.047	0.2329	--	-0.1116	-0.0151
2.017	26.99	0.386	0.024	0.3130	--	-0.1037	-0.0487
End of Table 33							

Table 34. Unvented Aileron, LEGR, δ=-30°, Re=2x10^6							
Rex10^{-6}	AOA	C_l	C_m	C_{dp}	C_{dw}	C_s	C_h
2.008	-5.98	-1.169	0.138	0.1850	--	-0.0622	0.2270
1.997	0.01	-1.069	0.173	0.1210	--	-0.1212	0.2165
2.004	3.03	-0.837	0.170	0.0895	--	-0.1336	0.1975
2.009	6.03	-0.583	0.170	0.0756	--	-0.1364	0.1859
2.016	9.04	-0.320	0.168	0.0706	--	-0.1200	0.1726
2.007	12.02	-0.044	0.159	0.0749	--	-0.0824	0.1524
1.998	15.06	0.167	0.148	0.0878	--	-0.0414	0.1329
1.998	18.05	0.515	0.095	0.1136	--	0.0516	0.0489
2.011	20.02	0.474	0.064	0.1620	--	0.0101	0.0221
1.998	24.02	0.290	0.046	0.2449	--	-0.1056	0.0171
2.014	27.00	0.249	0.075	0.2866	--	-0.1423	0.0600
End of Table 34							

Table 35. Unvented Aileron, LEGR, δ=-45°, Re=2x10^6							
Rex10^{-6}	AOA	C_l	C_m	C_{dp}	C_{dw}	C_s	C_h
2.010	-6.02	-1.463	0.187	0.3065	--	-0.1514	0.3269
2.006	0.05	-1.389	0.223	0.2262	--	-0.2274	0.3166
2.011	3.06	-1.279	0.234	0.1925	--	-0.2605	0.3184
1.998	6.04	-1.050	0.236	0.1712	--	-0.2807	0.3073
1.995	9.02	-0.803	0.233	0.1546	--	-0.2786	0.2916
2.002	12.05	-0.537	0.227	0.1458	--	-0.2547	0.2733
1.996	15.02	-0.262	0.211	0.1435	--	-0.2065	0.2424
2.001	18.01	0.113	0.158	0.1442	--	-0.1022	0.1589
1.992	20.01	0.413	0.036	0.1825	--	-0.0302	0.0005
2.001	23.99	0.550	0.004	0.2838	--	-0.0357	-0.0408
1.996	27.02	0.484	0.010	0.3366	--	-0.0800	-0.0322
End of Table 35							

Table 36. Unvented Aileron, LEGR, δ=-57°, Re=2x10^6							
Rex10^{-6}	AOA	C_l	C_m	C_{dp}	C_{dw}	C_s	C_h
1.997	-6.01	-1.640	0.201	0.3729	--	-0.1991	0.4085
1.998	-0.03	-1.517	0.222	0.2913	--	-0.2905	0.3781
1.998	3.01	-1.504	0.250	0.2831	--	-0.3617	0.3971
1.988	6.02	-1.309	0.254	0.2649	--	-0.4007	0.3855
1.994	9.03	-1.097	0.257	0.2554	--	-0.4244	0.3763
1.996	12.02	-0.869	0.256	0.2460	--	-0.4216	0.3640
1.996	15.00	-0.617	0.247	0.2312	--	-0.3830	0.3375
2.004	17.99	-0.333	0.226	0.2153	--	-0.3076	0.3011
2.006	19.99	-0.086	0.190	0.2009	--	-0.2182	0.2468
1.997	24.02	0.560	0.006	0.2314	--	0.0150	-0.0378
2.005	27.01	0.572	-0.020	0.2931	--	-0.0014	-0.0869
End of Table 36							

Table 37. Unvented Aileron, LEGR, δ=-87°, Re=2x10^6							
Rex10^{-6}	AOA	C_l	C_m	C_{dp}	C_{dw}	C_s	C_h
1.988	-6.01	-1.728	0.161	0.5052	--	-0.3215	0.5414
2.006	-0.01	-1.644	0.187	0.4195	--	-0.4192	0.5073
1.987	3.01	-1.693	0.221	0.4427	--	-0.5310	0.5504
1.970	6.01	-1.578	0.238	0.4639	--	-0.6266	0.5705
1.980	9.02	-1.423	0.248	0.4776	--	-0.6948	0.5775
1.993	12.02	-1.248	0.252	0.4778	--	-0.7272	0.5699
2.001	14.99	-1.060	0.249	0.4644	--	-0.7228	0.5496
2.002	17.99	-0.864	0.245	0.4597	--	-0.7041	0.5299
2.002	19.98	-0.713	0.236	0.4567	--	-0.6728	0.5113
1.995	23.98	-0.255	0.174	0.4277	--	-0.4944	0.3867
2.001	27.01	0.367	0.057	0.3949	--	-0.1852	0.1166
End of Table 37							

Vented Aileron, Re=1x10^6

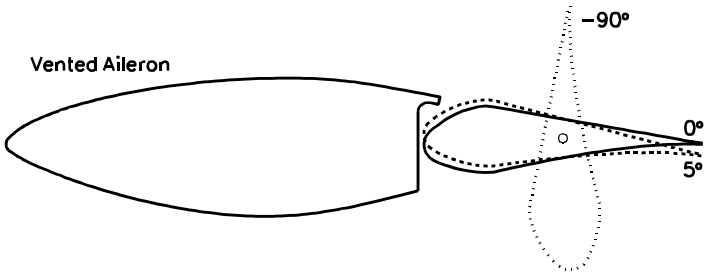

Table 38. Vented Aileron, Clean, δ=5°, Re=1x10^6							
Rex10^{-6}	AOA	C_l	C_m	C_{dp}	C_{dw}	C_s	C_h
1.003	-6.03	-0.288	-0.064	0.0168	0.0122	0.0181	0.0016
1.010	0.03	0.358	-0.084	0.0116	0.0135	-0.0133	0.0263
1.010	3.03	0.670	-0.089	0.0181	0.0127	0.0227	0.0342
1.009	6.04	0.835	-0.073	0.0256	--	0.0624	0.0279
1.007	9.04	0.966	-0.056	0.0361	--	0.1161	0.0220
1.004	12.06	1.160	-0.055	0.0579	--	0.1857	0.0302
0.998	15.04	1.208	-0.070	0.1101	--	0.2071	0.0400
0.981	18.03	0.684	-0.127	0.3105	--	-0.0835	0.0427
0.990	20.05	0.719	-0.138	0.3577	--	-0.0895	0.0467
1.003	24.04	0.780	-0.160	0.4574	--	-0.1008	0.0467
1.003	26.89	0.886	-0.189	0.5739	--	-0.1111	0.0450
End of Table 38							

Table 39. Vented Aileron, Clean, δ=0°, Re=1x10^6							
Rex10^{-6}	AOA	C_l	C_m	C_{dp}	C_{dw}	C_s	C_h
0.995	-5.97	-0.504	-0.009	0.0240	--	0.0286	-0.0241
0.997	-0.02	0.108	-0.029	0.0096	0.0124	-0.0124	0.0030
0.997	3.00	0.427	-0.038	0.0081	0.0141	0.0083	0.0129
0.995	6.02	0.695	-0.037	0.0098	0.0146	0.0584	0.0168
0.991	9.01	0.809	-0.021	0.0213	0.0265	0.1005	0.0068
0.990	12.00	1.052	-0.023	0.0294	--	0.1900	0.0328
0.985	14.97	1.167	-0.030	0.0653	--	0.2384	0.0422
0.953	17.96	0.618	-0.093	0.2569	--	-0.0538	0.0449
0.943	19.97	0.621	-0.104	0.2991	--	-0.0690	0.0474
1.008	23.97	0.664	-0.121	0.3786	--	-0.0762	0.0428
0.993	26.99	0.770	-0.149	0.4850	--	-0.0827	0.0510
0.963	29.99	0.936	-0.193	0.6266	--	-0.0748	0.0688
1.004	34.98	1.102	-0.250	0.8513	--	-0.0657	0.0914
0.970	39.95	1.181	-0.297	1.0604	--	-0.0546	0.1078
0.938	44.97	1.210	-0.341	1.2675	--	-0.0416	0.1202
1.007	60.02	1.108	-0.474	1.8813	--	0.0197	0.1538
0.974	70.02	0.869	-0.552	2.1945	--	0.0669	0.1708
0.953	80.02	0.533	-0.605	2.3636	--	0.1153	0.1778
0.946	90.02	0.148	-0.662	2.4851	--	0.1489	0.1841
1.023	119.99	-0.713	-0.620	1.7465	--	0.2554	0.1571
0.989	150.04	-0.438	-0.347	0.4989	--	0.2135	0.0520
1.072	180.05	0.070	0.022	0.0215	--	0.0214	-0.0044
0.992	210.06	0.489	0.365	0.5209	--	0.2059	-0.0209
1.017	240.01	0.775	0.633	1.7719	--	0.2144	-0.1085
0.948	269.02	-0.096	0.619	2.3240	--	0.1357	-0.1523
End of Table 39							

Table 40. Vented Aileron, Clean, δ=-5°, Re=1x10^6							
Rex10^{-6}	AOA	C_l	C_m	C_{dp}	C_{dw}	C_s	C_h
1.021	-6.01	-0.632	0.044	0.0545	--	0.0120	-0.0366
1.011	-0.01	-0.182	0.037	0.0144	0.0127	-0.0127	-0.0328
1.012	3.03	0.122	0.028	0.0092	0.0131	-0.0066	-0.0242
1.011	6.02	0.428	0.018	0.0101	0.0127	0.0323	-0.0125
1.011	9.06	0.611	0.019	0.0187	0.0187	0.0777	-0.0177
1.009	12.04	0.781	0.023	0.0279	--	0.1356	0.0148
1.004	15.03	0.952	0.014	0.0514	--	0.1972	0.0282
1.004	18.00	0.889	-0.017	0.1139	--	0.1664	0.0414
1.005	20.01	0.474	-0.058	0.2603	--	-0.0824	0.0400
1.004	25.52	0.515	-0.078	0.3473	--	-0.0915	0.0348
1.005	26.90	0.609	-0.098	0.4145	--	-0.0941	0.0416
End of Table 40							

Table 41. Vented Aileron, Clean, δ=-10°, Re=1x10^6							
Rex10^{-6}	AOA	C_l	C_m	C_{dp}	C_{dw}	C_s	C_h
1.002	-5.98	-0.708	0.087	0.0699	--	0.0042	-0.0346
1.009	-0.02	-0.402	0.091	0.0226	0.0169	-0.0168	-0.0676
1.012	3.03	-0.118	0.084	0.0154	0.0139	-0.0201	-0.0592
1.015	6.03	0.189	0.073	0.0107	0.0129	0.0070	-0.0465
1.014	8.99	0.381	0.059	0.0229	0.0204	0.0394	-0.0197
1.011	12.02	0.588	0.053	0.0386	--	0.0847	-0.0147
1.007	15.02	0.753	0.047	0.0584	--	0.1387	-0.0035
0.997	17.99	0.777	0.024	0.1095	--	0.1358	0.0134
1.004	19.99	0.356	-0.016	0.2475	--	-0.1109	0.0116
1.007	23.99	0.475	-0.048	0.3396	--	-0.1171	0.0150
0.994	26.88	0.527	-0.061	0.4042	--	-0.1223	0.0199
End of Table 41							

Table 42. Vented Aileron, Clean, δ=-20°, Re=1x10^6							
Rex10^{-6}	AOA	C_l	C_m	C_{dp}	C_{dw}	C_s	C_h
1.002	-5.99	-0.812	0.138	0.0948	--	-0.0095	-0.0314
1.011	0.04	-0.675	0.147	0.0389	--	-0.0394	-0.0990
1.011	3.03	-0.509	0.161	0.0325	--	-0.0594	-0.1140
1.014	6.03	-0.404	0.190	0.0170	0.0179	-0.0602	-0.1889
1.014	9.02	-0.142	0.184	0.0119	0.0156	-0.0377	-0.1909
1.013	12.04	0.131	0.160	0.0163	--	0.0150	-0.1570
1.005	15.02	0.814	0.065	0.0710	--	0.1424	0.0405
1.001	18.04	0.883	0.054	0.1111	--	0.1678	0.0552
0.998	19.99	0.524	0.106	0.1181	--	0.0681	-0.0213
1.000	23.98	0.040	0.076	0.2235	--	-0.1619	-0.1222
1.005	26.89	0.283	0.035	0.3184	--	-0.1560	-0.1009
End of Table 42							

Table 43. Vented Aileron, Clean, δ=-30°, Re=1x10^6							
Rex10^{-6}	AOA	C_l	C_m	C_{dp}	C_{dw}	C_s	C_h
1.003	-6.00	-0.807	0.171	0.1456	--	-0.0604	-0.0319
1.012	0.00	-0.719	0.170	0.0753	--	-0.0753	-0.1280
1.015	3.04	-0.548	0.181	0.0658	--	-0.0948	-0.1413
1.014	6.03	-0.339	0.185	0.0558	--	-0.0911	-0.1405
1.006	9.01	-0.135	0.194	0.0490	--	-0.0695	-0.1455
1.005	12.04	0.098	0.177	0.0423	--	-0.0209	-0.1247
1.005	15.01	0.362	0.151	0.0486	--	0.0468	-0.0875
1.006	18.00	0.315	0.186	0.0565	--	0.0436	-0.1888
1.005	20.01	0.312	0.188	0.0741	--	0.0371	-0.2032
0.997	23.97	-0.108	0.146	0.1869	--	-0.2147	-0.2790
0.998	26.91	0.007	0.121	0.2422	--	-0.2128	-0.2611
End of Table 43							

Table 44. Vented Aileron, Clean, δ=-45°, Re=1x10^6							
Rex10^{-6}	AOA	C_l	C_m	C_{dp}	C_{dw}	C_s	C_h
1.003	-6.02	-0.642	0.148	0.2419	--	-0.1732	-0.0167
1.001	0.01	-0.505	0.160	0.2621	--	-0.2622	-0.0858
1.004	3.05	-0.331	0.174	0.2614	--	-0.2786	-0.0877
1.007	6.03	-0.139	0.178	0.2410	--	-0.2543	-0.0861
1.001	9.02	0.025	0.168	0.2251	--	-0.2184	-0.0753
1.006	12.03	0.206	0.160	0.2065	--	-0.1590	-0.0576
1.006	15.05	0.423	0.143	0.1992	--	-0.0825	-0.0421
1.008	18.00	0.686	0.104	0.2128	--	0.0096	-0.0129
0.985	19.99	0.733	-0.084	0.3404	--	-0.0693	-0.0047
1.005	23.99	0.712	-0.076	0.4213	--	-0.0954	-0.0066
1.003	26.97	0.683	-0.065	0.4924	--	-0.1291	-0.0131
0.997	30.01	0.645	-0.056	0.5536	--	-0.1568	-0.0188
0.990	35.03	0.436	-0.002	0.6177	--	-0.2555	-0.0360
0.979	39.99	0.284	0.037	0.6647	--	-0.3267	-0.0457
0.987	44.94	0.220	0.043	0.7173	--	-0.3509	-0.0486
0.998	60.03	0.416	-0.080	1.0709	--	-0.1746	-0.2178
0.985	70.04	0.507	-0.211	1.4406	--	-0.0152	-0.0737
0.982	80.03	0.483	-0.317	1.7055	--	0.1804	0.0532
0.984	90.05	0.362	-0.393	1.8703	--	0.3636	0.1603
0.994	120.03	-0.076	-0.406	1.7438	--	0.8069	0.2872
0.992	150.10	-0.178	-0.262	0.6954	--	0.5141	-0.0241
1.037	180.05	-0.201	-0.142	0.2618	--	0.2620	-0.1030
1.023	210.06	0.364	0.128	0.3947	--	0.1593	-0.0611
0.964	240.03	0.829	0.397	1.0117	--	-0.2128	0.1348
0.973	269.08	0.356	0.396	1.5177	--	-0.3316	0.2186
End of Table 44							

Table 45. Vented Aileron, Clean, δ=-60°, Re=1x10^6							
Rex10^{-6}	AOA	C_l	C_m	C_{dp}	C_{dw}	C_s	C_h
1.001	-6.03	-0.588	0.149	0.4150	--	-0.3509	-0.0062
0.999	0.01	-0.376	0.172	0.3968	--	-0.3969	-0.0355
0.998	3.05	-0.248	0.156	0.3755	--	-0.3882	-0.0793
1.001	6.05	-0.173	0.172	0.3949	--	-0.4109	-0.0889
1.003	9.05	-0.079	0.175	0.3871	--	-0.3947	-0.0903
1.009	12.08	0.046	0.171	0.3638	--	-0.3461	-0.0874
1.012	15.04	0.204	0.161	0.3587	--	-0.2935	-0.0786
1.017	18.04	0.378	0.139	0.3487	--	-0.2145	-0.0688
0.995	20.03	0.626	-0.039	0.3974	--	-0.1589	-0.0598
0.988	23.99	0.644	-0.050	0.4545	--	-0.1534	-0.0669
1.006	26.99	0.650	-0.052	0.5121	--	-0.1613	-0.0667
1.001	30.01	0.633	-0.054	0.5520	--	-0.1614	-0.0688
0.994	35.01	0.641	-0.060	0.6574	--	-0.1707	-0.0686
1.000	39.99	0.647	-0.071	0.7681	--	-0.1727	-0.0688
0.995	45.03	0.298	-0.005	0.7967	--	-0.3522	-0.0969
1.004	60.04	0.076	-0.013	0.9978	--	-0.4325	-0.1059
0.999	70.05	0.017	-0.031	1.0620	--	-0.3464	-0.3500
0.989	80.02	0.145	-0.154	1.3147	--	-0.0850	-0.1875
0.986	90.03	0.183	-0.245	1.5133	--	0.1838	-0.0131
0.986	120.01	0.086	-0.270	1.5773	--	0.8634	0.3101
1.007	150.05	-0.060	-0.190	0.7316	--	0.6039	0.0163
1.016	180.07	-0.162	-0.123	0.4620	--	0.4622	-0.0686
1.012	210.03	0.016	-0.056	0.3624	--	0.3057	-0.1315
0.995	240.03	0.711	0.264	0.7362	--	-0.2482	0.2973
0.974	269.10	0.440	0.361	1.4237	--	-0.4176	0.2689
End of Table 45							

Table 46. Vented Aileron, Clean, δ=-90°, Re=1x10^6							
Rex10^{-6}	AOA	C_l	C_m	C_{dp}	C_{dw}	C_s	C_h
1.006	-6.06	-0.333	0.028	0.5545	--	-0.5162	0.0324
1.007	0.05	-0.104	0.050	0.5500	--	-0.5501	0.0143
1.008	3.10	-0.021	0.060	0.5406	--	-0.5409	0.0036
1.005	6.08	-0.042	0.054	0.5797	--	-0.5809	-0.0615
1.004	9.11	0.031	0.060	0.5848	--	-0.5725	-0.0684
1.006	12.08	0.084	0.064	0.5822	--	-0.5517	-0.0812
1.007	16.63	0.148	0.060	0.5837	--	-0.5169	-0.0992
1.008	18.07	0.251	0.051	0.5777	--	-0.4713	-0.1113
1.011	20.07	0.332	0.037	0.5413	--	-0.3945	-0.1186
0.990	24.04	0.346	-0.023	0.6437	--	-0.4469	-0.1491
0.994	26.99	0.425	-0.034	0.7255	--	-0.4536	-0.1548
0.997	30.04	0.426	-0.038	0.7807	--	-0.4626	-0.1629
0.996	35.04	0.646	-0.069	0.8903	--	-0.3580	-0.1581
0.997	40.00	0.649	-0.080	0.9872	--	-0.3391	-0.1619
1.006	45.08	0.569	-0.084	1.0623	--	-0.3472	-0.1643
1.004	60.05	0.243	-0.097	1.1609	--	-0.3690	-0.1681
1.006	70.06	-0.218	-0.093	1.1141	--	-0.5849	-0.1898
1.006	80.05	-0.394	-0.116	1.1215	--	-0.5819	-0.1950
1.005	90.05	-0.551	-0.140	1.0767	--	-0.5501	-0.1870
1.002	120.06	-0.120	-0.107	1.0293	--	0.4117	0.0981
1.010	150.07	0.103	-0.023	0.7191	--	0.6746	0.1225
1.009	180.07	-0.050	0.045	0.6477	--	0.6478	0.0226
1.004	210.07	0.005	0.071	0.5756	--	0.4956	-0.0640
0.980	240.02	0.327	0.175	1.0700	--	0.2514	-0.0106
0.995	269.08	0.552	0.170	1.1255	--	-0.5339	0.1493
End of Table 46							

Table 47. Vented Aileron, LEGR, δ=5°, Re=1x10^6							
Rex10^{-6}	AOA	C_l	C_m	C_{dp}	C_{dw}	C_s	C_h
1.012	-6.01	-0.291	-0.029	0.0244	0.0277	0.0029	0.0157
1.011	0.00	0.215	-0.060	0.0135	0.0187	-0.0187	0.0098
0.999	3.03	0.449	-0.058	0.0192	0.0222	0.0016	0.0081
0.995	6.03	0.665	-0.055	0.0290	0.0283	0.0417	0.0077
0.995	9.04	0.881	-0.053	0.0444	--	0.0946	0.0181
1.000	12.05	1.060	-0.056	0.0714	--	0.1515	0.0297
0.987	15.02	1.014	-0.085	0.1489	--	0.1190	0.0410
0.986	18.00	0.891	-0.115	0.2494	--	0.0381	0.0430
0.985	20.01	0.894	-0.137	0.3342	--	-0.0081	0.0452
0.993	23.99	0.930	-0.154	0.4634	--	-0.0452	0.0499
0.982	26.95	0.900	-0.167	0.5288	--	-0.0635	0.0508
End of Table 47							

Table 48. Vented Aileron, LEGR, δ=0°, Re=1x10^6							
Rex10^{-6}	AOA	C_l	C_m	C_{dp}	C_{dw}	C_s	C_h
1.011	-6.00	-0.425	0.002	0.0293	--	0.0153	0.0029
1.010	0.00	0.022	-0.018	0.0091	0.0149	-0.0149	-0.0020
1.010	3.04	0.298	-0.023	0.0116	0.0171	-0.0013	0.0029
1.008	6.04	0.520	-0.021	0.0198	0.0226	0.0322	-0.0006
1.005	9.01	0.698	-0.018	0.0293	0.0318	0.0779	0.0035
0.999	12.03	0.946	-0.019	0.0367	--	0.1613	0.0307
0.997	15.01	0.993	-0.041	0.0904	--	0.1699	0.0436
1.001	18.00	0.804	-0.071	0.1787	--	0.0785	0.0452
0.999	20.01	0.815	-0.097	0.2648	--	0.0301	0.0497
0.993	24.01	0.819	-0.117	0.3828	--	-0.0164	0.0570
0.997	26.94	0.711	-0.127	0.4339	--	-0.0647	0.0571
End of Table 48							

Table 49. Vented Aileron, LEGR, δ=-5°, Re=1x10^6							
Rex10^{-6}	AOA	C_l	C_m	C_{dp}	C_{dw}	C_s	C_h
1.011	-6.02	-0.494	0.028	0.0368	--	0.0152	-0.0060
1.006	0.00	-0.158	0.033	0.0126	0.0190	-0.0190	-0.0093
1.006	3.04	0.097	0.029	0.0087	0.0156	-0.0104	-0.0129
1.007	6.03	0.358	0.020	0.0125	0.0180	0.0197	-0.0175
1.007	9.04	0.499	0.024	0.0228	0.0242	0.0545	-0.0260
1.005	12.04	0.681	0.026	0.0376	--	0.1053	0.0160
0.999	15.04	0.838	0.015	0.0690	--	0.1508	0.0304
1.001	18.00	0.693	-0.024	0.1523	--	0.0693	0.0403
1.002	20.00	0.657	-0.050	0.2268	--	0.0116	0.0445
1.001	24.00	0.612	-0.074	0.3436	--	-0.0650	0.0504
1.001	26.96	0.628	-0.084	0.4052	--	-0.0764	0.0567
End of Table 49							

Table 50. Vented Aileron, LEGR, δ=-10°, Re=1x10^6							
Rex10^{-6}	AOA	C_l	C_m	C_{dp}	C_{dw}	C_s	C_h
1.000	-6.03	-0.415	0.045	0.0596	--	-0.0157	0.0093
1.008	0.01	-0.232	0.058	0.0209	0.0277	-0.0277	-0.0039
1.010	3.05	-0.026	0.063	0.0139	0.0206	-0.0220	-0.0189
1.014	6.04	0.189	0.061	0.0117	0.0171	0.0029	-0.0397
1.010	9.05	0.342	0.059	0.0190	0.0210	0.0331	-0.0519
1.011	12.06	0.473	0.057	0.0420	--	0.0578	-0.0146
1.008	15.04	0.640	0.049	0.0673	--	0.1011	-0.0057
0.999	18.00	0.600	0.015	0.1377	--	0.0544	0.0087
0.997	20.00	0.519	-0.004	0.1950	--	-0.0057	0.0112
0.992	23.99	0.520	-0.035	0.3116	--	-0.0733	0.0263
1.011	26.96	0.490	-0.046	0.3770	--	-0.1139	0.0360
End of Table 50							

Table 51. Vented Aileron, LEGR, δ=-20°, Re=1x10^6							
Rex10^{-6}	AOA	C_l	C_m	C_{dp}	C_{dw}	C_s	C_h
1.004	-6.02	-0.783	0.129	0.0855	--	-0.0029	-0.0124
1.002	0.00	-0.394	0.144	0.0599	--	-0.0599	-0.0412
1.005	3.03	-0.146	0.110	0.0338	--	-0.0415	-0.0350
1.006	6.04	-0.072	0.123	0.0274	--	-0.0348	-0.0731
1.007	9.03	-0.095	0.158	0.0165	--	-0.0312	-0.1586
1.006	12.02	0.097	0.158	0.0270	--	-0.0062	-0.1336
1.003	15.03	0.779	0.055	0.0826	--	0.1222	0.0448
0.996	18.01	0.624	0.035	0.1466	--	0.0535	0.0476
1.000	20.02	0.322	0.108	0.1477	--	-0.0285	-0.0317
1.001	23.98	0.308	0.060	0.2334	--	-0.0881	-0.0899
0.992	26.96	0.313	0.043	0.2965	--	-0.1224	-0.0863
End of Table 51							

Table 52. Vented Aileron, LEGR, δ=-30°, Re=1x10^6							
Rex10^{-6}	AOA	C_l	C_m	C_{dp}	C_{dw}	C_s	C_h
1.008	-6.01	-0.749	0.163	0.1336	--	-0.0544	0.0009
1.004	0.01	-0.384	0.170	0.0985	--	-0.0986	-0.0349
1.005	3.04	-0.140	0.161	0.0811	--	-0.0884	-0.0378
1.007	6.04	-0.103	0.142	0.0506	--	-0.0612	-0.0951
1.006	9.03	-0.127	0.177	0.0439	--	-0.0633	-0.1365
1.009	12.02	0.094	0.168	0.0473	--	-0.0267	-0.1179
1.005	15.04	0.371	0.138	0.0557	--	0.0425	-0.0865
1.007	18.01	0.383	0.143	0.1052	--	0.0184	-0.0989
1.001	20.00	0.144	0.177	0.1039	--	-0.0484	-0.2346
1.005	24.00	0.018	0.154	0.1541	--	-0.1335	-0.2695
0.999	26.98	0.020	0.139	0.2040	--	-0.1727	-0.2701
End of Table 52							

Table 53. Vented Aileron, LEGR, δ=-45°, Re=1x10^6							
Rex10^{-6}	AOA	C_l	C_m	C_{dp}	C_{dw}	C_s	C_h
1.009	-6.04	-0.606	0.165	0.2620	--	-0.1968	0.0194
1.018	0.03	-0.245	0.161	0.2079	--	-0.2080	-0.0006
1.002	3.05	-0.176	0.143	0.2114	--	-0.2205	-0.0560
1.002	6.04	-0.203	0.165	0.2413	--	-0.2613	-0.0716
1.002	9.06	-0.024	0.163	0.2274	--	-0.2283	-0.0649
1.005	12.04	0.178	0.154	0.2133	--	-0.1715	-0.0566
1.009	15.04	0.404	0.128	0.2026	--	-0.0908	-0.0396
0.998	18.02	0.711	0.008	0.2408	--	-0.0090	-0.0039
0.999	20.01	0.797	-0.049	0.3131	--	-0.0215	-0.0042
0.992	24.00	0.729	-0.083	0.4052	--	-0.0737	-0.0117
0.993	26.98	0.687	-0.074	0.4654	--	-0.1031	-0.0160
End of Table 53							

Table 54. Vented Aileron, LEGR, δ=-60°, Re=1x10^6							
Rex10^{-6}	AOA	C_l	C_m	C_{dp}	C_{dw}	C_s	C_h
1.007	-6.03	-0.517	0.163	0.4564	--	-0.3996	0.0311
1.011	0.02	-0.254	0.176	0.4038	--	-0.4039	0.0081
1.021	3.05	-0.172	0.129	0.3367	--	-0.3454	-0.0636
1.007	6.06	-0.227	0.156	0.3862	--	-0.4080	-0.0835
1.005	9.03	-0.156	0.166	0.3823	--	-0.4020	-0.0918
1.011	12.05	0.000	0.160	0.3602	--	-0.3523	-0.0886
1.005	15.04	0.152	0.148	0.3484	--	-0.2970	-0.0853
1.010	18.04	0.432	0.079	0.3246	--	-0.1749	-0.0693
1.002	20.01	0.560	0.015	0.3650	--	-0.1513	-0.0723
0.999	24.01	0.627	-0.045	0.4284	--	-0.1362	-0.0744
0.998	26.98	0.616	-0.053	0.4756	--	-0.1444	-0.0736
End of Table 54							

Table 55. Vented Aileron, LEGR, δ=-90°, Re=1x10^6							
Rex10^{-6}	AOA	C_l	C_m	C_{dp}	C_{dw}	C_s	C_h
1.007	-6.02	-0.207	0.041	0.5432	--	-0.5185	0.0750
1.009	0.01	0.028	0.050	0.5279	--	-0.5279	0.0416
1.014	3.05	0.033	0.061	0.4973	--	-0.4948	0.0209
1.004	6.05	-0.003	0.038	0.5650	--	-0.5622	-0.0670
1.006	9.03	-0.027	0.052	0.5804	--	-0.5774	-0.0818
1.006	12.05	0.055	0.054	0.5867	--	-0.5623	-0.0887
1.004	15.02	0.141	0.050	0.5853	--	-0.5288	-0.1025
1.011	18.03	0.232	0.027	0.5587	--	-0.4595	-0.1183
1.013	20.01	0.298	0.003	0.5638	--	-0.4278	-0.1291
1.006	24.00	0.404	-0.018	0.5910	--	-0.3756	-0.1390
1.002	26.98	0.387	-0.029	0.6649	--	-0.4170	-0.1484
End of Table 55							

Spoiler Flap, Re=1x10^6

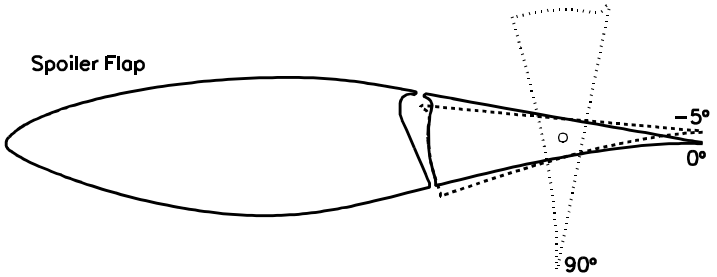

Table 56. Spoiler Flap, Clean, δ=-5°, Re=1x10^6							
Rex10^{-6}	AOA	C_l	C_m	C_{dp}	C_{dw}	C_s	C_h
0.995	-6.04	-0.696	0.044	0.0213	--	0.0520	-0.0473
0.997	0.01	-0.231	0.023	-0.0263*	--	0.0263	-0.0462
0.997	3.04	0.081	0.017	-0.0296*	--	0.0338	-0.0302
1.000	6.05	0.400	0.010	-0.0321*	--	0.0741	-0.0143
0.999	9.05	0.619	0.007	-0.0189*	0.0302	0.0675	-0.0105
0.996	12.07	0.746	0.011	0.0027	0.0441	0.1129	-0.0221
0.998	15.01	0.835	0.016	0.0196	0.0655	0.1530	-0.0295
0.995	17.99	0.902	0.003	0.0628	0.0641	0.2176	-0.0272
0.993	20.02	0.514	-0.049	0.2220	--	-0.0326	-0.0325
1.001	24.03	0.566	-0.066	0.3006	--	-0.0441	-0.0268
0.992	27.01	0.635	-0.083	0.3756	--	-0.0463	-0.0198
End of Table 56							

*Negative pressure drag due to an insufficient number of taps on the leading edge of the second airfoil element that didn't allow accurate pressure resolution in the integration of pressure drag.

Table 57. Spoiler Flap, Clean, δ=0°, Re=1x10^6							
Rex10^{-6}	AOA	C_l	C_m	C_{dp}	C_{dw}	C_s	C_h
1.000	-5.98	-0.530	-0.026	0.0179	0.0115	0.0438	-0.0145
1.007	-0.02	0.121	-0.045	0.0142	0.0098	-0.0098	0.0167
1.010	2.99	0.458	-0.054	0.0219	0.0100	0.0139	0.0334
1.010	6.01	0.758	-0.058	0.0236	0.0112	0.0682	0.0478
1.009	9.00	0.837	-0.042	0.0422	--	0.0893	0.0216
1.007	12.00	0.957	-0.040	0.0659	--	0.1345	0.0232
1.003	15.00	1.039	-0.043	0.0998	--	0.1725	0.0303
0.990	17.95	0.955	-0.067	0.1676	--	0.1349	0.0389
1.021	19.97	0.617	-0.112	0.3254	--	-0.0951	0.0418
1.004	23.99	0.705	-0.135	0.4271	--	-0.1036	0.0499
0.993	26.98	0.848	-0.172	0.5523	--	-0.1075	0.0604
0.985	29.96	0.986	-0.210	0.6936	--	-0.1085	0.0715
1.002	34.95	1.127	-0.267	0.9182	--	-0.1070	0.0834
0.992	39.93	1.198	-0.314	1.1341	--	-0.1007	0.0960
0.980	44.95	1.197	-0.348	1.3175	--	-0.0868	0.1014
0.999	59.95	1.062	-0.467	1.8928	--	-0.0286	0.1261
0.985	70.01	0.807	-0.542	2.1816	--	0.0126	0.1426
1.000	79.96	0.485	-0.587	2.3273	--	0.0718	0.1499
0.996	89.99	0.127	-0.617	2.3281	--	0.1266	0.1473
1.039	119.96	-0.759	-0.627	1.7725	--	0.2276	0.1118
1.003	150.01	-0.635	-0.388	0.5710	--	0.1771	0.0191
1.019	180.00	-0.013	-0.030	0.0077	--	0.0077	0.0008
0.994	210.00	0.609	0.366	0.5605	--	0.1809	-0.0057
0.921	239.97	0.744	0.627	1.7779	--	0.2456	-0.1003
0.958	269.01	-0.060	0.621	2.3193	--	0.1001	-0.1567
End of Table 57							

Table 58. Spoiler Flap, Clean, δ=5°, Re=1x10^6							
Rex10^{-6}	AOA	C_l	C_m	C_{dp}	C_{dw}	C_s	C_h
1.005	-6.01	-0.302	-0.062	0.0247	0.0202	0.0115	0.0324
1.005	-0.02	0.327	-0.081	0.0252	0.0216	-0.0217	0.0621
1.004	2.98	0.627	-0.085	0.0218	0.0268	0.0058	0.0836
1.001	6.02	0.853	-0.110	0.0307	0.0337	0.0559	0.0644
0.997	9.05	0.845	-0.066	0.0458	--	0.0877	0.0198
1.004	12.02	1.002	-0.058	0.0652	--	0.1449	0.0248
1.004	15.01	1.106	-0.063	0.0972	--	0.1926	0.0331
0.985	17.98	0.732	0.143	0.3124	--	-0.0712	0.0443
0.985	19.99	0.714	-0.141	0.3440	--	-0.0792	0.0465
1.001	24.01	0.795	-0.163	0.4472	--	-0.0850	0.0536
0.990	27.01	0.954	-0.203	0.5881	--	-0.0907	0.0623
End of Table 58							

Table 59. Spoiler Flap, Clean, δ=10°, Re=1x10^6							
Rex10^{-6}	AOA	C_l	C_m	C_{dp}	C_{dw}	C_s	C_h
1.008	-6.01	-0.343	-0.091	0.0189	--	0.0171	0.0471
1.008	-0.01	-0.035	-0.052	0.0233	--	-0.0233	-0.0062
1.010	2.99	0.200	-0.049	0.0294	--	-0.0189	-0.0015
1.008	6.00	0.488	-0.057	0.0400	--	0.0112	0.0069
1.008	9.00	0.724	-0.075	0.0749	--	0.0393	0.0153
1.008	12.01	0.948	-0.078	0.0981	--	0.1013	0.0200
1.007	15.01	1.123	-0.081	0.1316	--	0.1637	0.0225
0.987	17.97	0.763	-0.157	0.3514	--	-0.0989	0.0273
0.994	19.95	0.767	-0.163	0.3965	--	-0.1110	0.0294
0.995	23.98	0.870	-0.192	0.5226	--	-0.1239	0.0375
0.992	27.01	1.026	-0.233	0.6727	--	-0.1334	0.0493
End of Table 59							

Table 60. Spoiler Flap, Clean, δ=20°, Re=1x10^6							
Rex10^{-6}	AOA	C_l	C_m	C_{dp}	C_{dw}	C_s	C_h
1.004	-6.00	-0.826	0.030	0.1040	--	-0.0171	-0.0142
1.004	-0.02	-0.123	-0.067	0.1291	--	-0.1291	0.0055
1.003	2.98	0.127	-0.070	0.1408	--	-0.1340	0.0105
1.003	6.00	0.390	-0.078	0.1558	--	-0.1142	0.0146
1.006	9.01	0.652	-0.105	0.1546	--	-0.0506	0.0244
1.003	11.97	0.891	-0.118	0.1739	--	0.0147	0.0194
1.009	15.00	1.081	-0.121	0.1915	--	0.0948	0.0203
0.997	17.96	0.843	-0.193	0.3998	--	-0.1204	0.0192
0.995	19.96	0.865	-0.204	0.4543	--	-0.1317	0.0227
0.986	24.01	1.009	-0.241	0.6070	--	-0.1439	0.0342
0.987	27.00	1.161	-0.284	0.7670	--	-0.1563	0.0445
End of Table 60							

Table 61. Spoiler Flap, Clean, δ=30°, Re=1x10^6							
Rex10^{-6}	AOA	C_l	C_m	C_{dp}	C_{dw}	C_s	C_h
1.003	-6.01	-0.704	-0.016	0.2130	--	-0.1381	-0.0064
1.001	0.00	-0.077	-0.092	0.2456	--	-0.2456	0.0203
1.000	3.01	0.158	-0.097	0.2588	--	-0.2501	0.0259
0.997	5.99	0.386	-0.096	0.2646	--	-0.2229	0.0288
0.999	9.01	0.658	-0.142	0.2790	--	-0.1725	0.0314
1.002	12.01	0.877	-0.150	0.2859	--	-0.0971	0.0255
1.002	14.99	1.104	-0.161	0.3073	--	-0.0113	0.0255
0.977	17.98	0.984	-0.220	0.4762	--	-0.1492	0.0160
1.002	19.98	0.994	-0.231	0.5380	--	-0.1660	0.0190
0.994	24.00	1.081	-0.262	0.6894	--	-0.1901	0.0266
0.994	26.99	1.214	-0.302	0.8544	--	-0.2104	0.0339
End of Table 61							

Table 62. Spoiler Flap, Clean, δ=45°, Re=1x10^6							
Rex10^{-6}	AOA	C_l	C_m	C_{dp}	C_{dw}	C_s	C_h
1.005	-5.96	-0.427	-0.073	0.3302	--	-0.2841	0.0012
0.996	-0.01	0.055	-0.123	0.3695	--	-0.3695	0.0517
0.997	2.99	0.263	-0.121	0.3864	--	-0.3722	0.0552
0.996	6.00	0.445	-0.114	0.4001	--	-0.3514	0.0506
0.999	9.01	0.567	-0.140	0.4197	--	-0.3257	0.0248
1.003	12.02	0.816	-0.165	0.4189	--	-0.2398	0.0131
1.004	15.00	1.068	-0.181	0.4166	--	-0.1260	0.0047
0.996	17.97	0.992	-0.240	0.6140	--	-0.2780	0.0019
0.997	19.96	0.964	-0.243	0.6681	--	-0.2989	0.0030
1.008	23.97	1.022	-0.269	0.8240	--	-0.3377	0.0063
0.990	26.98	1.160	-0.311	1.0089	--	-0.3728	0.0100
0.999	29.98	1.210	-0.339	1.1549	--	-0.3902	0.0165
0.988	34.95	1.252	-0.375	1.3684	--	-0.4044	0.0195
0.989	39.96	1.246	-0.409	1.5778	--	-0.4091	0.0272
0.982	44.96	1.166	-0.434	1.7472	--	-0.4124	0.0316
1.009	59.97	0.760	-0.485	2.1187	--	-0.4023	0.0441
0.989	70.00	0.406	-0.530	2.2919	--	-0.4024	0.0566
1.011	79.95	0.018	-0.536	2.2690	--	-0.3782	0.0612
0.997	89.99	-0.324	-0.535	2.1284	--	-0.3244	0.0562
1.034	119.98	-0.965	-0.487	1.2721	--	-0.2002	0.0471
1.006	149.99	-0.266	-0.197	0.4024	--	0.2154	0.0788
0.993	180.02	0.374	0.182	0.4630	--	0.4629	0.0178
0.995	209.98	0.091	0.208	0.7616	--	0.6142	-0.0379
0.968	239.97	0.326	0.444	1.6062	--	0.5216	-0.1280
0.986	268.99	-0.003	0.337	1.6402	--	0.0319	0.0112
End of Table 62							

Table 63. Spoiler Flap, Clean, δ=60°, Re=1x10^6							
Rex10^{-6}	AOA	C_l	C_m	C_{dp}	C_{dw}	C_s	C_h
1.005	-6.06	-0.025	-0.132	0.4749	--	-0.4696	0.0865
0.994	0.03	0.287	-0.122	0.5139	--	-0.5137	0.0820
0.997	3.03	0.297	-0.112	0.5126	--	-0.4962	0.0580
1.003	6.02	0.414	-0.131	0.4989	--	-0.4527	0.0141
1.005	9.05	0.579	-0.163	0.4609	--	-0.3641	-0.0175
1.007	12.06	0.687	-0.178	0.4731	--	-0.3191	-0.0384
1.001	15.04	0.651	-0.161	0.5380	--	-0.3506	-0.0365
0.988	18.00	0.622	-0.158	0.6051	--	-0.3833	-0.0425
0.996	19.98	0.478	-0.182	0.7664	--	-0.5569	-0.0718
1.000	24.02	0.527	-0.202	0.9228	--	-0.6284	-0.0817
1.014	27.02	0.562	-0.211	1.0035	--	-0.6386	-0.0884
1.003	29.99	0.594	-0.217	1.0729	--	-0.6323	-0.0921
1.003	34.97	0.619	-0.233	1.2193	--	-0.6444	-0.0929
1.012	39.98	0.622	-0.259	1.3963	--	-0.6703	-0.0937
0.988	44.98	0.585	-0.280	1.5525	--	-0.6847	-0.0880
1.001	59.98	0.323	-0.322	1.8541	--	-0.6479	-0.0814
0.992	70.01	0.060	-0.340	1.9100	--	-0.5966	-0.0790
1.005	79.98	-0.199	-0.338	1.8212	--	-0.5128	-0.0733
1.001	89.99	-0.444	-0.335	1.6633	--	-0.4443	-0.0632
1.011	120.00	-0.944	-0.328	0.7418	--	-0.4466	-0.0072
1.004	150.00	0.008	-0.029	0.5158	--	0.4507	0.0721
0.988	180.01	0.199	0.128	0.6815	--	0.6815	-0.0140
0.992	210.01	-0.034	0.117	0.7876	--	0.6990	-0.0706
0.988	240.01	0.179	0.336	1.5047	--	0.5971	-0.1648
0.996	269.01	0.259	0.185	1.3840	--	-0.2350	-0.0224
End of Table 63							

Table 64. Spoiler Flap, Clean, δ=90°, Re=1x10^6							
Rex10^{-6}	AOA	C_l	C_m	C_{dp}	C_{dw}	C_s	C_h
1.000	-6.06	0.028	-0.069	0.6433	--	-0.6427	0.0830
1.003	0.03	0.116	-0.050	0.6135	--	-0.6134	0.0413
0.998	3.04	0.116	-0.045	0.6414	--	-0.6343	0.0269
0.995	6.07	0.184	-0.037	0.6538	--	-0.6307	0.0195
0.995	9.02	0.254	-0.032	0.6475	--	-0.5997	0.0037
0.998	12.05	0.319	-0.034	0.6394	--	-0.5587	-0.0164
0.999	15.04	0.378	-0.039	0.6386	--	-0.5186	-0.0306
1.004	18.00	0.400	-0.025	0.6247	--	-0.4705	-0.0476
1.008	20.00	0.420	-0.025	0.6186	--	-0.4376	-0.0616
0.992	24.01	0.365	-0.057	0.7863	--	-0.5697	-0.0940
0.994	27.00	0.399	-0.063	0.8760	--	-0.5994	-0.0965
0.998	30.02	0.476	-0.063	0.8536	--	-0.5009	-0.1051
0.981	34.99	0.497	-0.066	0.9449	--	-0.4891	-0.1091
0.985	39.97	0.512	-0.075	1.0544	--	-0.4792	-0.1152
0.985	44.98	0.478	-0.080	1.1407	--	-0.4690	-0.1180
1.010	60.00	0.157	-0.098	1.3043	--	-0.5162	-0.1177
1.026	70.02	-0.026	-0.109	1.3132	--	-0.4731	-0.1152
1.016	80.00	-0.213	-0.116	1.2595	--	-0.4285	-0.1078
1.041	90.04	-0.621	-0.115	0.9884	--	-0.6203	-0.0806
1.028	120.02	-0.348	-0.223	0.9997	--	0.1988	-0.0045
1.011	150.00	-0.001	-0.134	0.7345	--	0.6356	-0.0168
1.015	180.04	-0.191	-0.097	0.7195	--	0.7196	-0.0711
1.019	210.00	-0.141	-0.052	0.6163	--	0.6042	-0.0997
1.016	239.98	0.336	0.169	1.0329	--	0.2258	-0.0448
1.007	268.99	0.555	0.198	1.1527	--	-0.5346	0.0965
End of Table 64							

Table 65. Spoiler Flap, LEGR, δ=-5°, Re=1x10^6							
Rex10^{-6}	AOA	C_l	C_m	C_{dp}	C_{dw}	C_s	C_h
0.997	-5.98	-0.547	0.030	0.0356	--	0.0216	-0.0019
0.996	0.01	-0.279	0.037	0.0037	0.0296	-0.0296	-0.0603
0.998	3.00	-0.064	0.039	0.0156	0.0329	-0.0362	-0.0582
0.997	6.03	0.200	0.038	0.0111	0.0379	-0.0167	-0.0485
0.996	9.03	0.428	0.038	0.0015	0.0456	0.0221	-0.0456
1.007	12.03	0.619	0.031	0.0079	0.0566	0.0737	-0.0454
1.001	15.00	0.703	0.034	0.0271	0.0754	0.1091	-0.0516
1.009	18.00	0.701	0.007	0.0915	--	0.1296	-0.0505
0.996	20.00	0.624	-0.022	0.1689	--	0.0547	-0.0497
0.994	24.01	0.646	-0.055	0.2967	--	-0.0082	-0.0449
0.996	27.00	0.709	-0.064	0.3588	--	0.0022	-0.0395
End of Table 65							

Table 66. Spoiler Flap, LEGR, δ=0°, Re=1x10^6							
Rex10^{-6}	AOA	C_l	C_m	C_{dp}	C_{dw}	C_s	C_h
0.997	-6.01	-0.526	0.016	0.0319	--	0.0233	-0.0152
0.997	0.00	-0.011	-0.023	0.0088	0.0151	-0.0151	0.0052
0.999	3.01	0.255	-0.026	0.0142	0.0175	-0.0041	0.0101
0.996	6.04	0.469	-0.025	0.0257	--	0.0238	0.0031
1.000	9.04	0.650	-0.024	0.0414	--	0.0612	0.0040
0.991	12.02	0.783	-0.023	0.0656	--	0.0989	0.0104
0.999	15.01	0.867	-0.030	0.1015	--	0.1265	0.0169
1.002	17.97	0.700	-0.073	0.2019	--	0.0239	0.0226
0.997	19.98	0.702	-0.095	0.2675	--	-0.0115	0.0275
1.010	23.98	0.692	-0.120	0.3796	--	-0.0656	0.0315
0.999	27.01	0.777	-0.128	0.4496	--	-0.0477	0.0362
End of Table 66							

Table 67. Spoiler Flap, LEGR, δ=5°, Re=1x10^6							
Rex10^{-6}	AOA	C_l	C_m	C_{dp}	C_{dw}	C_s	C_h
1.001	-6.01	-0.182	-0.043	0.0019	0.0337	-0.0145	0.0547
1.002	0.01	0.215	-0.068	0.0027	0.0274	-0.0274	0.0596
1.002	3.00	0.457	-0.083	0.0188	0.0363	-0.0123	0.0465
1.002	6.04	0.593	-0.069	0.0378	--	0.0248	0.0175
1.001	9.02	0.754	-0.058	0.0537	--	0.0652	0.0168
0.999	12.02	0.912	-0.056	0.0772	--	0.1144	0.0251
1.012	15.02	0.984	-0.061	0.1173	--	0.1417	0.0314
0.994	17.99	0.819	-0.105	0.2211	--	0.0427	0.0403
1.001	19.98	0.786	-0.125	0.2897	--	-0.0037	0.0456
1.003	23.97	0.882	-0.158	0.4269	--	-0.0318	0.0551
1.012	27.00	0.795	-0.156	0.4683	--	-0.0563	0.0538
End of Table 67							

Table 68. Spoiler Flap, LEGR, δ=10°, Re=1x10^6							
Rex10^{-6}	AOA	C_l	C_m	C_{dp}	C_{dw}	C_s	C_h
1.000	-5.97	-0.681	0.022	0.0280	--	0.0430	-0.0086
0.996	0.06	-0.128	-0.016	0.0264	--	-0.0265	-0.0144
0.998	3.02	0.218	-0.050	0.0449	--	-0.0333	0.0007
0.998	6.05	0.467	-0.069	0.0672	--	-0.0176	0.0044
0.995	9.03	0.701	-0.077	0.0878	--	0.0233	0.0112
0.992	12.05	0.911	-0.079	0.1149	--	0.0778	0.0167
1.008	15.02	1.015	-0.084	0.1533	--	0.1150	0.0204
0.997	17.98	0.877	-0.130	0.2720	--	0.0120	0.0264
1.004	19.99	0.870	-0.156	0.3584	--	-0.0394	0.0321
0.996	23.98	0.948	-0.182	0.4913	--	-0.0636	0.0388
1.001	27.00	0.871	-0.190	0.5539	--	-0.0981	0.0384
End of Table 68							

Table 69. Spoiler Flap, LEGR, δ=20°, Re=1x10^6							
Rex10^{-6}	AOA	C_l	C_m	C_{dp}	C_{dw}	C_s	C_h
1.003	-6.00	-0.870	0.045	0.1076	--	-0.0161	-0.0107
1.003	0.01	-0.222	-0.018	0.1240	--	-0.1240	-0.0074
1.003	3.02	0.114	-0.054	0.1234	--	-0.1172	-0.0020
1.002	6.01	0.447	-0.103	0.1421	--	-0.0945	0.0216
0.999	9.04	0.669	-0.119	0.1715	--	-0.0642	0.0152
0.998	12.02	0.884	-0.123	0.1852	--	0.0030	0.0165
1.000	15.02	0.993	-0.131	0.2109	--	0.0536	0.0151
0.989	17.99	0.984	-0.185	0.3547	--	-0.0334	0.0211
1.001	19.98	1.009	-0.204	0.4379	--	-0.0668	0.0249
0.995	24.01	0.981	-0.220	0.5460	--	-0.0996	0.0305
1.005	27.01	1.108	-0.269	0.7155	--	-0.1343	0.0403
End of Table 69							

Table 70. Spoiler Flap, LEGR, δ=30°, Re=1x10^6							
Rex10^{-6}	AOA	C_l	C_m	C_{dp}	C_{dw}	C_s	C_h
0.998	-5.99	-0.758	0.004	0.2110	--	-0.1307	-0.0079
1.001	0.04	-0.165	-0.049	0.2370	--	-0.2371	0.0029
0.998	2.99	0.096	-0.064	0.2411	--	-0.2358	0.0107
0.997	6.03	0.433	-0.135	0.2544	--	-0.2075	0.0278
0.995	9.02	0.666	-0.155	0.2887	--	-0.1807	0.0225
0.999	12.03	0.860	-0.156	0.2991	--	-0.1133	0.0219
1.002	15.03	1.039	-0.166	0.3126	--	-0.0325	0.0208
1.000	17.98	1.070	-0.202	0.4120	--	-0.0616	0.0159
1.007	19.99	1.074	-0.218	0.4951	--	-0.0981	0.0185
1.001	24.01	1.027	-0.241	0.6173	--	-0.1460	0.0225
1.011	27.02	1.139	-0.281	0.7831	--	-0.1802	0.0308
End of Table 70							

Table 71. Spoiler Flap, LEGR, δ=45°, Re=1x10^6							
Rex10^{-6}	AOA	C_l	C_m	C_{dp}	C_{dw}	C_s	C_h
1.007	-6.01	-0.411	-0.076	0.3329	--	-0.2880	0.0194
1.002	0.00	0.033	-0.096	0.3611	--	-0.3611	0.0280
0.998	3.03	0.245	-0.099	0.3791	--	-0.3656	0.0356
1.000	6.01	0.368	-0.133	0.3885	--	-0.3478	0.0194
1.000	9.05	0.597	-0.169	0.4182	--	-0.3191	0.0112
1.002	12.03	0.826	-0.183	0.4246	--	-0.2431	0.0059
1.006	15.04	1.004	-0.194	0.4042	--	-0.1298	-0.0091
0.998	18.00	0.972	-0.211	0.5227	--	-0.1967	-0.0022
1.007	19.98	0.988	-0.226	0.6095	--	-0.2352	0.0000
0.993	24.00	0.951	-0.245	0.7396	--	-0.2888	0.0027
1.002	27.01	1.069	-0.288	0.9346	--	-0.3472	0.0070
End of Table 71							

Table 72. Spoiler Flap, LEGR, δ=60°, Re=1x10^6							
Rex10^{-6}	AOA	C_l	C_m	C_{dp}	C_{dw}	C_s	C_h
1.002	-6.04	0.015	-0.104	0.4711	--	-0.4701	0.0626
0.998	0.02	0.312	-0.104	0.5138	--	-0.5137	0.0687
1.006	3.02	0.291	-0.089	0.4920	--	-0.4760	0.0499
1.020	6.04	0.374	-0.157	0.4670	--	-0.4250	-0.0092
1.006	9.03	0.535	-0.178	0.4639	--	-0.3742	-0.0331
1.004	12.03	0.615	-0.178	0.4901	--	-0.3512	-0.0412
0.996	15.01	0.565	-0.166	0.5719	--	-0.4061	-0.0382
1.009	17.99	0.510	-0.169	0.6549	--	-0.4654	-0.0536
1.004	19.99	0.477	-0.161	0.6756	--	-0.4718	-0.0609
1.006	23.99	0.513	-0.180	0.8245	--	-0.5447	-0.0748
1.004	27.02	0.538	-0.198	0.9448	--	-0.5973	-0.0824
End of Table 72							

Table 73. Spoiler Flap, LEGR, δ=90°, Re=1x10^6							
Rex10^{-6}	AOA	C_l	C_m	C_{dp}	C_{dw}	C_s	C_h
0.995	-6.01	0.201	-0.064	0.6455	--	-0.6630	0.0934
1.011	-0.01	0.223	-0.045	0.5306	--	-0.5306	0.0582
1.003	3.02	0.162	-0.051	0.5481	--	-0.5388	0.0049
1.007	6.01	0.151	-0.054	0.6256	--	-0.6063	-0.0013
1.010	9.04	0.194	-0.045	0.6372	--	-0.5988	-0.0151
1.007	12.03	0.272	-0.041	0.6403	--	-0.5695	-0.0280
1.002	15.04	0.323	-0.037	0.6346	--	-0.5290	-0.0417
1.011	18.00	0.333	-0.035	0.6132	--	-0.4803	-0.0638
0.990	20.00	0.340	-0.034	0.6227	--	-0.4689	-0.0761
1.026	24.01	0.368	-0.043	0.6848	--	-0.4758	-0.0869
0.996	26.99	0.370	-0.048	0.7426	--	-0.4938	-0.0949
End of Table 73							

Appendix C: Pressure Distributions

List of Figures Page

S809 Baselline Configuration

Pressure Distributions, Re = 1 million

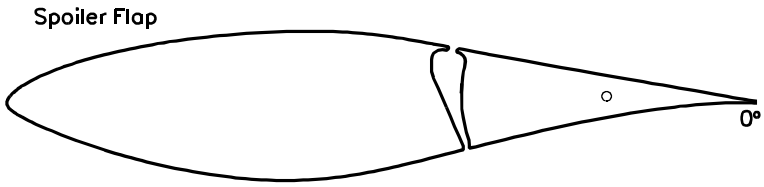

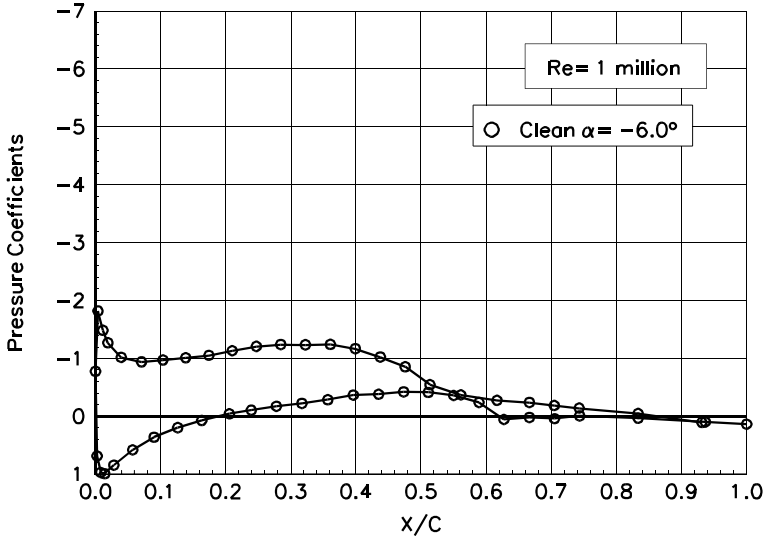

Figure 1. Baseline, α = -6.0°

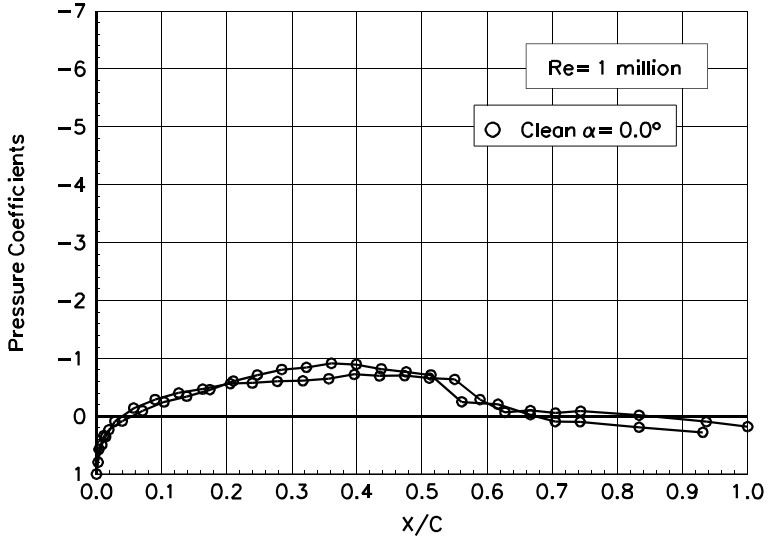

Figure 2. Baseline, α = 0.0°

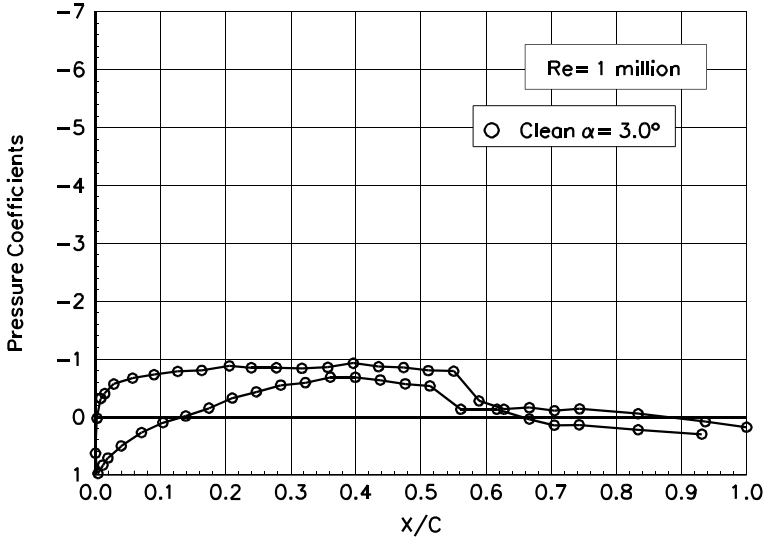

Figure 3. Baseline, α = 3.0°

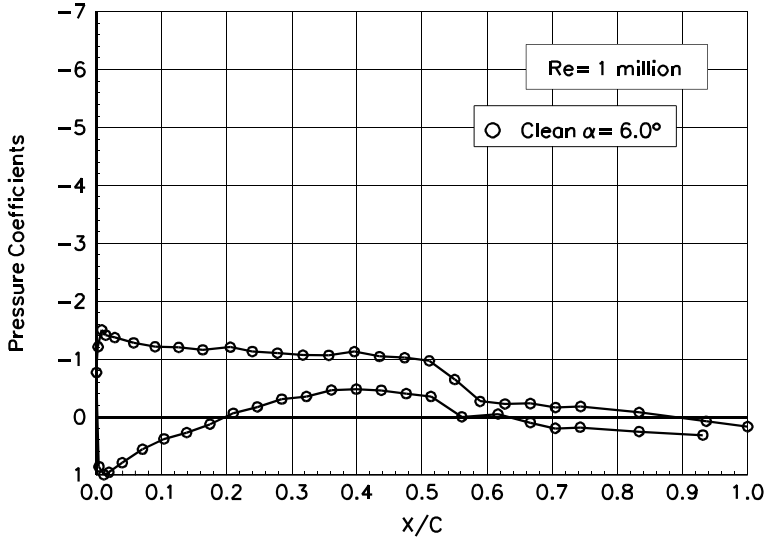

Figure 4. Baseline, α = 6.0°

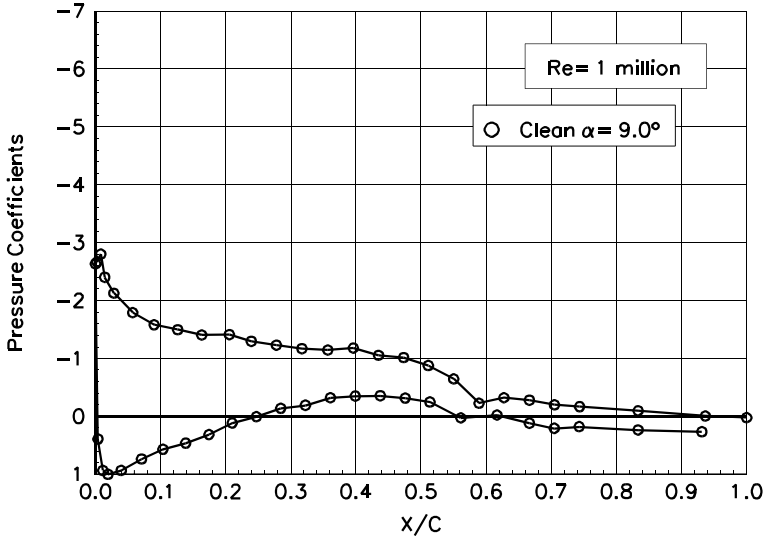

Figure 5. Baseline, α = 9.0°

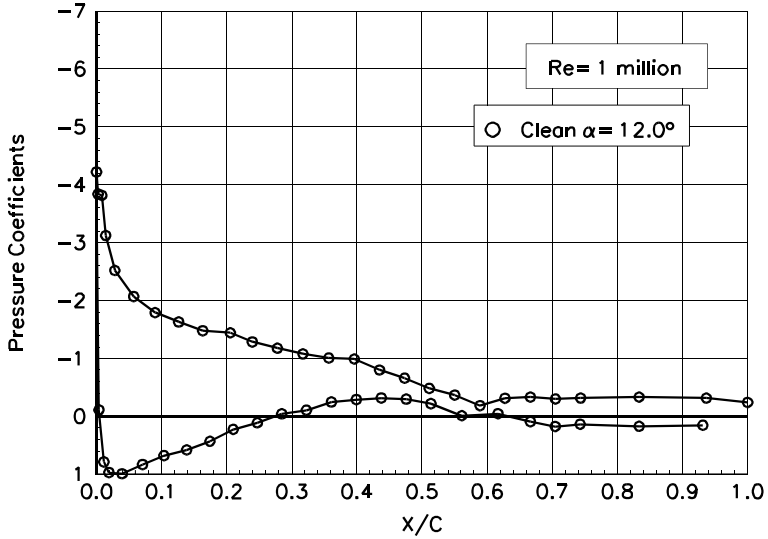

Figure 6. Baseline, α = 12.0°

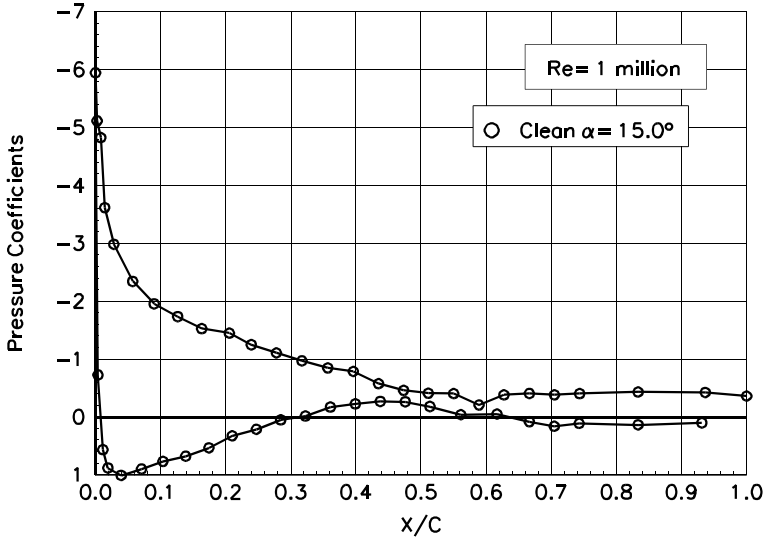

Figure 7. Baseline, α = 15.0°

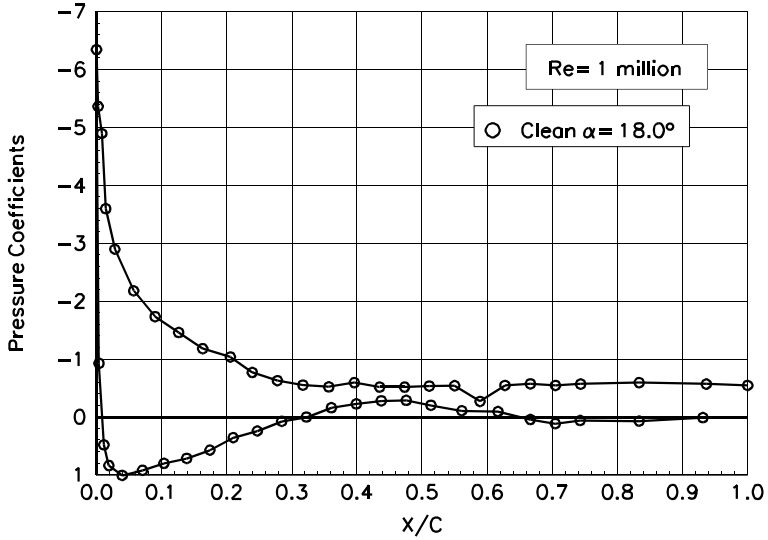

Figure 8. Baseline, α = 18.0°

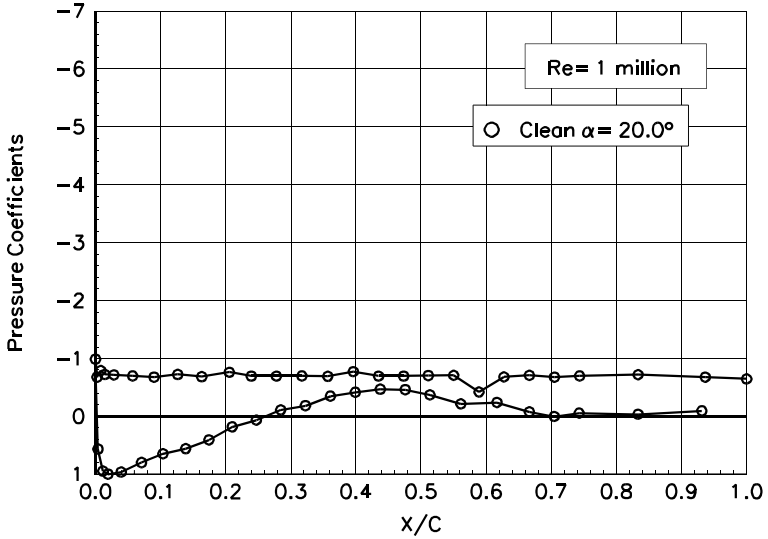

Figure 9. Baseline, α = 20.0°

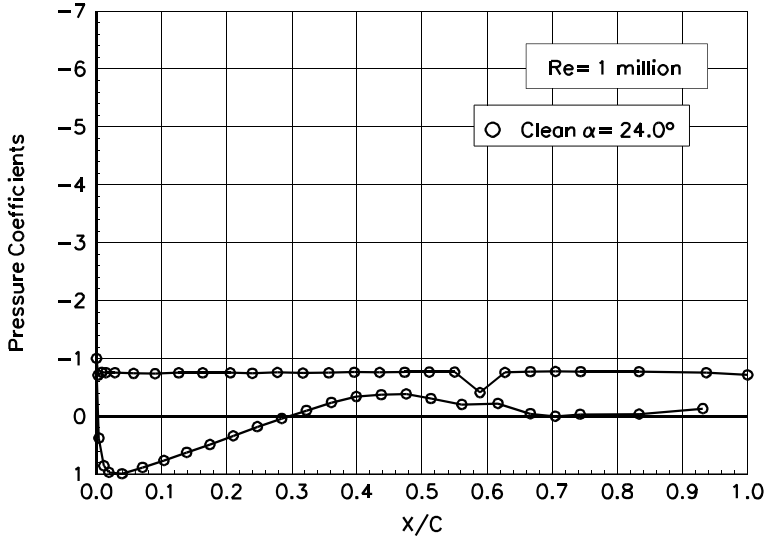

Figure 10. Baseline, α = 24.0°

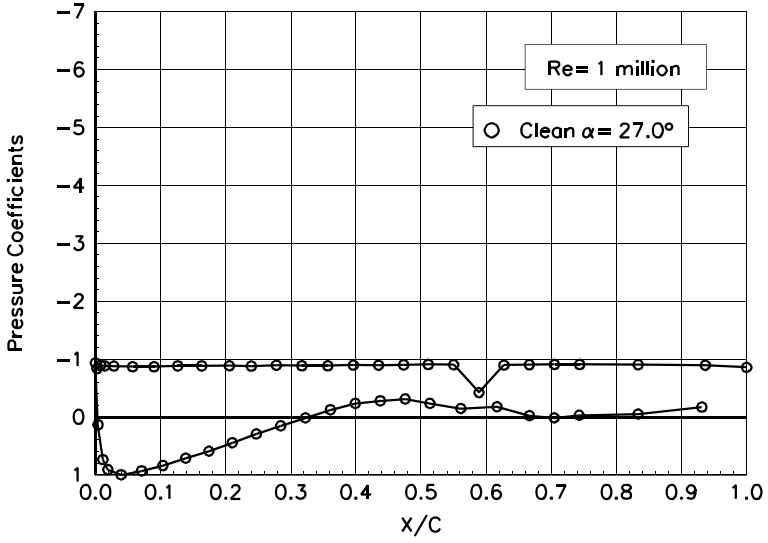

Figure 11. Baseline, α = 27.0°

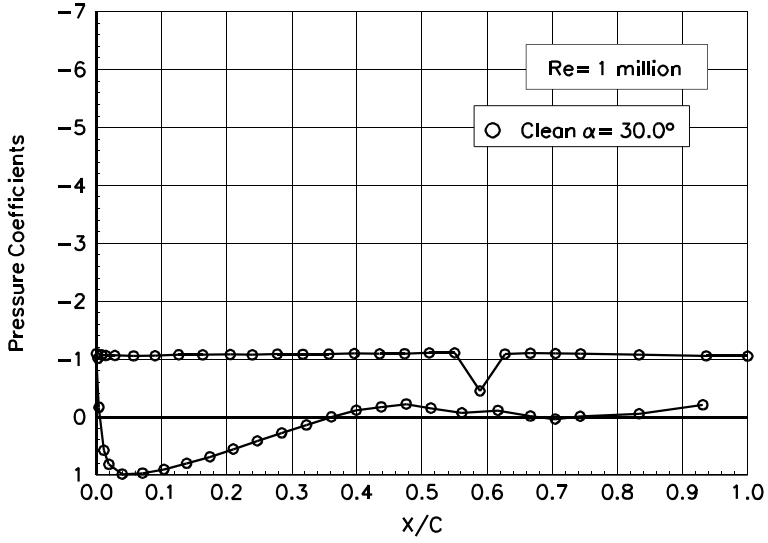

Figure 12. Baseline, α = 30.0°

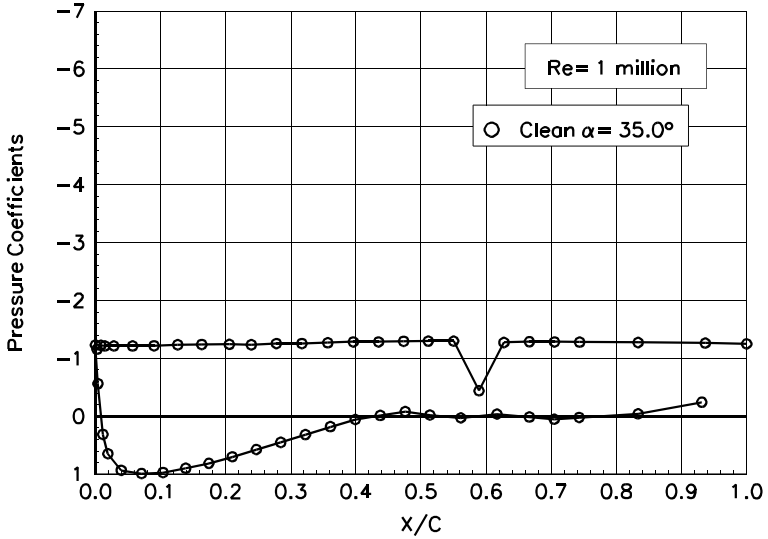

Figure 13. Baseline, α = 35.0°

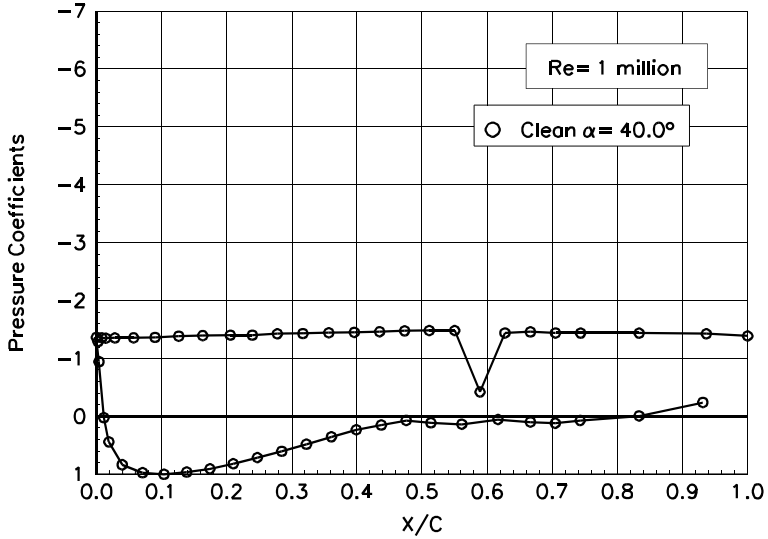

Figure 14. Baseline, α = 40.0°

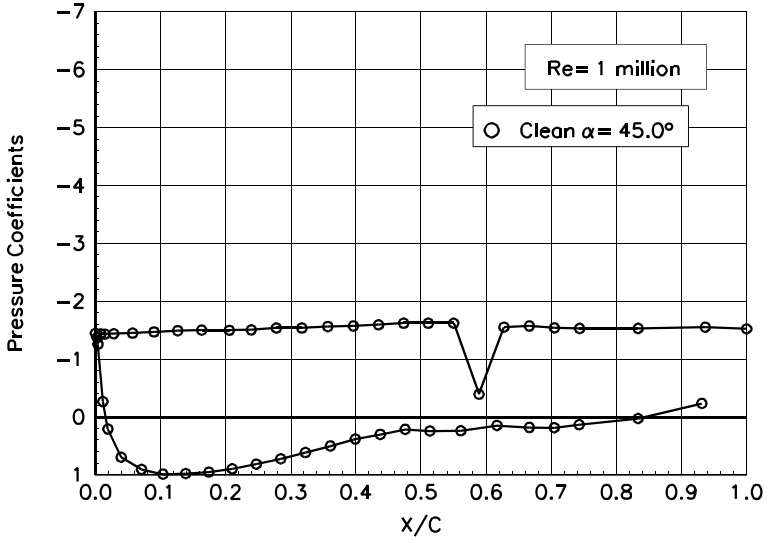

Figure 15. Baseline, α = 45.0°

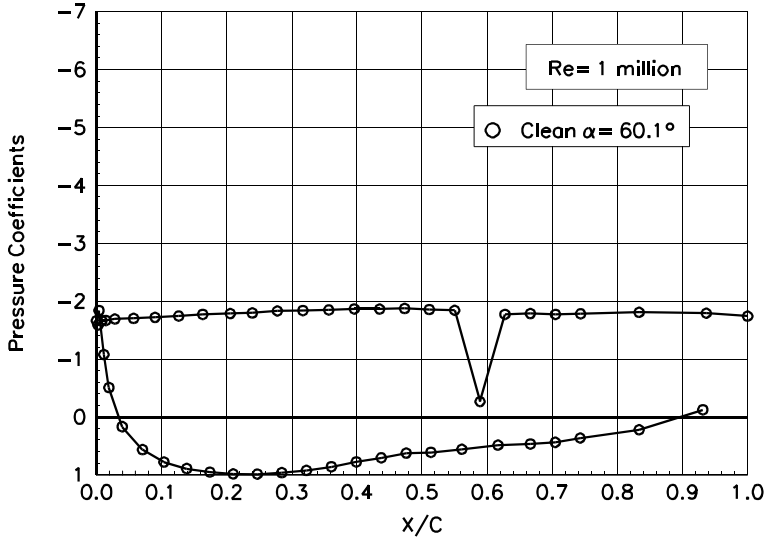

Figure 16. Baseline, α = 60.1°

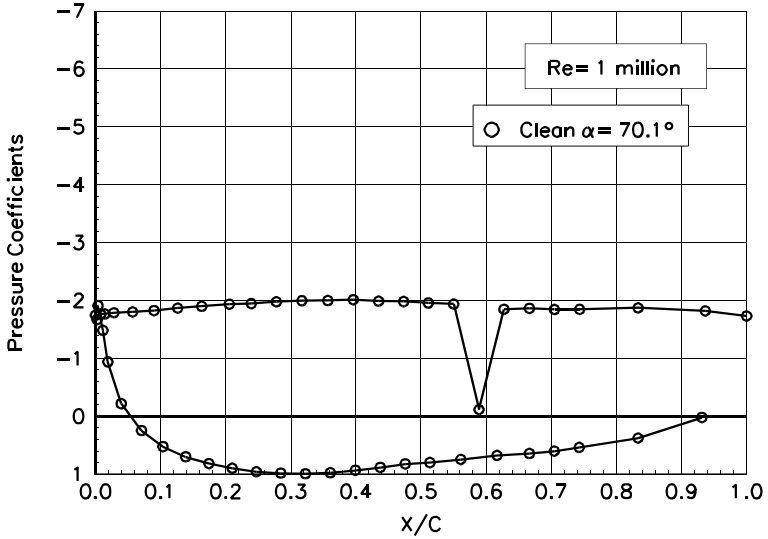

Figure 17. Baseline, α = 70.1°

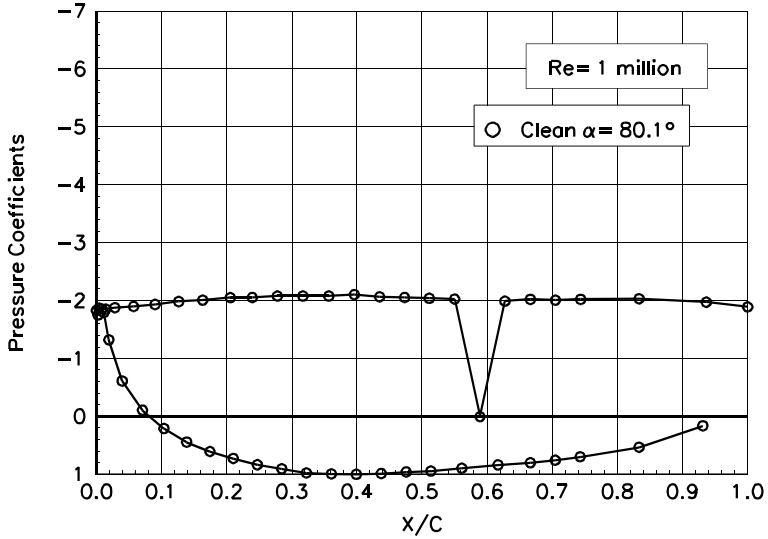

Figure 18. Baseline, α = 80.1°

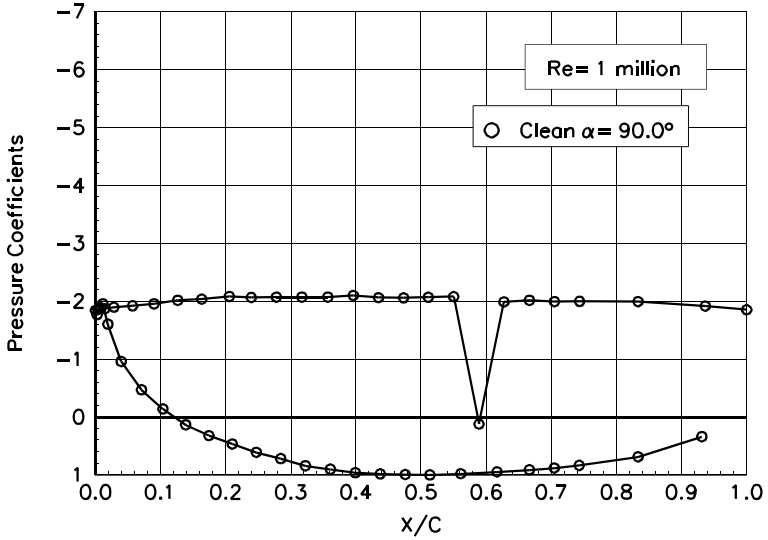

Figure 19. Baseline, α = 90.0°

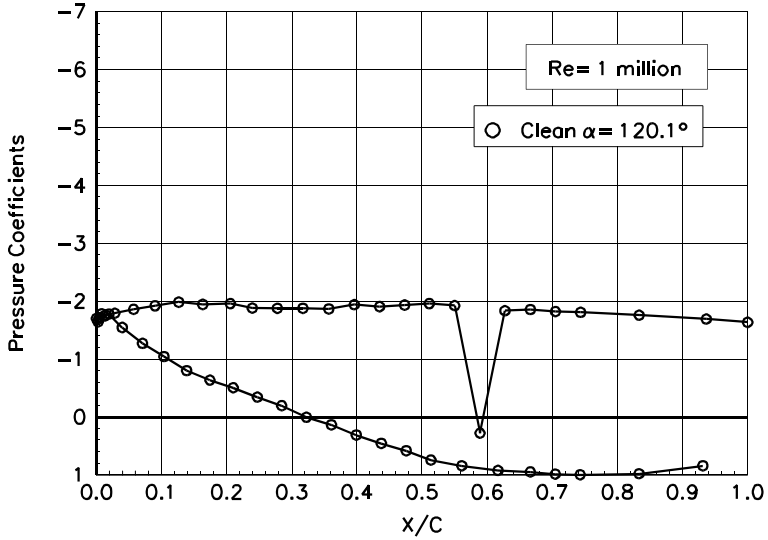

Figure 20. Baseline, α = 120.1°

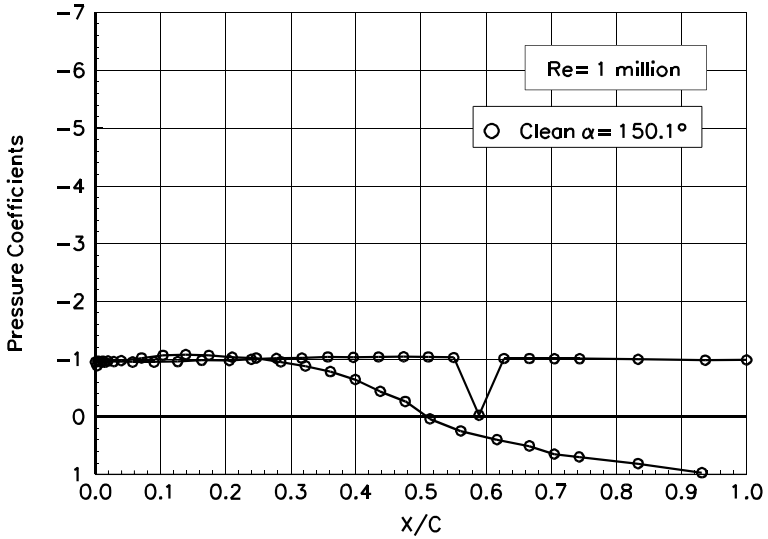

Figure 21. Baseline, α = 150.1°

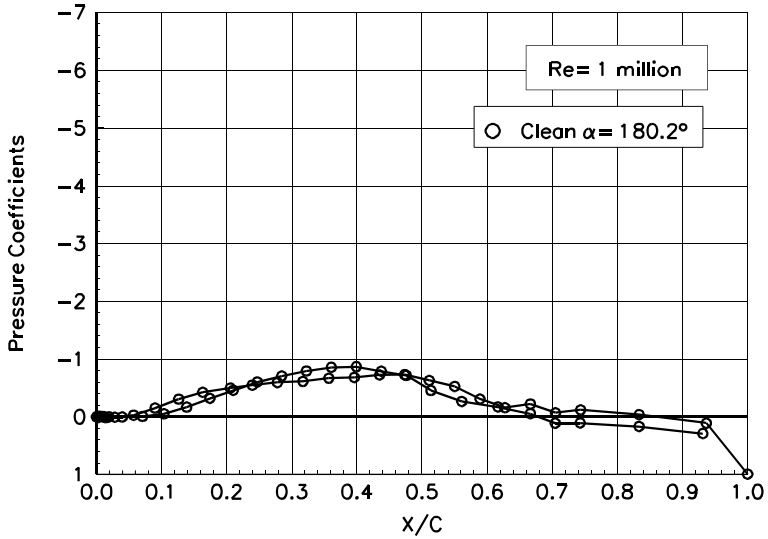

Figure 22. Baseline, α = 180.2°

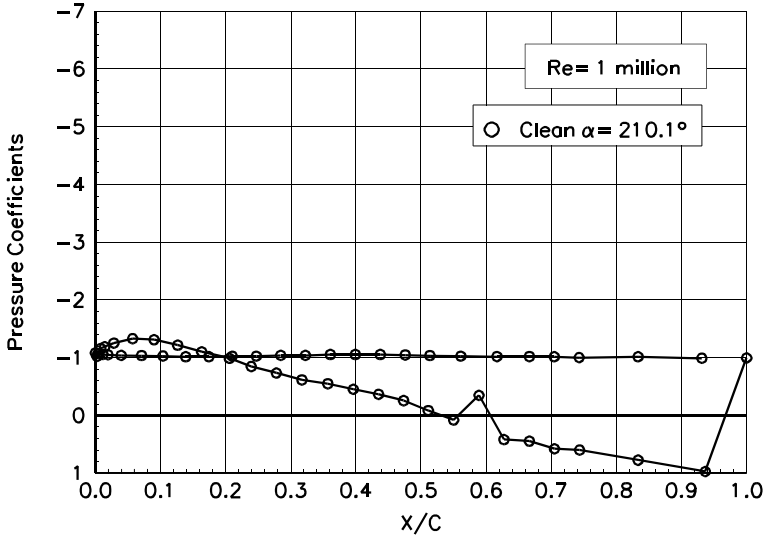

Figure 23. Baseline, α = 210.0°

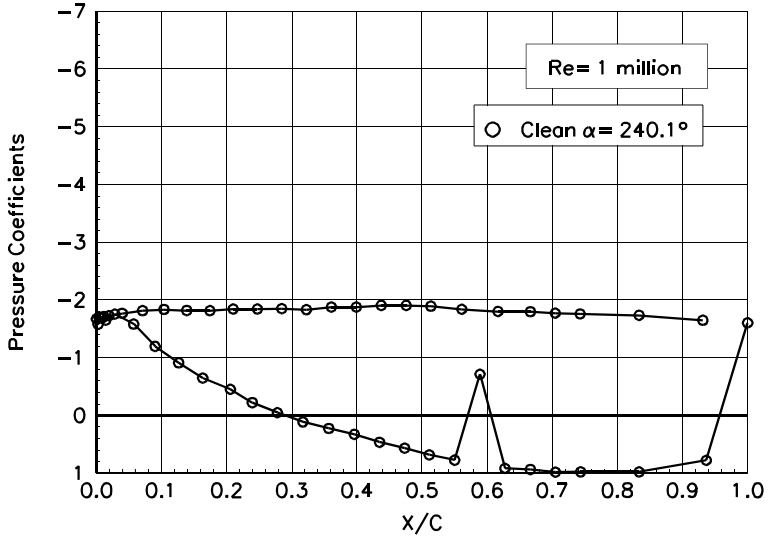

Figure 24. Baseline, α = 240.1°

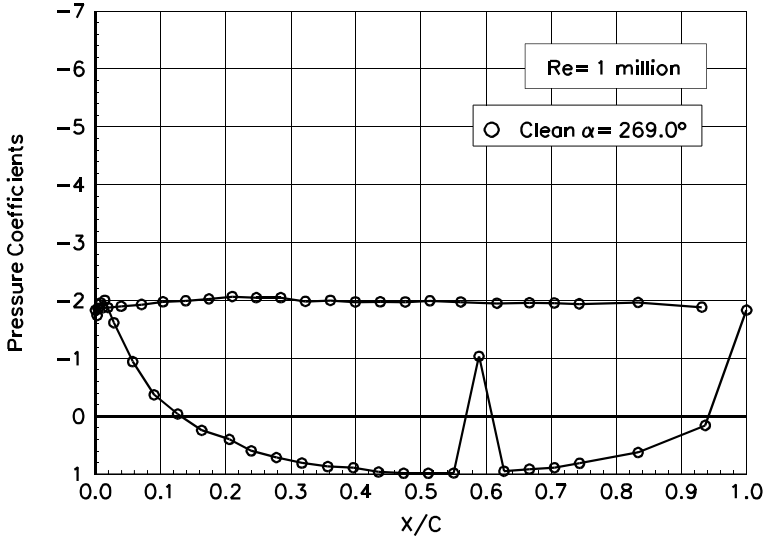

Figure 25. Baseline, α = 269.0°

S809 Unvented Aileron

Pressure Distributions, Re = 1 million, δ=5°

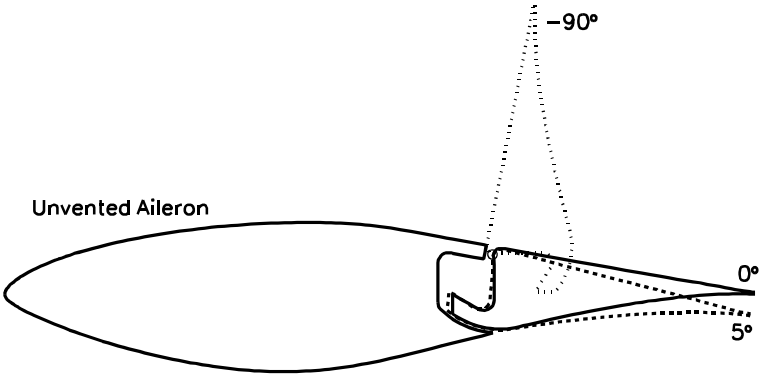

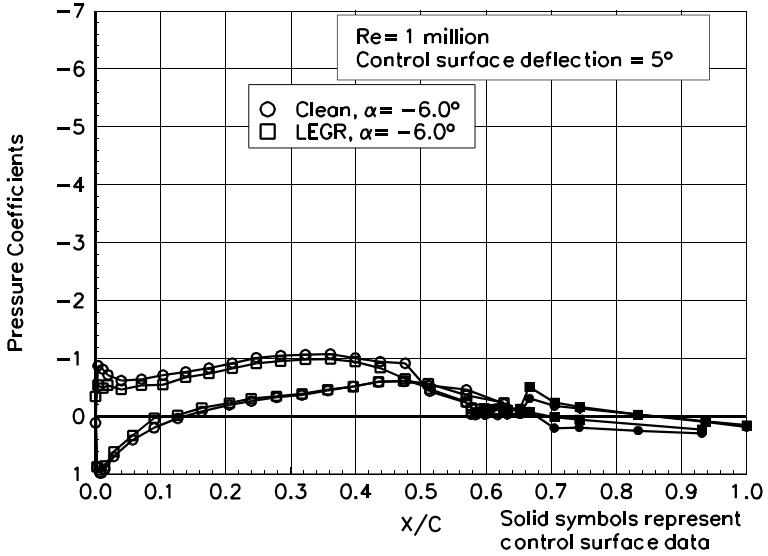

Figure 26. Unvented Aileron, α = -6.0°

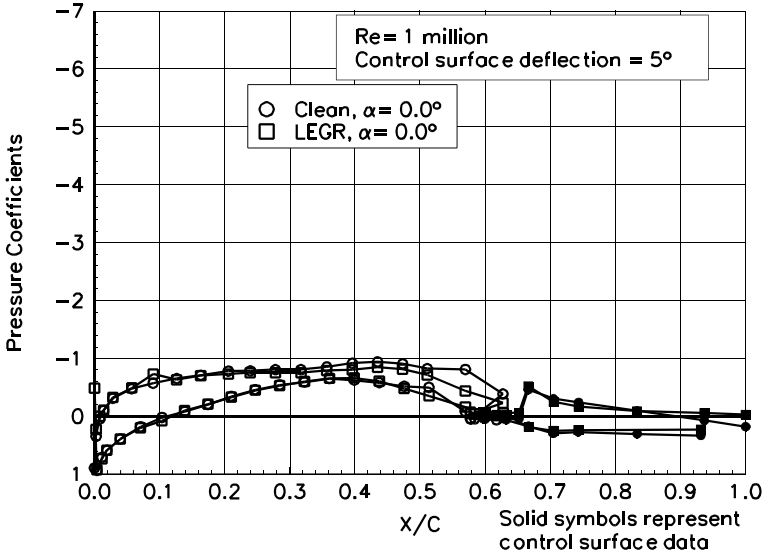

Figure 27. Unvented Aileron, α = 0.0°

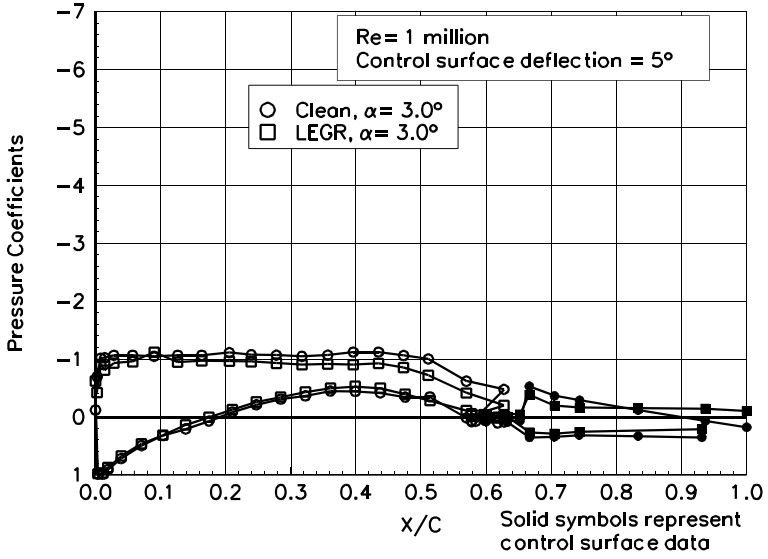

Figure 28. Unvented Aileron, α = 3.0°

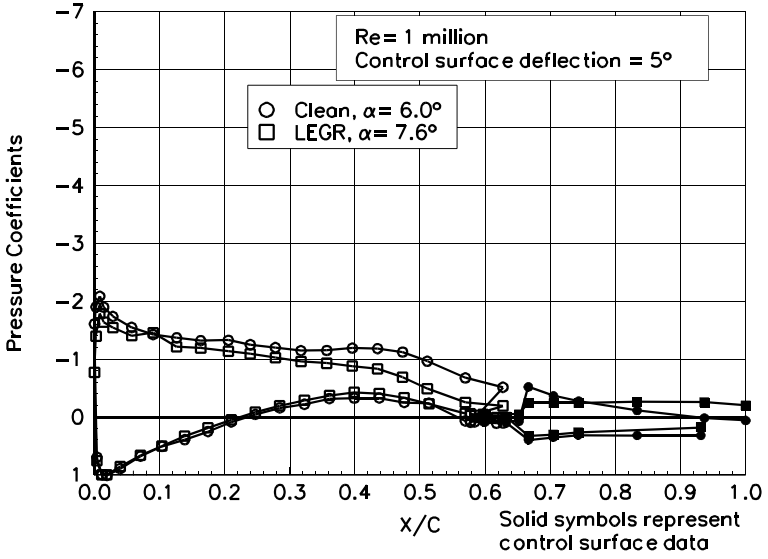

Figure 29. Unvented Aileron, α = 6.0°

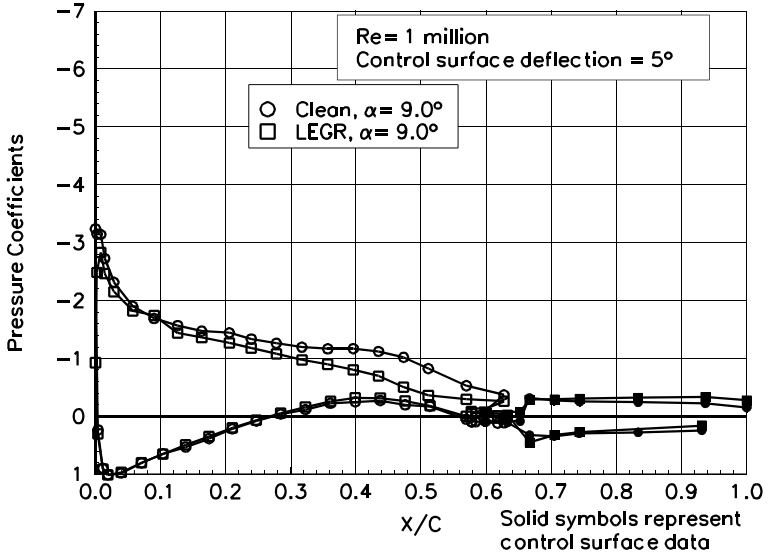

Figure 30. Unvented Aileron, α = 9.0°

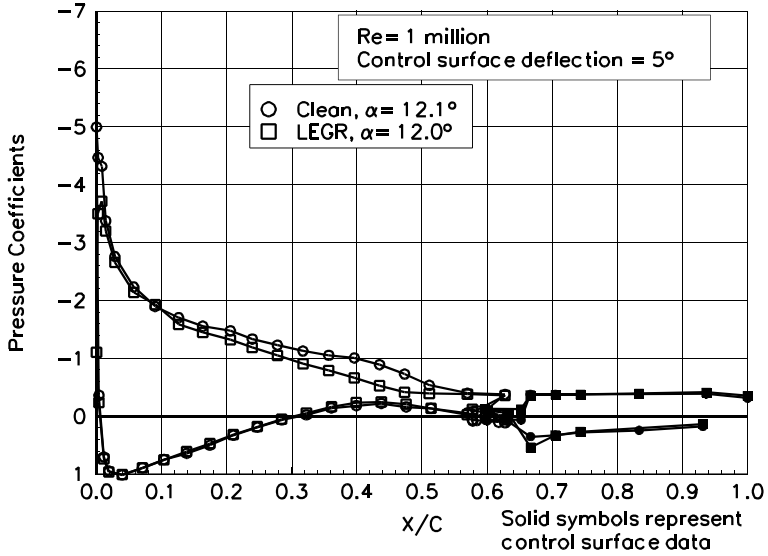

Figure 31. Unvented Aileron, α = 12.1°

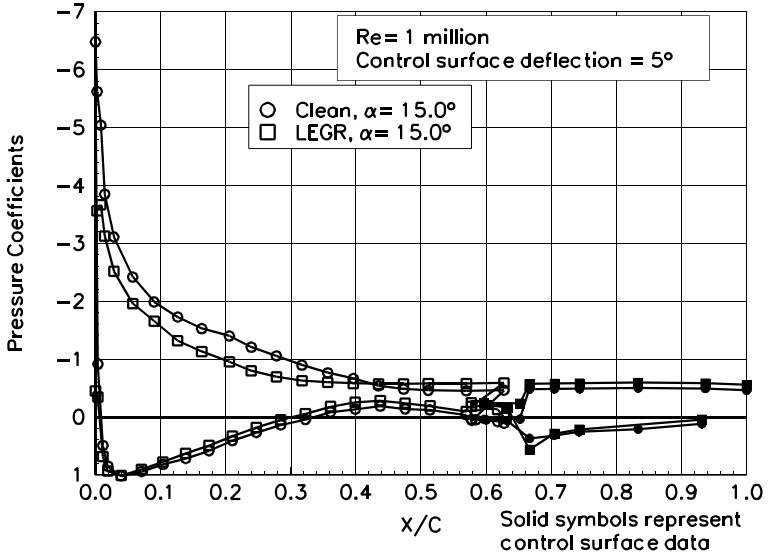

Figure 32. Unvented Aileron, α = 15.0°

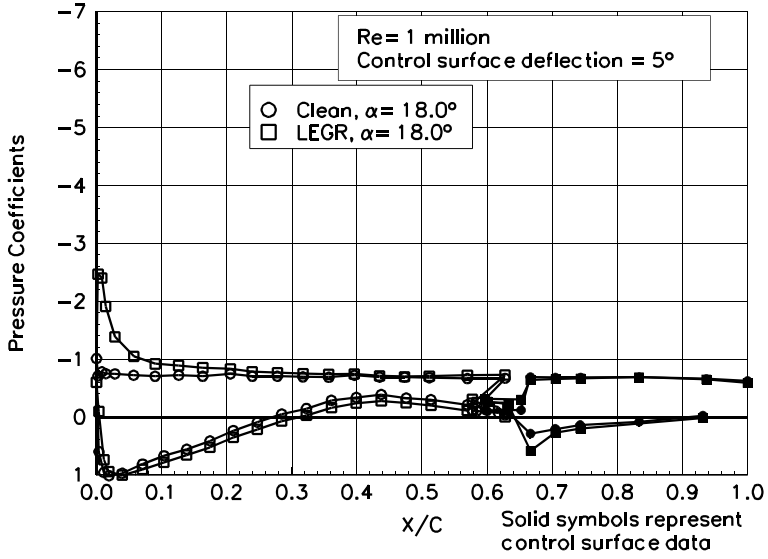

Figure 33. Unvented Aileron, α = 18.0°

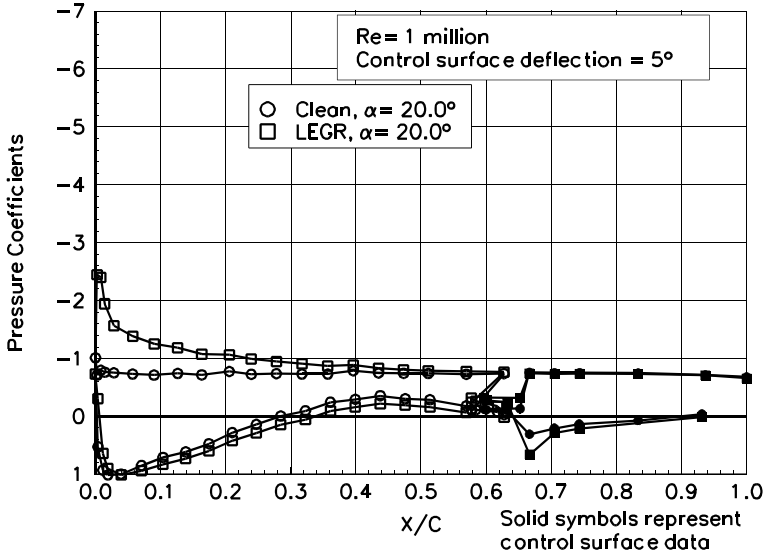

Figure 34. Unvented Aileron, α = 20.0°

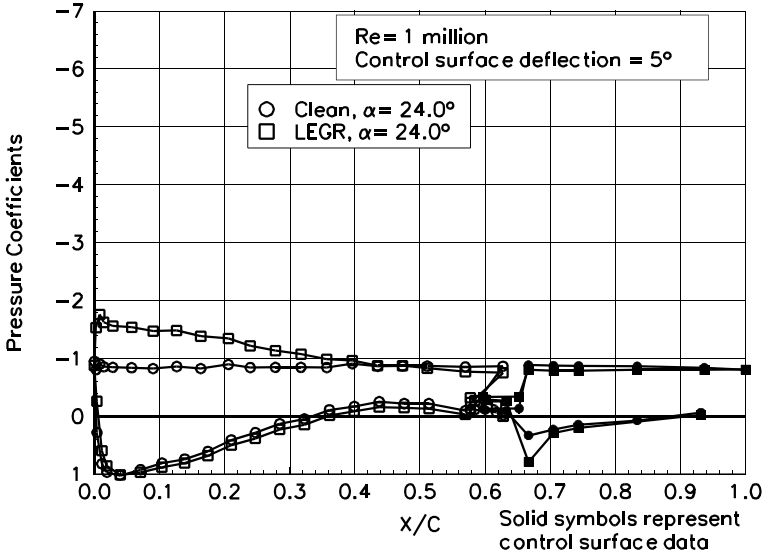

Figure 35. Unvented Aileron, α = 24.0°

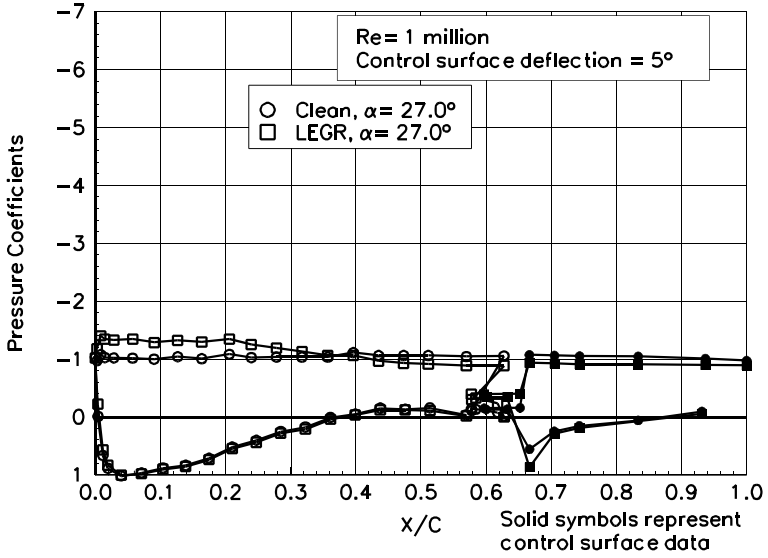

Figure 36. Unvented Aileron, α = 27.0°

S809 Unvented Aileron

Pressure Distributions, Re = 1 million, δ=0°

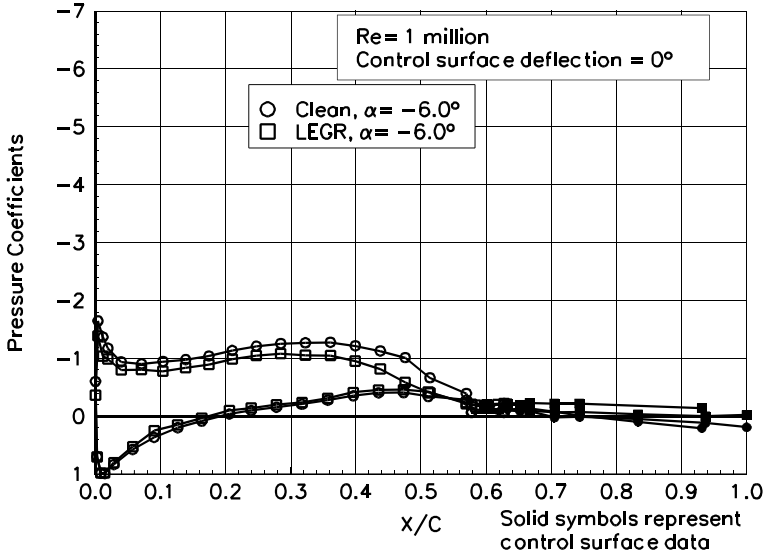

Figure 37. Unvented Aileron, α = -6.0°

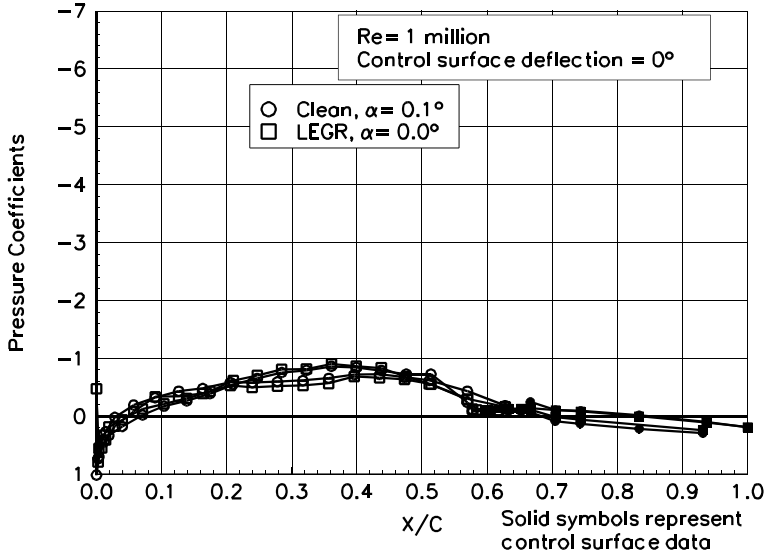

Figure 38. Unvented Aileron, α = 0.1°

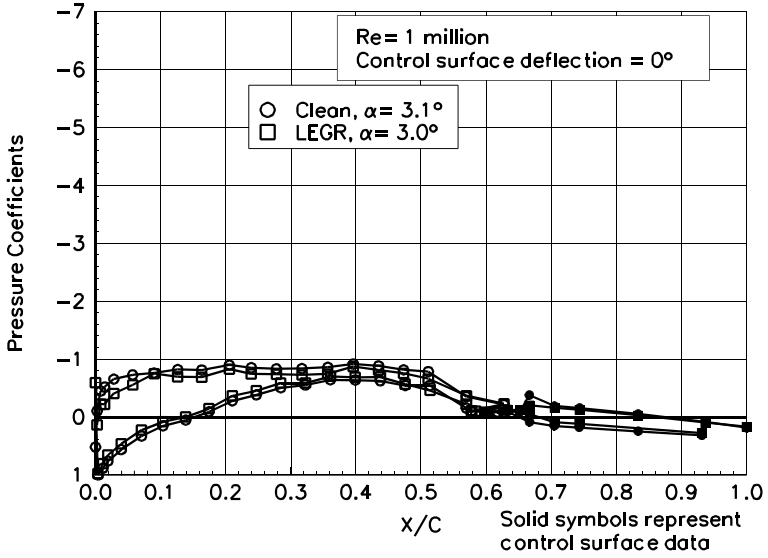

Figure 39. Unvented Aileron, α = 3.1°

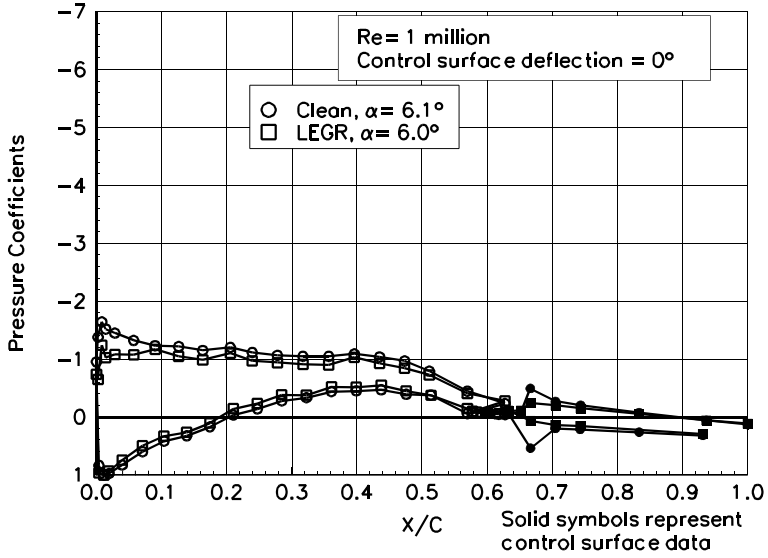

Figure 40. Unvented Aileron, α = 6.1°

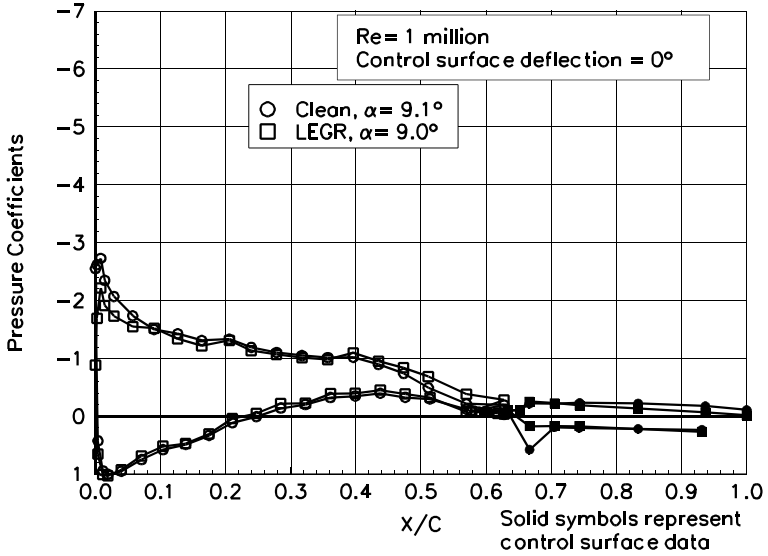

Figure 41. Unvented Aileron, α = 9.1°

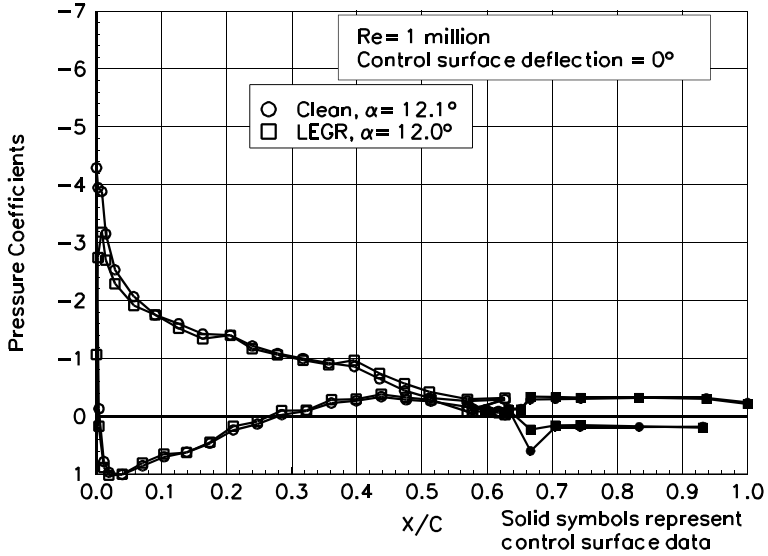

Figure 42. Unvented Aileron, α = 12.1°

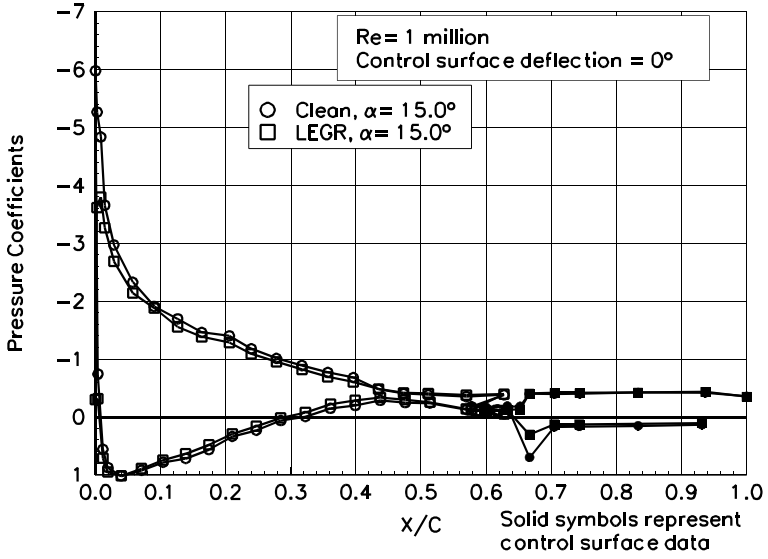

Figure 43. Unvented Aileron, α = 15.0°

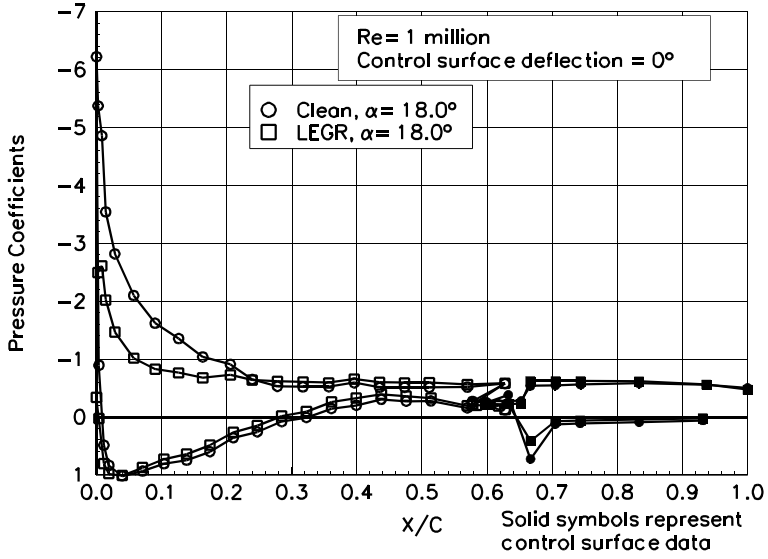

Figure 44. Unvented Aileron, α = 18.0°

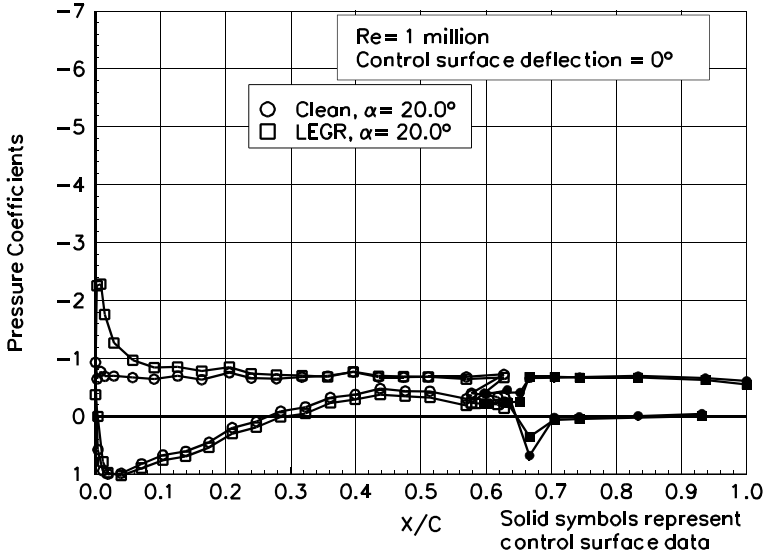

Figure 45. Unvented Aileron, α = 20.0°

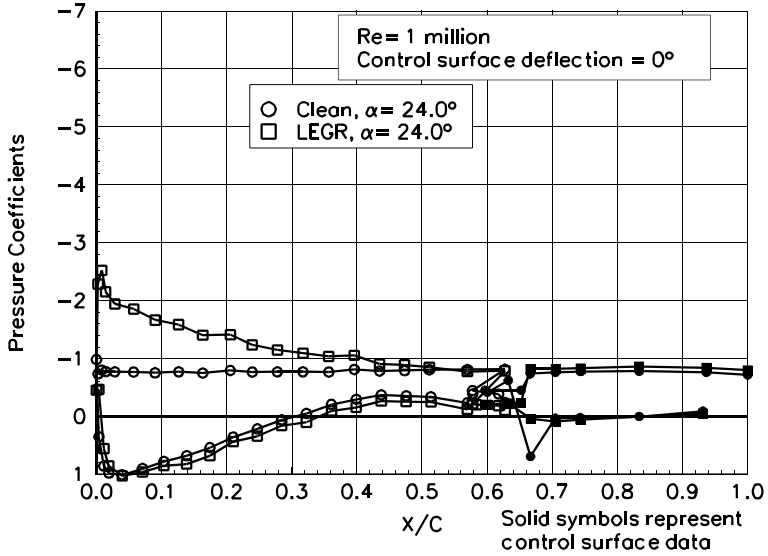

Figure 46. Unvented Aileron, α = 24.0°

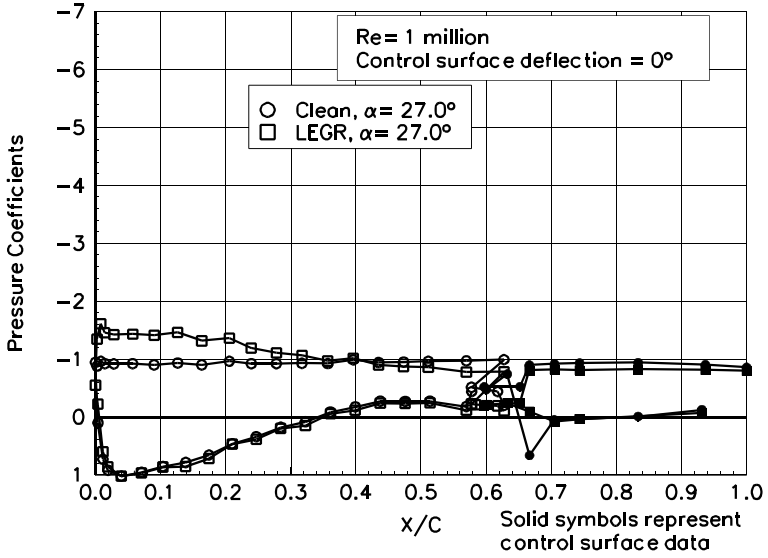

Figure 47. Unvented Aileron, α = 27.0°

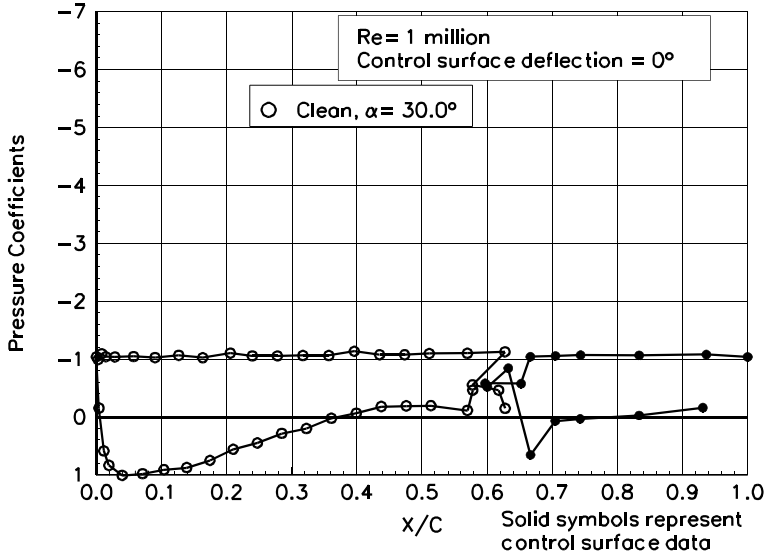

Figure 48. Unvented Aileron, α = 30.0°

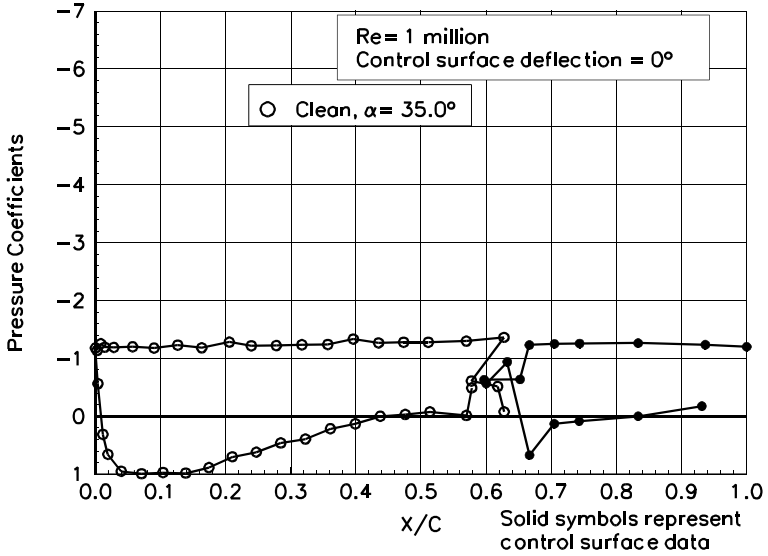

Figure 49. Unvented Aileron, α = 35.0°

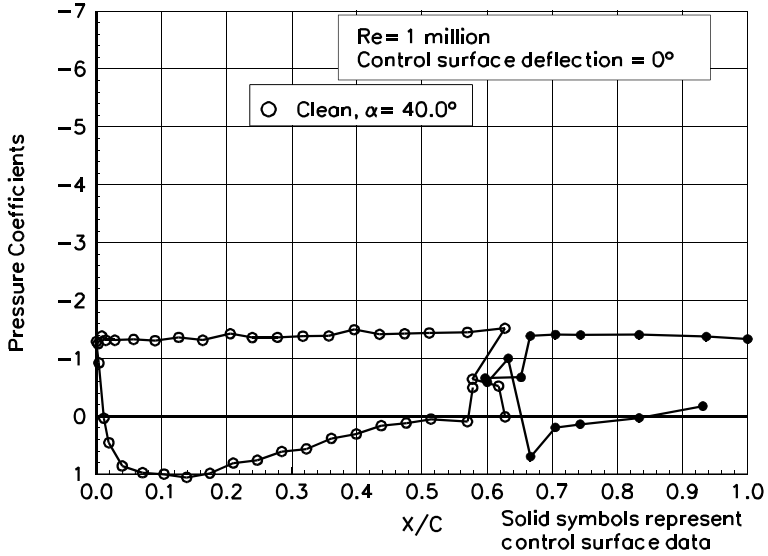

Figure 50. Unvented Aileron, α = 40.0°

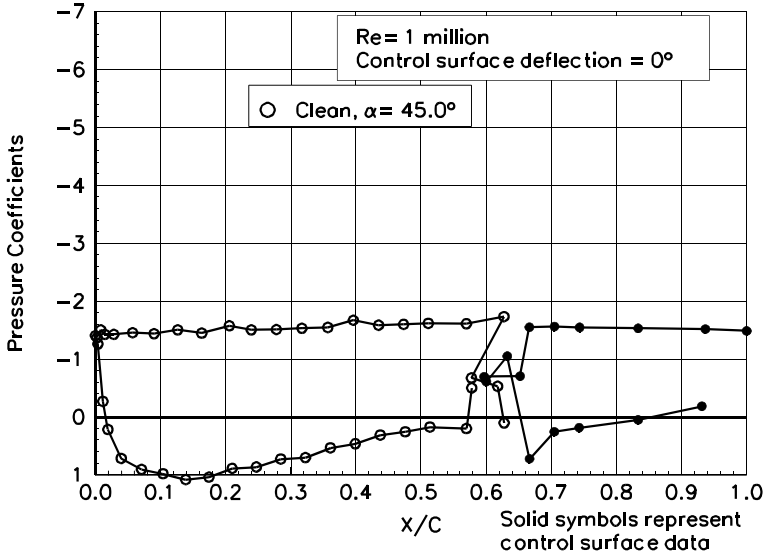

Figure 51. Unvented Aileron, α = 45.0°

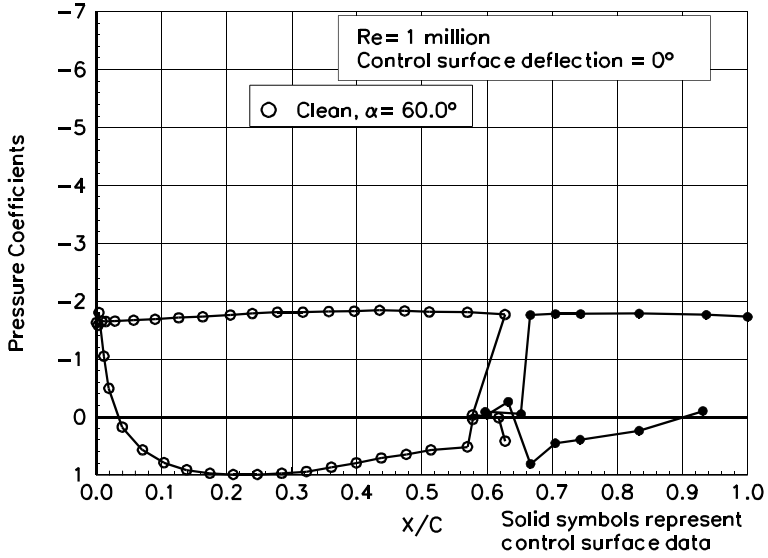

Figure 52. Unvented Aileron, α = 60.0°

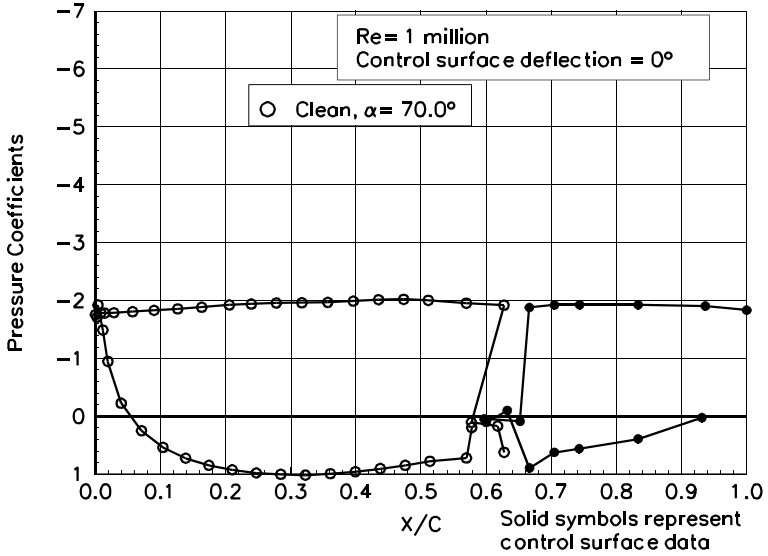

Figure 53. Unvented Aileron, α = 70.0°

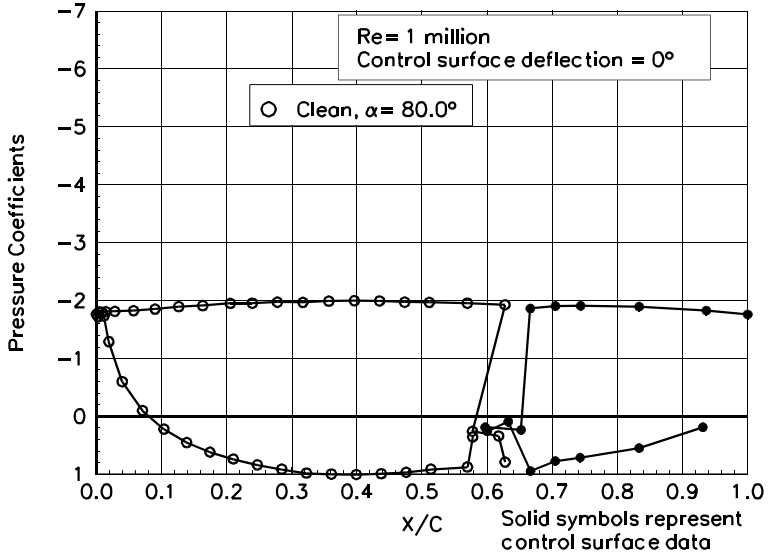

Figure 54. Unvented Aileron, α = 80.0°

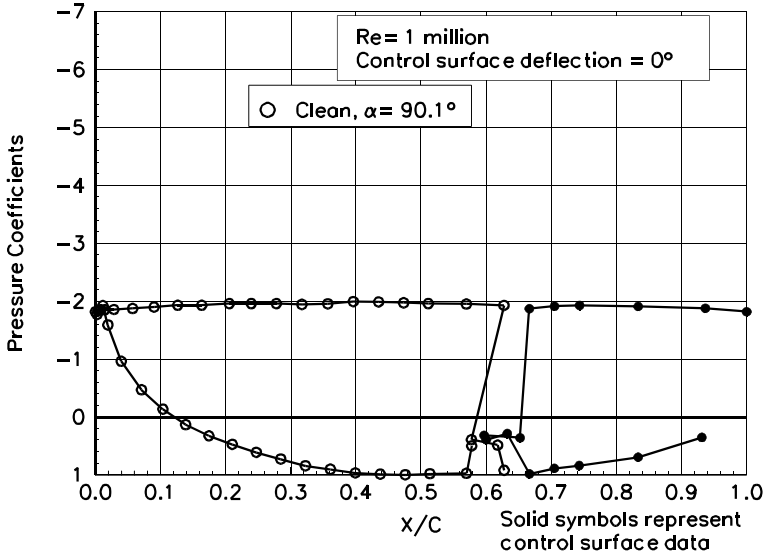

Figure 55. Unvented Aileron, α = 90.1°

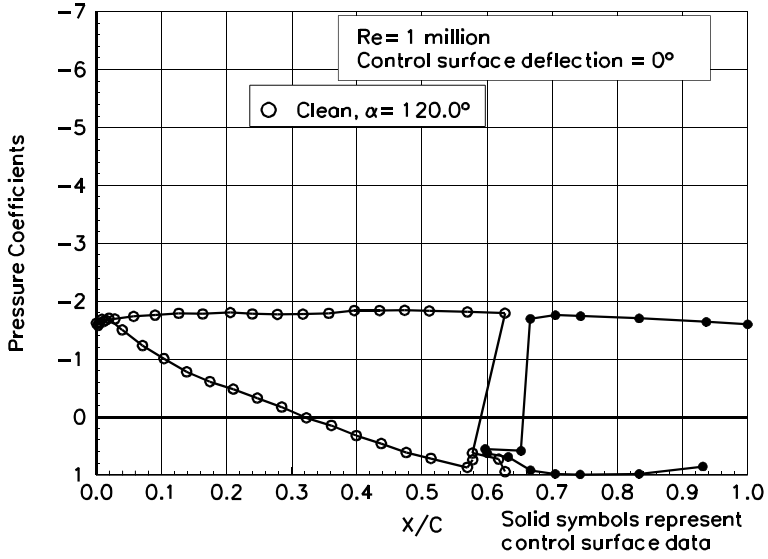

Figure 56. Unvented Aileron, α = 120.0°

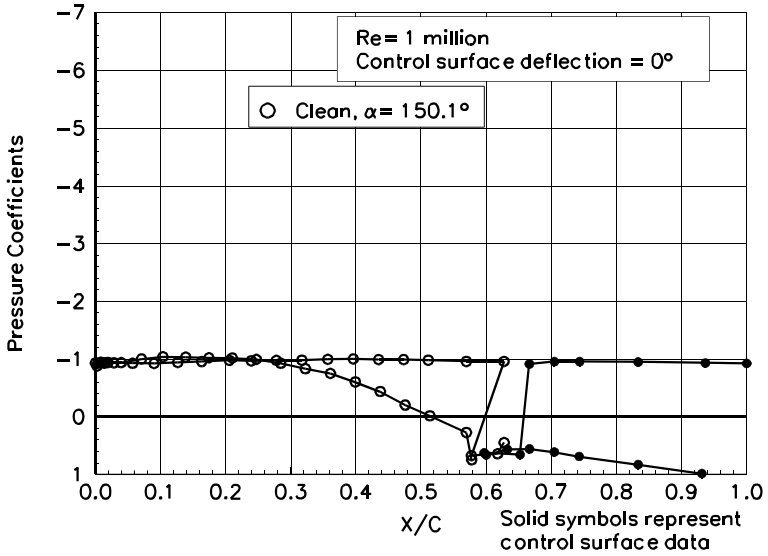

Figure 57. Unvented Aileron, α = 150.1°

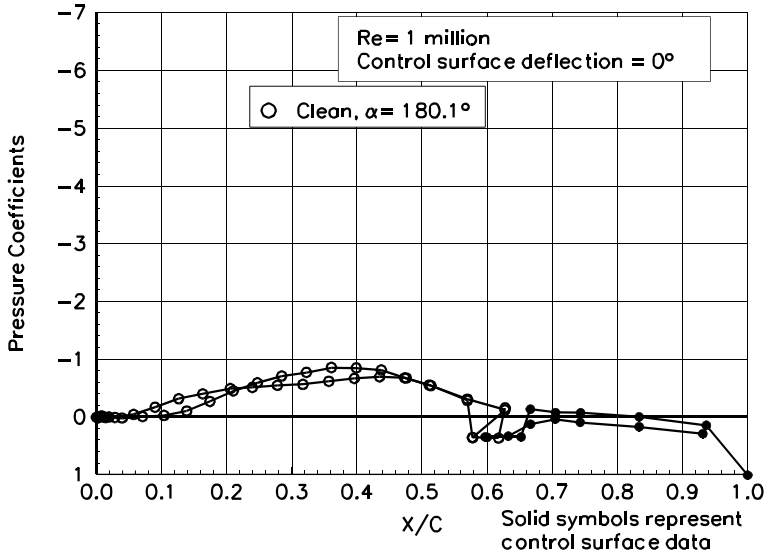

Figure 58. Unvented Aileron, α = 180.1°

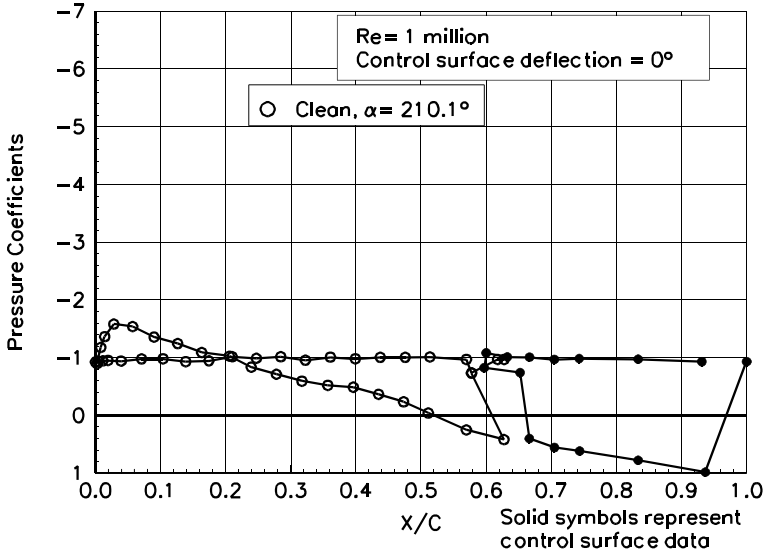

Figure 59. Unvented Aileron, α = 210.1°

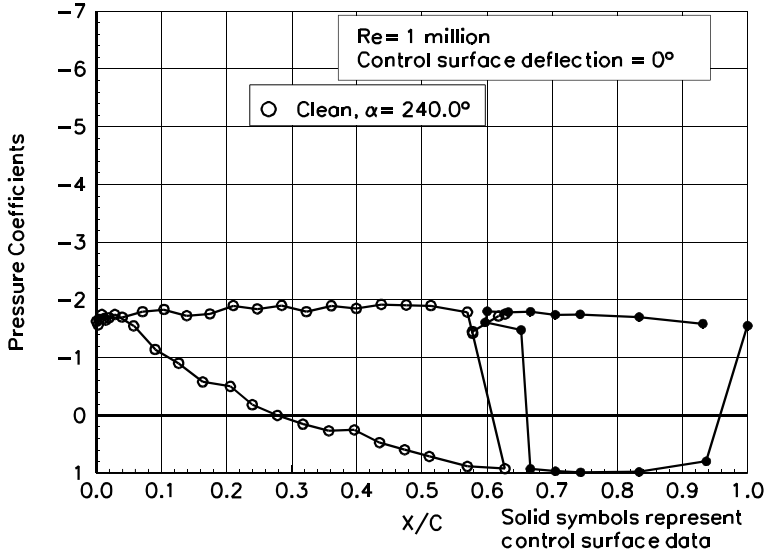

Figure 60. Unvented Aileron, α = 240.0°

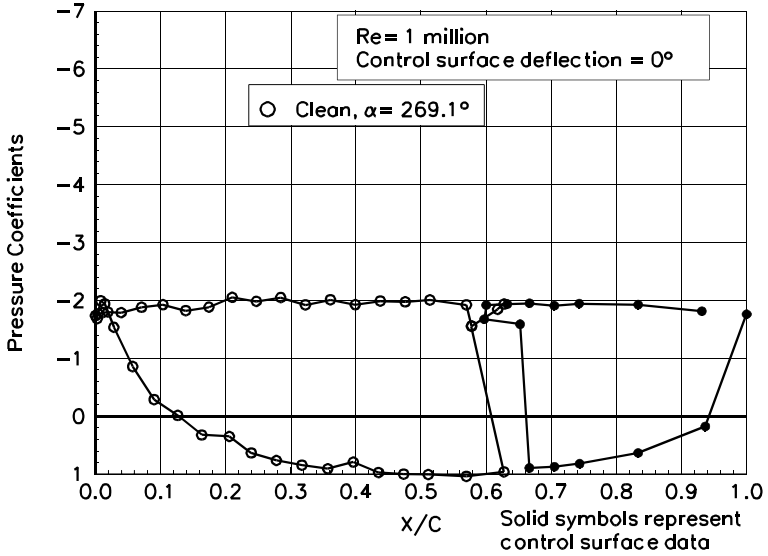

Figure 61. Unvented Aileron, α = 269.1°

S809 Unvented Aileron

Pressure Distributions, Re = 1 million, δ=-5°

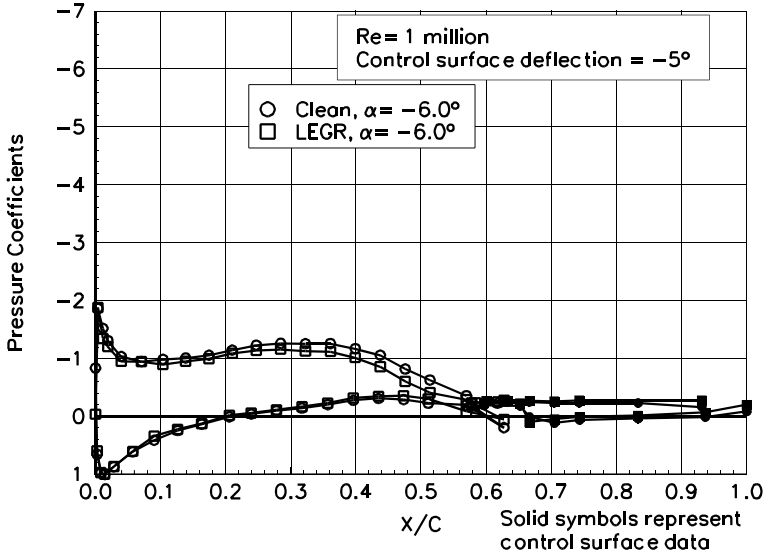

Figure 62. Unvented Aileron, α = -6.0°

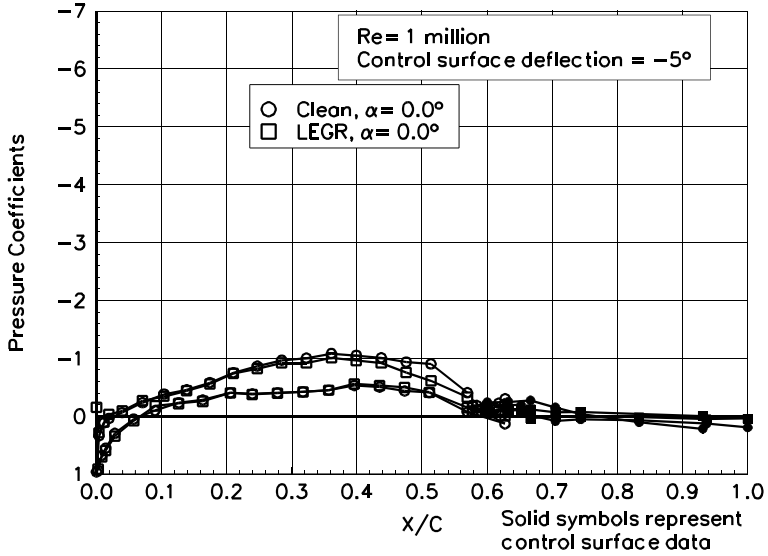

Figure 63. Unvented Aileron, α = 0.0°

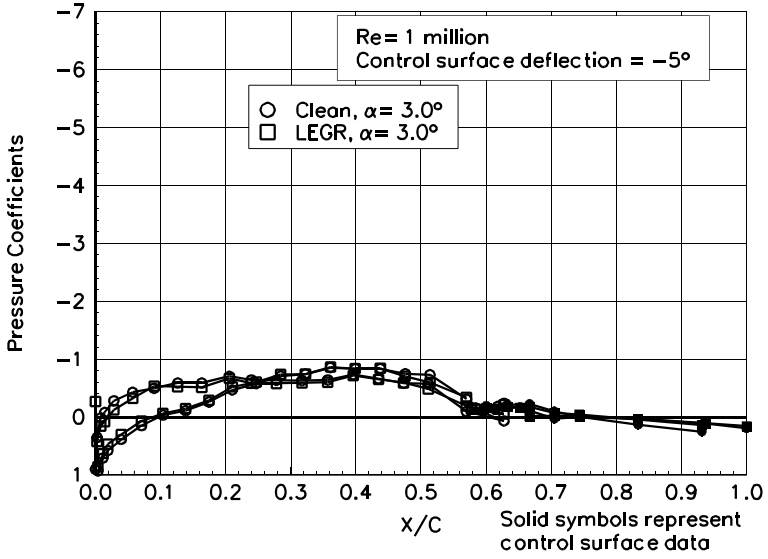

Figure 64. Unvented Aileron, α = 3.0°

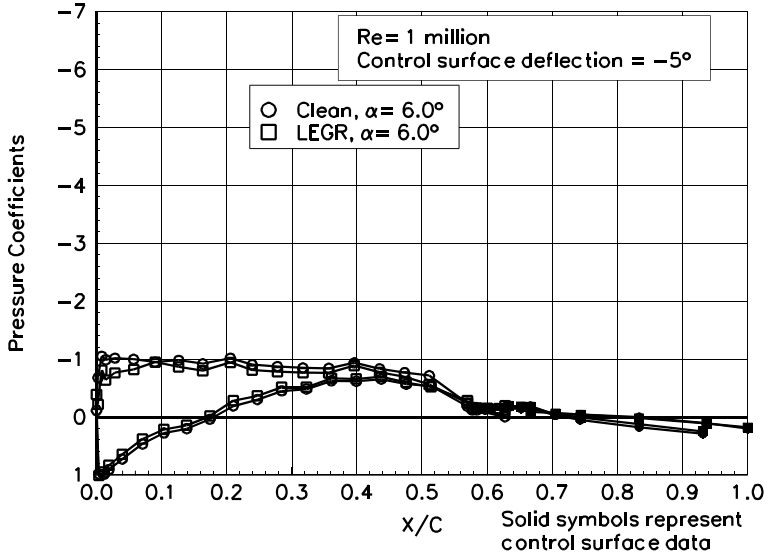

Figure 65. Unvented Aileron, α = 6.0°

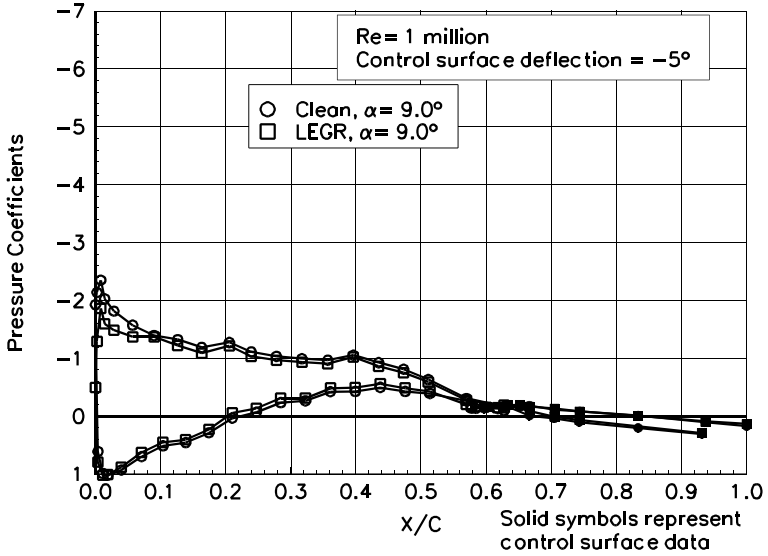

Figure 66. Unvented Aileron, α = 9.0°

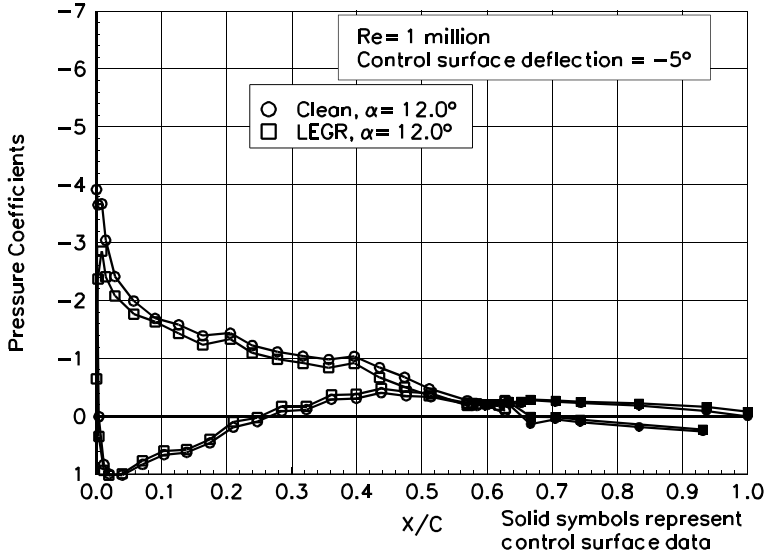

Figure 67. Unvented Aileron, α = 12.0°

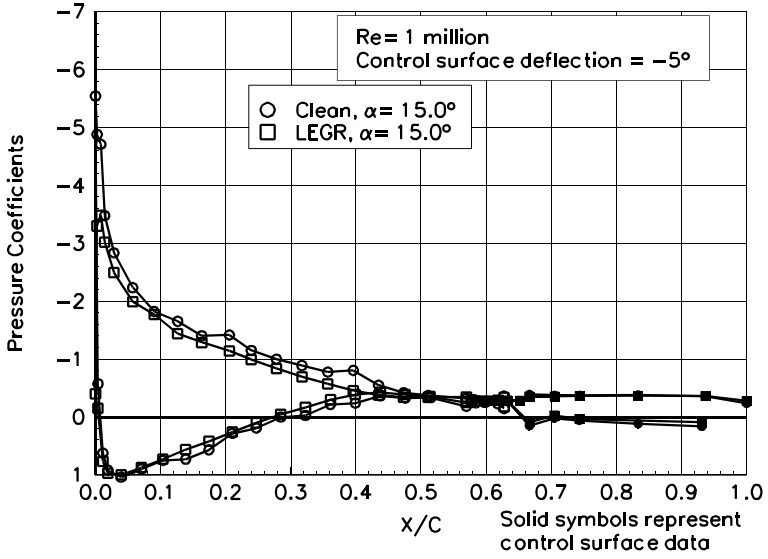

Figure 68. Unvented Aileron, α = 15.0°